Chapter 7

Dielectric Self Energy in Continuum Theories

7.1 Abstract

We investigate whether the accuracy of the Poisson-Boltzmann and Poisson-Nernst-Planck equations can be improved in biological ion channels by including a specific dielectric self energy term to overcome spurious shielding effects. By comparing results with Brownian dynamics simulation, we show that although significant qualitative improvements are obtained when considering single ion channels, large errors still exist in many cases. The inaccuracies are much greater in multi-ion channels. Thus neither theory can be reliably salvaged for quantitative studies of biological ion channels in this simple manner.

7.2 Introduction

As noted previously, the PB and PNP equations have been widely used in studies of biological ion channels. These include calculation of the forces and energy profiles seen by ions in channels [1, 29, 37, 54, 101, 121, 163, 171, 181, 182, 189, 211], the ionisation states of side chains [164, 174], and currents passing through the channel [31, 61, 62, 88, 89, 113]. The use of these techniques for calculation of potentials and currents in narrow channels whose radius was smaller than the Debye length of the electrolyte were called into question in chapters 5 and 6 as they were found to overestimate electrolytic shielding effects. When the PB equation is used in channels, high concentrations of counter ions accumulate around a fixed test ion, which act to eliminate the repulsive image force created by the dielectric boundary at the channel walls. Such high concentrations of counter ions around a test ion are not seen when the mobile ions are treated explicitly as in BD. In such simulations, the image

forces felt by individual counter ions prevent them from easily entering the channel and thereby suppress the large degree of shielding seen in the continuum theory. Similarly, in PNP calculations the currents passing through narrow channels are found to be much larger than in corresponding BD simulations, again as a direct consequence of higher ionic concentrations found in the former method.

Extensive comparisons with BD simulations indicate that the problems in both continuum theories arise from the fact that the dielectric self energy (DSE) contribution is not properly taken into account. Because the self energy is proportional to the square of the charge, it is positive for all ions, and it would repel them from the dielectric channel boundaries leading to a suppression of their concentrations. In numerical solutions of the PB and PNP equations, fractional charges are used in a given region of the channel, which means that only partial image charges are induced from that region. This is very different from the realistic case in which monovalent ions carry a full charge of e. In this situation image charges are induced in an 'all or nothing' way, either a large image force is induced (repelling the ion away from the boundary) or there is no ion and thus no force. This DSE problem is especially accentuated in those PNP calculations where equal amounts of positive and negative electrolyte are found in the channel resulting in the dielectric repulsion being completely cancelled out.

Given the computational simplicity of the continuum theories compared to simulation approaches and their widespread use, it would be desirable to find a solution to the DSE problem highlighted above. A possible approach is to include an explicit self energy term that would mimic the effect of the induced surface charges on ions entering the channel. Such a term would prevent the build up of large counter ion concentrations and possibly eradicate the spurious shielding effects seen in these continuum models. This approach to correct the continuum theories is also being pursued elsewhere [43, 134]. Here we examine the consequences of including a DSE term in the PB and PNP formalisms. The forces calculated using the modified PB and the currents found from the modified PNP equations are again compared with BD simulations to ascertain whether the suggested modification improves the performance of the continuum approaches in ion channels.

7.3 Theory

7.3.1 Modified PB equation

In the Poisson-Boltzmann theory, the mobile ions are treated as a continuous charge density distributed according to the Boltzmann factor

$$n_\nu(\mathbf{r}) = n_{0\nu} \exp(-U_\nu/kT), \quad U_\nu = z_\nu e\phi(\mathbf{r}). \tag{7.1}$$

Here $n_{0\nu}$ is a background (or reference) density of ions of species ν, U_ν is the electrostatic potential energy of an ion with charge $z_\nu e$, and $\phi(\mathbf{r})$ is the average potential at the position $\mathbf{r}$ determined from the solution of Poisson's equation (Eq. 2.1).

The crucial assumption of the PB theory in Eq. 7.1 is that at a given point, the same average potential acts on ions regardless of their valence, and hence the potential energy of anions and cations have opposite signs. This is a reasonable assumption to make in a homogeneous system but it cannot be justified in an inhomogeneous one with dielectric boundaries. Near a water-protein interface, a mobile ion with charge $z_\nu e$ induces polarization charges of the same sign on the boundary. These charges, in turn, generate a reaction potential ϕ_{R} that acts to repel the ion from the boundary. The potential energy due to this reaction field, called the dielectric self energy, is given by

$$U_{\nu\mathrm{R}} = \frac{1}{2} z_\nu e\phi_{\mathrm{R}}(\mathbf{r}). \tag{7.2}$$

Since ϕ_{R} is itself proportional to $z_\nu e$, $U_{\nu\mathrm{R}}$ depends on the square of the ionic charge, and hence it is always positive regardless of the valence of the ions. Thus the self energy contribution to the total potential energy of an ion is the same for cations and anions, which is incompatible with the assumption in Eq. 7.1. The PB equation often bypasses the self energy problem because it results in equal densities of anions and cations near a (neutral) dielectric boundary—since the average charge is zero, there are no induced charges or reaction potentials to give rise to a self energy contribution. The upshot is that the PB equation cannot lead to a suppression of ionic densities near a dielectric boundary because it fails to take into account the self energy contribution. A similar problem occurs in the Gouy-Chapman solutions of the PB equation where counter-ions build up at a charged electrode. In that case, this unphysical behavior is avoided by introducing a Stern or Helmholtz layer that excludes ions from the immediate neighborhood of the boundary. While the presence of this layer is motivated by the finite size of ions or the effect of the solvent layer, in practice its thickness is used as a free parameter to fit the experimental

data. In any case, the physics of repulsive self energy is very different and cannot be modeled by such a simple exclusion zone for ions.

The above discussion about the lack of self energy in the PB equation suggests an apparently simple remedy: modify the Boltzmann factor in Eq. 7.1 by adding a self energy term to the potential energy

$$n_\nu(\mathbf{r}) = n_{0\nu} \exp[-(U_\nu + U_{\nu \mathrm{R}})/kT], \tag{7.3}$$

so that the modified PB equation in a 1:1 electrolyte becomes

$$\epsilon_0 \nabla \cdot [\epsilon(\mathbf{r}) \nabla \phi(\mathbf{r})] = 2en_0 \sinh[e\phi(\mathbf{r})/kT] \exp[-U_{\mathrm{R}}/kT] - \rho_{\mathrm{ex}}. \tag{7.4}$$

As an ion approaches a dielectric boundary, U_{R} grows rapidly, and the exponential factor in Eq. 7.4 provides a natural mechanism to suppress the ion densities. The difficulty in this scheme, of course, lies in the calculation of U_{R} in a many-body system in a self-consistent manner. For a single-ion, self energy is well defined—one just needs to solve Poisson's equation for the single ion and substitute the computed reaction potential in Eq. 7.2. Indeed in a dilute electrolyte solution, where the effect of ion-ion correlations may be neglected, this simple recipe should be quite adequate for the self energy correction. However, at higher concentrations, the correlations among ions lead to screening of their charges at relatively shorter distances (Debye length), and the approximation of the reaction potential with that of a single-ion becomes problematic. Unfortunately, there is no known method for incorporating the ion-ion correlations in the calculation of the reaction potential. Nevertheless, it is of interest to see whether the inclusion of the self energy correction at the single-ion level improves the accuracy of the PB solutions sufficiently so that they can be used in ion channels with some confidence. For this purpose, we compare the results of the modified PB equation with those obtained from BD simulations.

The modified PB equation is solved using a finite difference method as described previously for the standard PB equation (chapter 5). The DSE values are calculated by solving the Poisson equation using the same technique, but with all the electrolyte concentrations set to zero. A unit charge is placed at each of the grid points used in the finite difference computation and the calculated values of U_{R} are stored in a table. Entries from this table are utilized during the solution of the modified PB equation (Eq. 7.4).

7.3.2 Modified PNP equations

As in the case of PB theory, the presence of dielectric boundaries creates problems for the application of PNP to narrow channels because DSE of ions is not properly taken into account.

The PNP equations can be modified in a similar manner to the PB equation by including a specific DSE term in the potential energy of an ion:

$$\mathbf{J}_\nu = -ez_\nu D_\nu \left(\nabla n_\nu + \frac{z_\nu e n_\nu}{kT} \nabla(\phi + \phi_{\mathrm{R}}/2) \right). \tag{7.5}$$

The analogy between Eq. 7.5 and the modified PB equation can be seen most clearly when the current vanishes. Then Eq. 7.5 can be easily integrated yielding the modified Boltzmann factor given in Eq. 7.3. Here we solve Eq. 7.5 simultaneously with Poisson's equation (Eq. 2.1) using a finite difference procedure as described previously for the PNP equations (chapter 6). The DSE values are implemented in this process using a table as in the solution of the modified PB equation.

7.4 Results

7.4.1 Self energy in continuum theories

In continuum electrostatics, self energy refers to the intrinsic potential energy of a charge or charge distribution. This is different from the DSE discussed above, which arises from the interaction of a charge with a dielectric boundary. Because an ion's self energy is constant and has no effect on most results, it is routinely ignored in electrostatic calculations involving discrete charges, and only the Coulomb interactions among the charges are considered. In continuum theories, however, charges are distributed continuously and it is not possible to isolate the self energy from the Coulomb interaction. Thus when Poisson's equation is solved in the PB and PNP theories, the calculated potential energy of ions necessarily contains a self energy contribution. This is not a concern in typical applications of continuum theories, which involve a large number of ions ($N \gg 1$) in a nearly neutral electrolyte solution. First, the self energy is proportional to N whereas Coulomb interaction scales as N^2, so its relative contribution would be negligible for large N. Secondly, near electroneutrality in a large system means that the self energy due to any excess charge has to be small. To give an example, when a charge q is uniformly spread in a water filled sphere of radius R, the self energy associated with this distribution is given by

$$U_{\mathrm{s}} = \frac{1}{4\pi\epsilon_0\epsilon_w} \frac{3q^2}{5R}. \tag{7.6}$$

For a unit charge with a dielectric constant of $\epsilon_w = 80$, this yields $U_{\mathrm{s}} = (4.2/R)$ kT where R is in Å. Thus in large system (e.g. $R > 100$ Å), self energy due to an excess ionic charge is negligible.

Ion channels do not satisfy either condition: they contain a rather small volume of electrolyte which is far from being electroneutral—at least for the majority of channels that are either cation or anion selective. Because the PB and PNP equations strive to maintain electroneutrality, this was not an apparent problem in earlier applications of the continuum theories to ion channels. The introduction of the DSE term, however, leads to a suppression of the counter ions in the channel and thereby exposes the self energy problem more conspicuously. To get a feel for the size of this effect, we show in Fig. 7.1 its influence in the simple case of electrolyte contained within a sphere. In Fig. 7.1 A, a single ionic charge is confined inside a 4 Å radius sphere with $\epsilon = 80$ everywhere so that there are no dielectric boundaries. A single ion should move freely within the sphere occupying all space evenly. In contrast, the average concentration found using the (standard) PB equation (Fig. 7.1 A) exhibits a central depression, which is simply caused by the Coulomb repulsion amongst the charges distributed at all the grid points. The size of the corresponding potential energy of the system can be simply calculated by summing the energy at each of the grid points, i, in the finite difference solution to Poisson's equation as follows:

$$U_{\mathrm{s}} = \frac{1}{2}\sum_i q_i \phi_i, \tag{7.7}$$

in which q_i is the total charge of the electrolyte contained within the grid volume and ϕ_i is the potential at the grid point. The potential energy of the charge distribution shown in Fig. 7.1 is about 1 kT. This self energy is, of course, entirely spurious because the potential energy of an isolated ion is zero.

With increasing number of ions in the system, things get worse before recovering at the large N limit. This is illustrated in Fig. 7.1 B, where the potential energy of the system is plotted as a function of the number of monovalent ions in the sphere. The solid line shows the potential energy obtained from the solution of the PB equation at room temperature ($T = 298$ K). As the charge in the sphere is increased, the potential energy is seen to increase roughly proportional to the charge squared. Thus for 2 ions it is about 4 kT and for 3 ions, 9 kT. The dotted line in the figure shows the minimum electrostatic energy of the system that would be obtained at $T = 0$ K when all the charges collapse to the boundary. Because the two curves are quite similar, we simply present the potential energy for the corresponding discrete charge configurations at $T = 0$ K (dashed line in Fig. 7.1 B). The discrepancy between the continuum and discrete representations of the potential energy is seen to grow with increasing number of ions. For two ions, contribution of the spurious self-energy to the total potential energy is about 3 kT which may have a sizable impact on the continuum theory results. The error introduced by spurious self

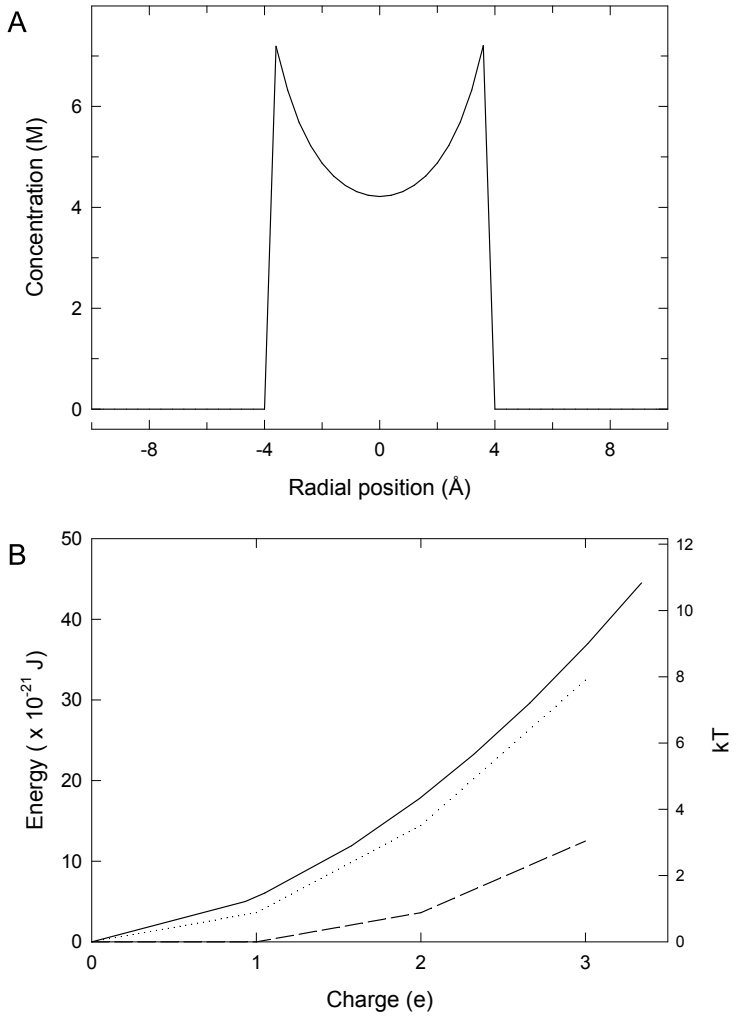

Figure 7.1: Effect of self energy created by spreading the charge on an ion in a continuous fashion. (A) The concentration found using the standard PB equation is plotted against the radial position when a total of one ionic charge is contained in a 4 Å radius sphere. (B) The energy of the system as the charge in the sphere is increased. Results are shown as found from the PB equation at 298° K (solid line), 0 ° (dotted line) and as calculated with discrete ions at 0° (dashed line). In both cases $\epsilon = 80$ is used everywhere.

energy would obviously be greater when dealing with divalent ions.

While channels are cylindrical and do not absolutely confine ions, we expect the order of magnitude estimates presented above will have a bearing on the results of the modified PB and PNP equations, particularly in multi-ion channels. Whenever there is a net charge build up inside the channel, the repulsion arising from the spurious self energy will push the electrolyte out of the channel, leading to a lowering of the concentration inside. This process of self repulsion is required to understand some of the results presented later.

7.4.2 Modified PB equation

The modified PB equation is tested by calculating the force on fixed test ions as well as potential and concentration profiles within schematic channel models, in a similar manner to that done in chapter 5 for the standard PB equation. The first tests are made in cylindrical channels of varying radii whose shape is indicated in Fig. 5.4. The dielectric constants are set to 2 in the protein and 80 for the water. An average concentration of 300 mM is used in all cases, determined from the average charge of cations and anions in the modified PB equation, and corresponding to 24 Na^+ and 24 Cl^- ions in the BD simulations.

Rather than repeating all the tests made previously for bare cylindrical channels (no fixed charge), we show in Fig. 7.2 the summary of how the screening charge (A) and force on a test ion (B) change with the channel radius when using the modified PB equation. In both cases a test ion is held fixed at $z = 12.5$ Å, where the force on the ion is greatest. It can be seen that the inclusion of the DSE term dramatically reduces the concentration of counter ions in the channel, well below that seen with the standard PB equation. In Fig. 7.2 A the total electrolyte charge in the channel (screening charge) is plotted against the radius of the channel. In the narrowest channel studied ($r = 3$ Å) there is essentially no screening charge in the channel, in agreement with the BD results. So, in this case the unwanted shielding effects found in the standard PB equation are removed as desired. But, at larger channel radii, the amount of counter charge in the channel stays below that found in the BD simulations, suggesting that the electrolyte screening may be suppressed too much. Suppression of the counter charges in modified PB persists even after an agreement between the standard PB, and BD results is obtained at $r > 12$ Å.

The dynamics of an ion in the channel is determined by the force acting on it, and so this is a primary quantity of concern. In Fig. 7.2 B the axial component of the force on the test ion, normalised by the force experienced by a single ion is plotted against the channel radius. A single ion in the channel experiences a

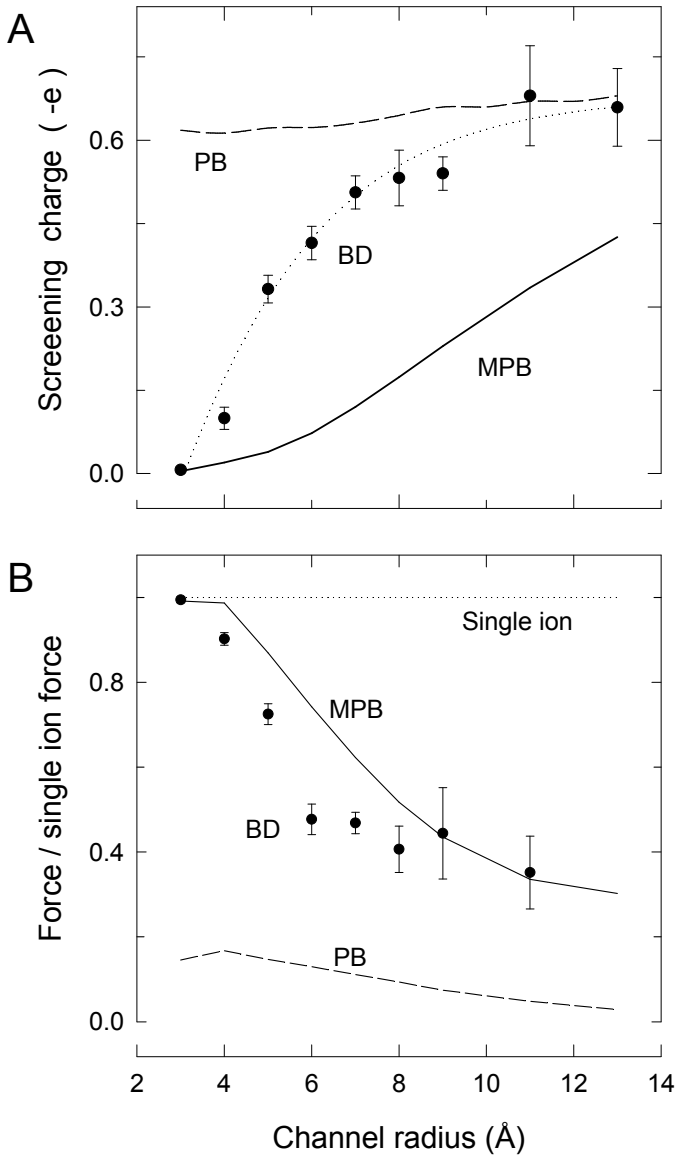

Figure 7.2: Pore size dependence of the screening charge and force on a cation held at $z = 12.5$ Å in a cylindrical channel. (A) The net screening charge in the channel (from $z = -15$ to 15 Å) is plotted as a function of the channel radius. The modified PB results (MPB) are shown by the solid line, standard PB by the dashed line and the BD values by the filled circles fitted with the dotted line. (B) The force on the cation normalised by the force on a single ion (no electrolyte) is plotted as the channel radius is increased. Symbols are as in A and the single ion results (dotted line) are indicated for reference.

large force repelling it out of the channel due to the surface charges it induces along the dielectric boundary of the channel. This force is found by solving Poisson's equation and is indicated by the dotted line in the figure for reference. As expected in the narrow $r = 3$ Å channel, both the BD and modified PB results agree with the single ion result as no screening charge finds its way into the channel. In intermediate radii channels the BD and modified PB results diverge, the forces calculated from the modified PB equation lying closer to the single ion results as there is less screening charge in this case. The two results converge again at a channel radius of around 10 Å. Looking at the force felt by the test ion in Fig. 7.2 B, it is clear that the inclusion of the DSE term has lead to a dramatic improvement in the PB results. However, in the intermediate radii channels, the discrepancy in the force from that found in BD is still large ($\sim 50\%$), and is likely to be important in quantitative studies of ion channels. The modified PB equation overcompensates for the problems experienced by the standard PB equation, and now underestimates shielding rather than overestimating it.

Biological ion channels contain fixed charges in the channel walls that help one type of ion to permeate through the channel. For completeness, we also examine the more realistic case of a $r = 4$ Å channel with negative monopoles in the walls making it cation selective. Here, we place a ring of eight negative monopoles each with charge $-0.09e$ spread evenly near each channel mouth at $z = -12.5$ and $z = 12.5$ Å and set 1 Å inside the boundary as done previously. The inclusion of negatively charged monopoles at the channel ends, cancels the dielectric barriers seen by cations, whilst doubling their height for anions. In Fig. 7.3 A we plot the potential profile through the channel as found from the PB equation (dashed line), modified PB equation (solid line), BD simulations (dash-dot line) and with no electrolyte (ie. from Poisson's equation), with no test ion present. The potential found from the modified PB equation drops below that found with the standard PB equation and is closer to the BD result, showing a significant improvement compared to the standard PB results.

The improvement in the concentration profiles is also quite good as shown in Fig. 7.3 B. Here we plot the cation concentration in the channel, corresponding to the potential profiles shown in Fig. 7.3 A. The concentration found from the modified PB equation is significantly lower than that found from the standard PB equation, and only a little lower than that of the BD simulations. This slight reduction in concentration compared to BD is presumably caused by the self energy repulsion.

It is worthwhile to stress that, unlike the PB equations, the modified PB equations are not self consistent because the DSE term is included in Eq. 7.4 in an ad

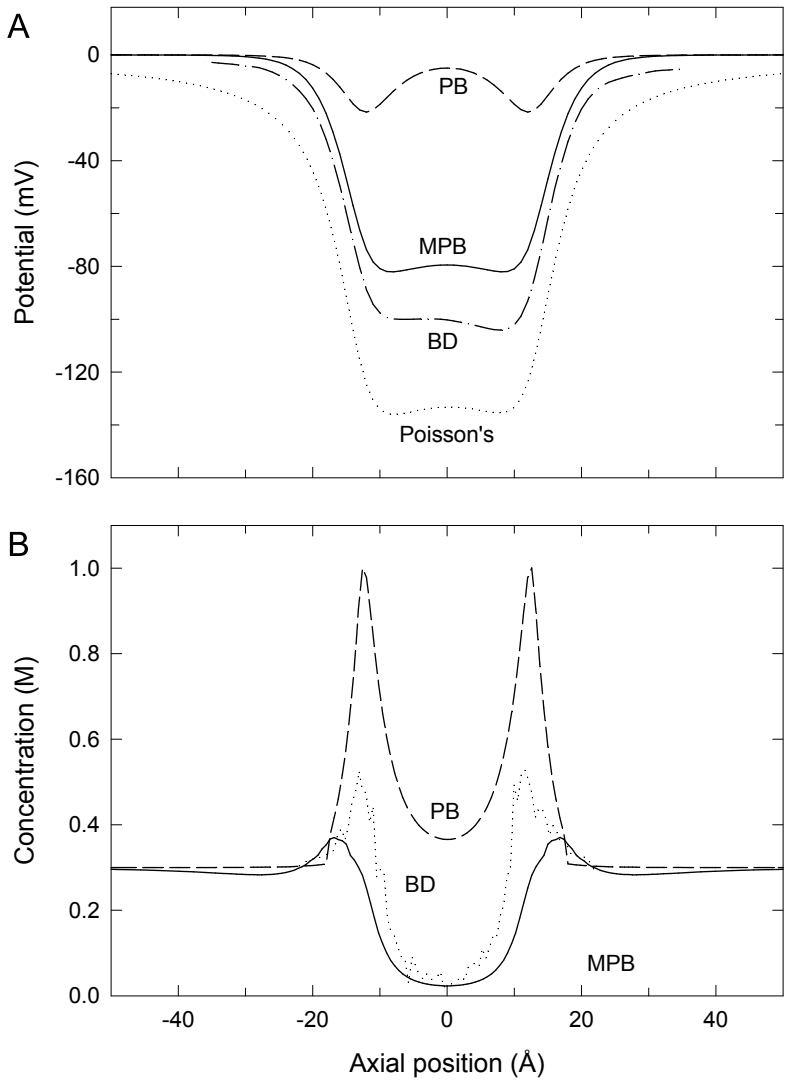

Figure 7.3: (A) Potential profiles found in a 4 Å radius cylindrical channel with charges in the protein and no fixed test ion found using the standard PB equation (dashed line), modified PB equation (solid line), BD (dash-dot line) with 300 mM NaCl solution in the baths. The potential found from Poisson's equation with no electrolyte is shown by the dotted line. (B) Concentration profiles corresponding to the results in (A). The BD results are indicated by the dotted line.

hoc manner. A consequence of this can be seen in a comparison of Figs. 7.3 A and B. In the potential plot, the modified PB results lie closer to the standard PB results than those found from BD simulations. However, in the concentration plot the reverse is true. The reason for this is that the potential plotted is ϕ found from Eq. 7.4, whereas the concentration is determined from $\phi + \phi_R/2$ as indicated in Eq. 7.3.

We next turn our attention to the slightly more complex case of the gramicidin A channel. A model of the channel is constructed from recent NMR data [104] including the partial charges of all the protein atoms. This model is described in detail in chapter 9, and for the point of this study may be considered as a very narrow, roughly cylindrical channel. The shape of the channel is shown in the inset of Fig. 7.4. In Fig. 7.4 A and B, we again show the potential profile and concentration of cations found in this channel without a test ion using each of the methods described. Without any electrolyte the potential has a deep well created by the distribution of partial charges in the protein, which act to attract cations into the channel. Using the standard PB equation the potential is flattened out as a large concentration of cations enters the channel negating the effect of the distribution of partial charges. Using the modified PB equation, however, we find that this potential profile remains largely unchanged from the solution of Poisson's equation, as only a small concentration of cations finds its way into the channel. The potential found from the modified PB equation is remarkably similar to that found from the BD simulations, the two agree to within a few percent. Comparing the concentration profiles in Fig. 7.4 B, we find that in both cases the concentration of ions in the channel is quite low. In this very narrow channel the inclusion of the DSE term in the PB equation yields a dramatic improvement. This may not be surprising as the channel is very narrow and, in fact, is found to be occupied only 10% of the time. This means that the dielectric repulsion from the channel boundary is a dominant effect, and can be approximated quite well by the repulsion felt by a single ion.

We finally test the modified PB equation in a less favourable, and more complicated case: the KcsA potassium channel. Not only does this channel have a more complicated geometry, it is also always occupied by multiple ions. This means that the calculation of the DSE term using a single ion may be less accurate, ion-ion interactions that are difficult to describe in a continuum approach may become important, and errors due to the spurious self energy are more likely to be significant. An open state channel shape is made from the KcsA crystal structure as described previously [41] and is shown at the top of Fig. 7.5. The narrow 'selectivity filter' of

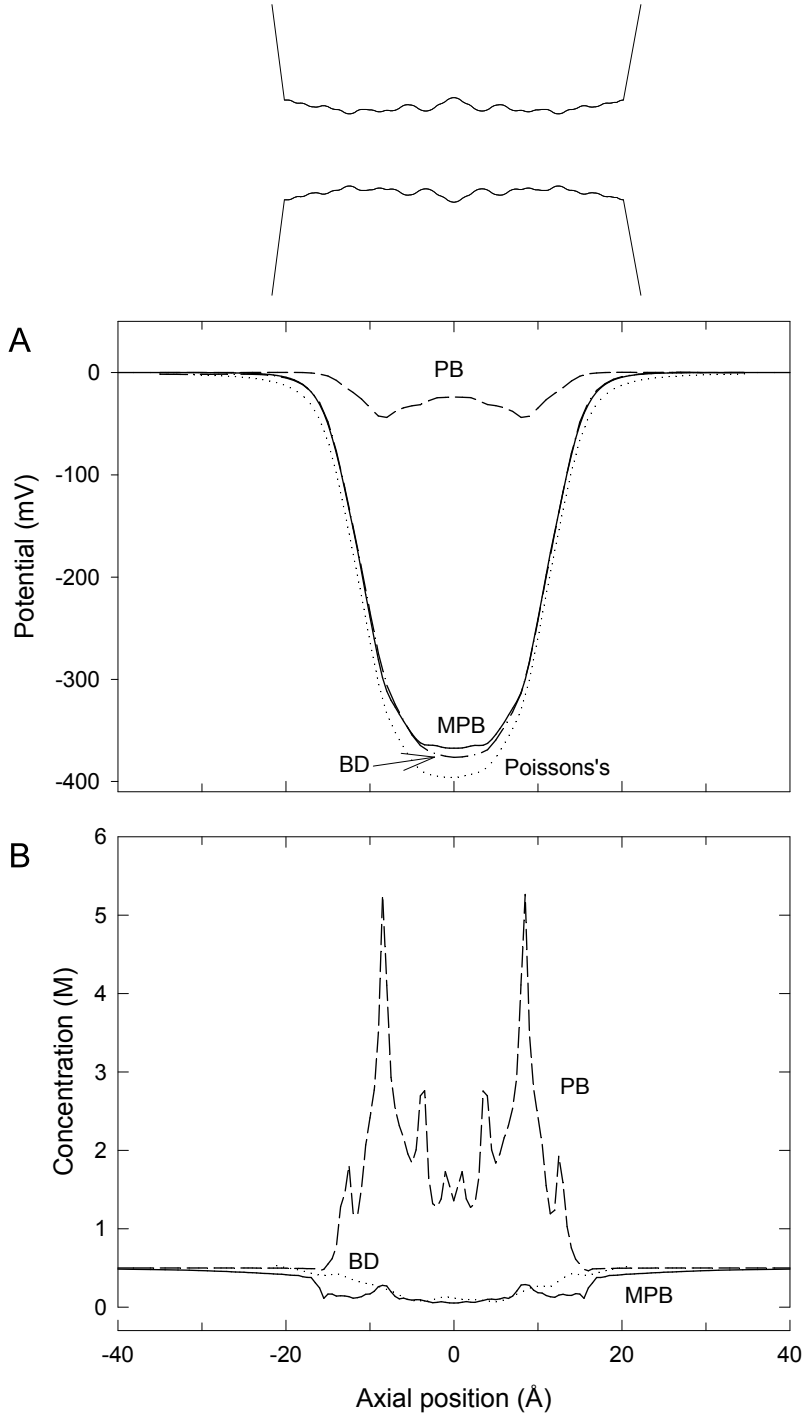

Figure 7.4: (A) Potential and (B) concentration profiles as in Fig. 4 except for the gramicidin A channel. 500 mM KCl is used in both cases. The shape of the channel is indicated in the inset.

the channel is surrounded by carbonyl oxygen atoms whose partial negative charges create a deep potential well as seen from the solution of Poisson's equation indicated by the dotted line in Fig. 7.5 A. These negative charges attract potassium ions into the channel, whose presence decreases the size of this well. Using the standard PB equation, enough cations enter the channel to roughly cancel out the energy well. In BD simulations, at least 2 ions are always present in the narrow section of the channel. Because the volume of this section of the channel is very small, this leads to a very large concentration there as seen in Fig. 7.5 B. The two peaks in the concentration plot show clearly where the ions are most likely to be found. These ions again act to cancel the potential well in the channel. The inclusion of the DSE term in the PB equations however, leads to a worse agreement with the BD results than is found with the standard PB equation. Less cation concentration builds up in the channel, and consequently the potential well remains deeper in the modified PB equation. Indeed, the difference in potential found using BD and the modified PB equation is very large at over 700 mV.

Examining the concentration profiles in Fig. 7.5 B, it is interesting to note that even the standard PB equation predicts a much lower concentration than is found using BD. Indeed, whereas BD predicts a total of 4 ions in the channel, the PB equation predicts only 2.5. (Note that the channel is wider at the left hand side, and so even though the peak in concentration there looks small it represents at least 1 ion). The reason for this may be erroneous self repulsion in the PB solution. In the KcsA channel, multiple ions are present in the narrow selectivity filter, and the self energy of this charge will act to reduce the concentration there in both the standard and modified PB equations. The inclusion of the DSE term lowers the number of ions found in the channel using the modified PB equation to just 1.5.

7.4.3 Modified PNP equations

Following the tests carried out in chapter 6 we calculated the current passing through cylindrical channels of varying radii using the modified PNP equations and compared them to currents found from BD simulations. In Fig. 7.6 we plot the channel conductance for cylindrical channels of varying radius. Here the conductance has been normalised by the cross sectional area of the channel to factor out the trivial increase in current with increasing area. All plots are carried out using symmetrical 300 mM NaCl solution and an applied potential of 105 mV between the reservoir ends. The PNP results from chapter 6 are indicated by the dashed lines and show the slight downward trend created by access resistance effects. The currents in narrow channels found from BD (data points fitted by dotted lines) are

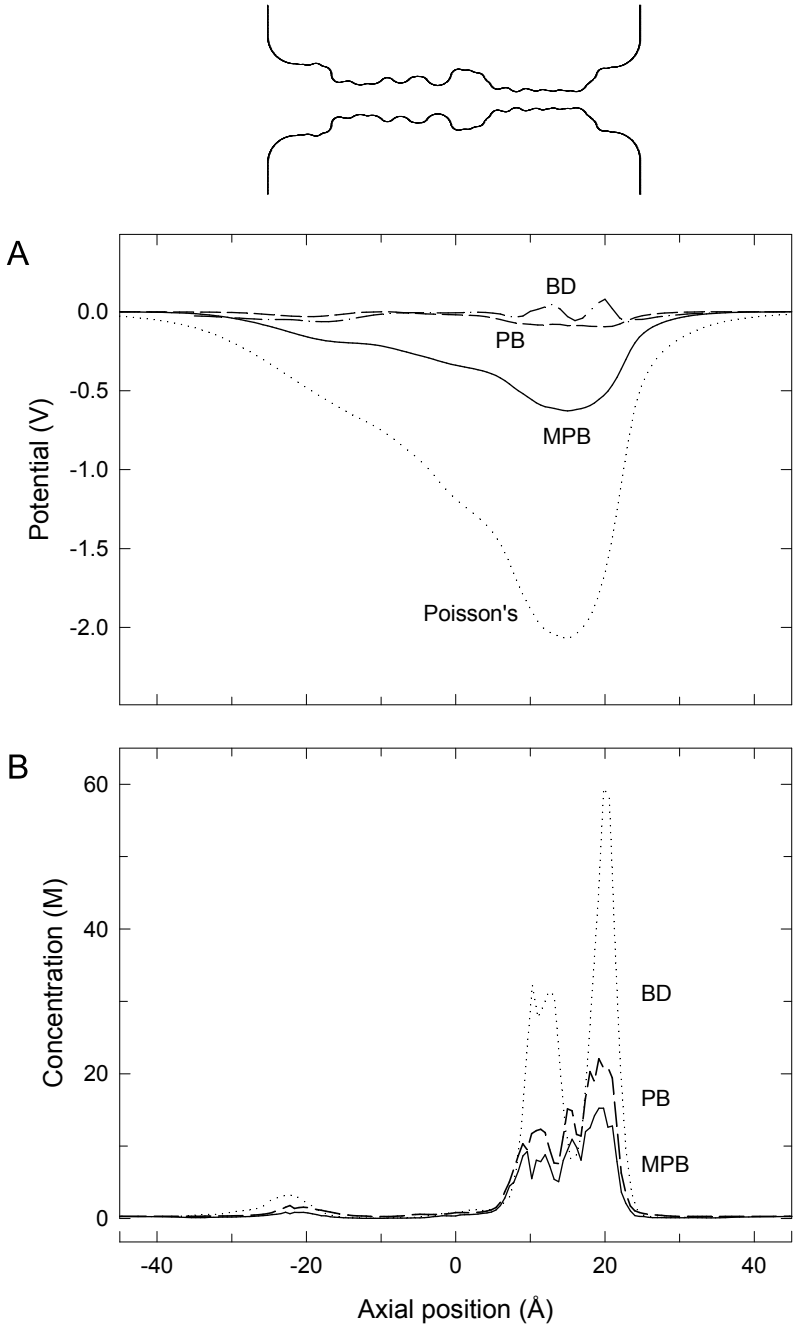

Figure 7.5: (A) Potential and (B) concentration profiles as in Fig. 4 except in the KcsA potassium channel. 300 mM KCl is used in both cases. The shape of the channel is indicated in the inset.

well below the PNP values due to dielectric repulsion slowing the progress of ions through the channel. When the DSE term is included explicitly in the modified PNP equations the current is also suppressed in the narrow channels. Indeed, the conductance is essentially zero in the 3 Å radius channel in agreement with the BD results. The normalised conductance also climbs as the channel radius is increased in a similar manner to that seen in BD. There are some differences in intermediate radii channels, but the differences are remarkably small ($\sim 35\%$). It appears that the inclusion of an explicit self energy term in the PNP equations can reproduce the BD results reasonably well in these bare cylindrical channels.

Next we consider the simple cation selective channel, discussed previously when looking at the modified PB equation. It has been seen that in PNP these charges spoil the coexistence of anions and cations and reduce the perfect shielding seen in PNP studies of bare channels. The modified PNP equations, however, do not perform as well in this case as in the bare channels as demonstrated by plotting the normalised conductance in channels of varying radii in Fig. 7.7. The anion currents found using the modified PNP equations agree closely with the BD results at all radii. However, the cation agreement is not as good. Both predict very small currents in the narrowest channel, but in BD the current climbs rapidly to more than double that found with the modified PNP equations in the intermediate radii channels. The results from both techniques converge again at large radii.

The reason for the discrepancy between the modified PNP and BD results is demonstrated in Fig. 7.8, where we plot the cation (A) and anion (B) concentrations in the 4 Å radius channel with fixed charges. The inclusion of the DSE term stops anions entering the channel, preventing the large concentration found using the standard PB equation and yielding a good agreement with BD. But the cation concentration is reduced too much by this self energy term, and the concentrations found in the channel peak at a lower value than is found in BD near the fixed charges. Obviously, the lower cation concentration results in a smaller current in the modified PNP equations.

The inclusion of a DSE term leads to a dramatic improvement in bare channels, in which the standard PNP equations once predicted perfect shielding of induced surface charges. But, in the charged channels the modification appears to over compensate for the electrolyte shielding. The results are, however, more realistic and demonstrate a more accurate qualitative behaviour. But, the magnitude of the currents predicted can be less than half what is found in the same situations using BD.

So far we have considered only single ion cylindrical channels for examining

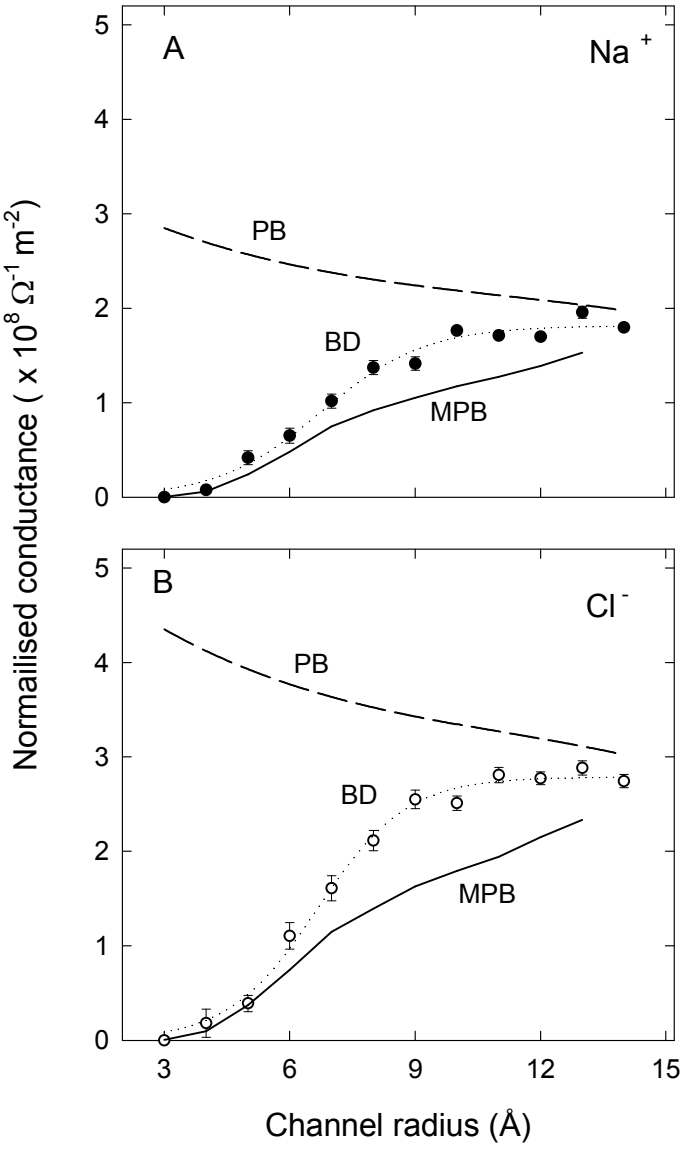

Figure 7.6: Conductance of Na^+ (A) and Cl^- (B) ions in bare cylindrical channels of varying radii normalised by the cross sectional area. The results of the modified PNP equations (MPNP - solid lines), standard PNP (dashed lines) and BD simulations (data points fitted by dotted lines) are shown. The ions are driven across the channel with an applied field of 105 mV between the reservoir ends and a 300 mM NaCl solution is maintained in the reservoirs.

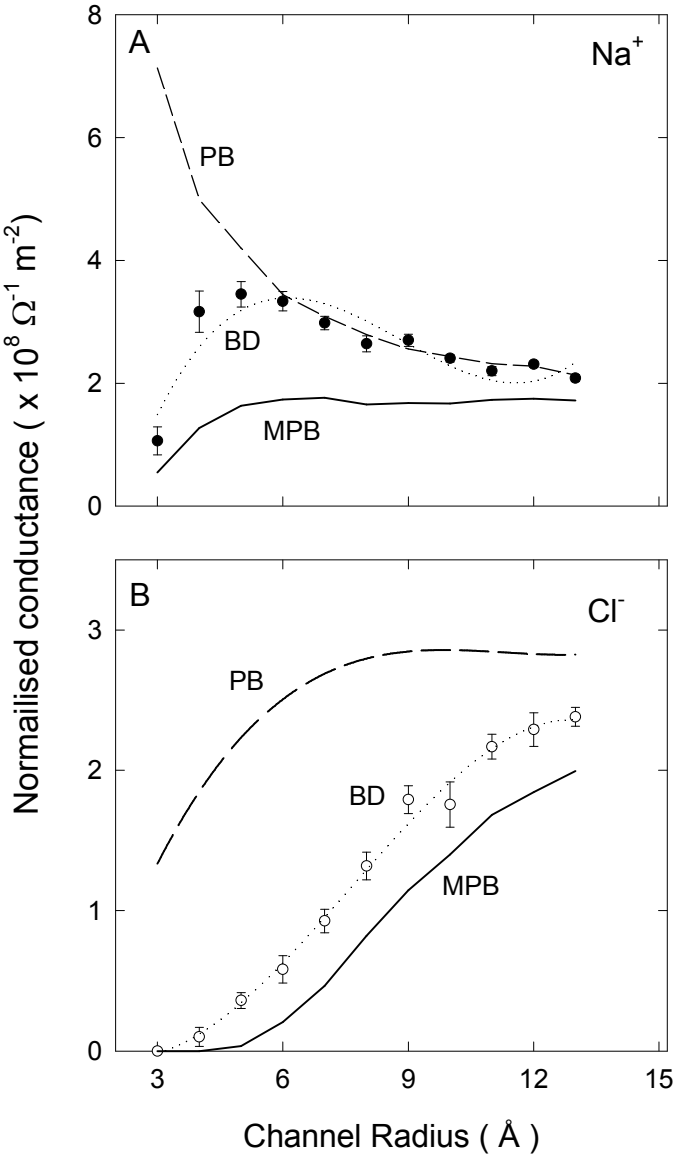

Figure 7.7: Normalised Conductance in cylindrical channels with fixed charges in the channel walls. Otherwise as in Fig. 7.

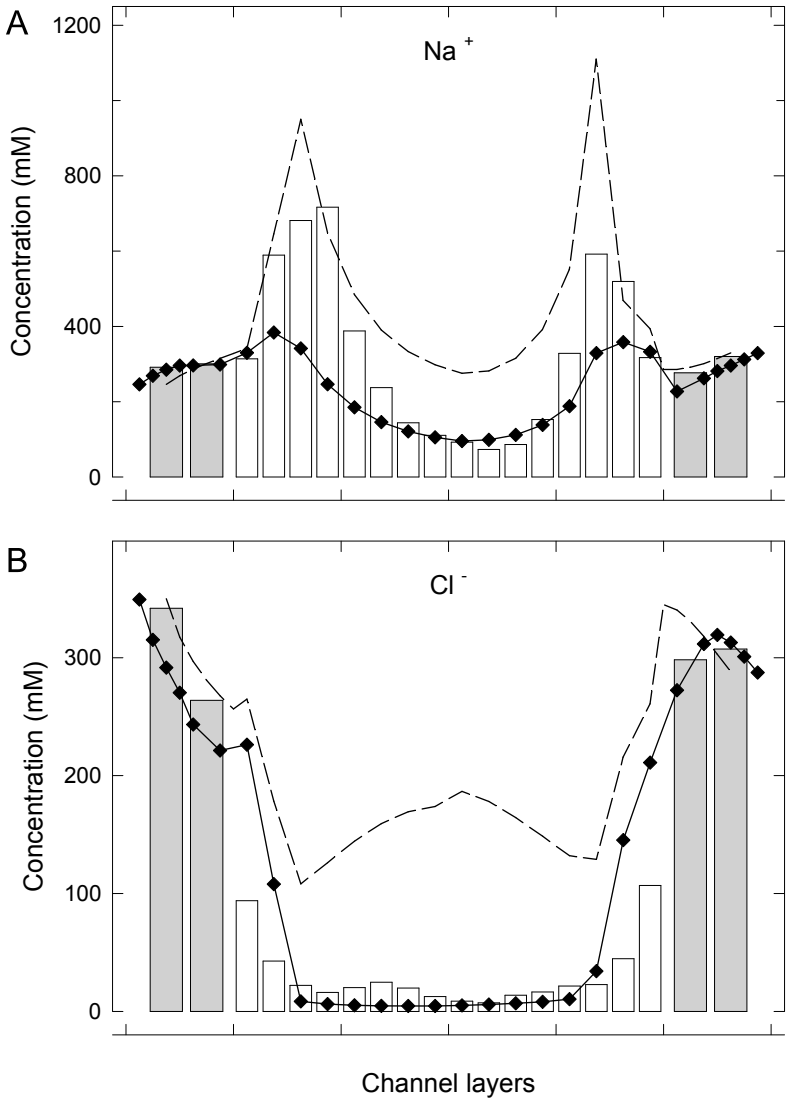

Figure 7.8: Concentration profiles for (A) Na^+ and (B) Cl^- ion in a 4 Å radius cylindrical channel with fixed charges as found from the modified PNP equations (diamonds and solid line), standard PNP (dashed line) and BD simulations (bars).

the modified PNP equations. We next examine a multi ion channel, in which the continuum approximation may have further problems in describing the interactions between ions. We examine the currents found passing through a model L-type calcium channel discussed in detail in chapter 8. The shape of the channel is shown in the inset at the top of Fig. 7.9, and includes a narrow selectivity filter surrounded by four negatively charged glutamate residues. These residues strongly attract cations, holding one calcium ion, or two sodium ions permanently in the channel. Conduction requires the entry of another ion making it a two calcium ion, or three sodium ion process. Full details of the model are described in the following chapter.

The standard PNP equations give very poor results in this channel. The magnitude of the calcium currents predicted are too large by an order of magnitude. Indeed the calcium currents are greater than the sodium currents, the reverse of what is found using BD and in experiment. The results found using the modified PNP equation are more sensible. Notably, the calcium current is reduced to a more appropriate value, only around 35% greater than expected. The current shows an initial non-linearity at low concentrations, suggesting that saturation has been obtained. But after this it appears to increase fairly linearly. The sodium current is only reduced a small amount when the DSE term is added. The calcium current is reduced much more due to the larger DSE experienced by divalent ions. But, whereas the calcium current found from modified PNP is larger than the corresponding value from BD, the sodium current is only about half that found in BD.

The modified PNP equations perform remarkably well in this multi ion channel, but the errors in currents are still quite large. In our BD studies of the calcium channel, we have been able to simulate mixtures of calcium and sodium ions to better understand channel selectivity. The divalent calcium ions are more strongly bound to the glutamate charges than a sodium ion. Unfortunately, a down side of the continuum approach is that this feature cannot be reproduced as it requires the localization of divalent and monovalent charges in discrete positions. Thus, the continuum approach is more limited in the types of questions it can be used to answer.

7.5 Conclusions

The continuum approach to studying ion channels is considerably simpler and less time consuming than carrying out simulations, and it would be desirable, if at all possible, to salvage it. In a simple attempt to do this we modified the PB

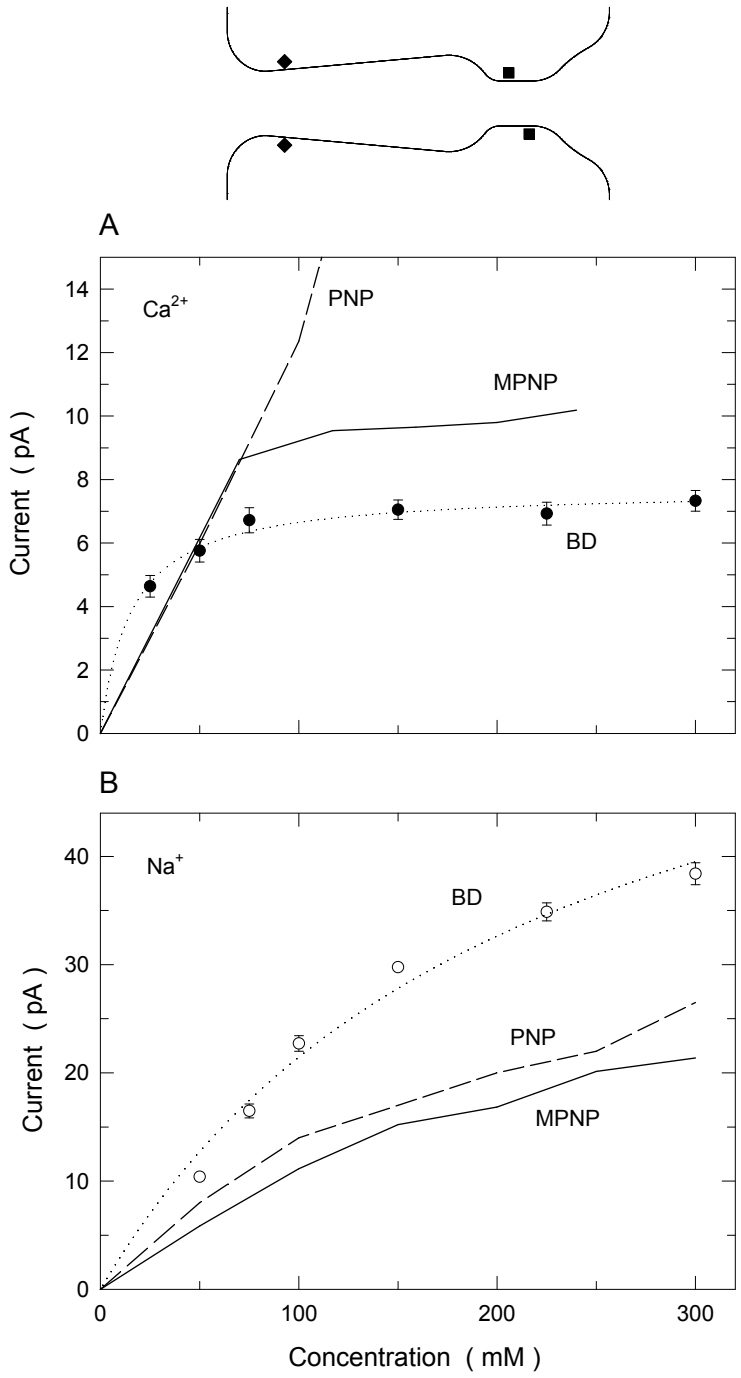

Figure 7.9: Current-concentration relationships for (A) 300 mM $CaCl_2$ and (B) 300 mM NaCl in the L-type calcium channel. The currents found using the standard PNP equations (dashed lines), modified PNP equations (solid lines) and BD simulations (data points fitted by dotted line) are shown. The shape of the channel and the locations of 2 of the 4 glutamate residues is shown in the inset (squares).

and PNP theories to include an explicit dielectric self energy term when calculating electrolyte concentrations, as the lack of such self energy was shown previously to create problems with these continuum models. Including this DSE term leads to a significant improvement in the performance of the PB and PNP equations. However, although fairly accurate in some situations the modified continuum methods are not quantitatively reliable in all cases.

The modified PB equation accurately mimics the BD results in the narrowest channels studied. This is not surprising, however, as it can be seen that the effect of including the DSE term in the PB equation is to almost eradicate ion concentrations in the channel, reducing us back to Poisson's equation. In such narrow channels we had already seen that counter ions were unable to enter and so Poisson's equation, which does not include any mobile electrolyte, gave accurate results. Agreement between the modified PB theory and BD simulations is retained in wide channels with $r > 2$ Debye lengths. However, at intermediate channel radii the agreement was not as good, and errors of up to 50% were common. The validity of the modified PNP theory mimicked that of the modified PB equation. Accurate results were obtained in very narrow and very wide single ion channels, but errors were present at intermediate radii. The inclusion of a DSE term yields a general qualitative improvement, but where the standard continuum equations overestimate electrolyte shielding, in many cases the modified continuum equations underestimates it.

Unfortunately the performance of the modified continuum equations is much worse in the more realistic multi ion channel models we examined. When the modified PB equation was used to calculate concentration in the KcsA potassium channel the results were found to be incorrect by an order of magnitude. The qualitative shape, and magnitude of the potential found using the modified PB theory are both incorrect. Using the modified PNP equation in a highly charged calcium channel model led to similarly poor results. The predicted calcium currents were too high and the sodium currents too low. In both the KcsA and calcium channel models, the channel is highly charged and there are usually multiple ions resident in the channel. This means that interactions between the discrete ions may be important in determining the ion dynamics, a property that is not well described in the continuum picture where the ions are not localised, but rather spread across many grid points. Also, the magnitude of the dielectric repulsion acting on an ion will change when a second ion enters, thus the DSE correction term may be a less accurate representation of the forces felt by the ions in the multi-ion case. In addition, we showed that the continuum theories also introduce erroneous energy due to self repulsion which may be important in these multi-ion channels. The problems highlighted in

these and earlier studies also indicate that the validity of using the PB equation for calculating pK_A values in ion channels also needs to be assessed.

More sophisticated statistical mechanical descriptions of electrolytes are being developed, but at this stage, as far as we are aware, none of these theories can correctly take into account the self energy terms in ion channels. The prime applications of density functional theory in inhomogeneous systems are concerned with electrolytes near a highly charged plane [80] or hard-sphere fluids in a cavity [70], neither of which is directly relevant to ion channels. In the former, the image forces are simply ignored (considering the high charge on the planes, this is presumably a good approximation), while in the latter there are no image forces. The only study that comes close to an ion channel like situation is that of Lehamani et al. [118], who discuss transport of ions in the pores of Nafion membranes. The authors employ the mean spherical approximation (MSA) to improve on the PB results but ignore the ion-boundary interactions. Given that these are large pores with radius 20 Å, our tests suggest that PB/PNP theories should work quite well, and their neglect of ion-boundary interaction is justified. Interestingly, Lehamani et al. [118] find that the ion-size effects taken into account via MSA, play a negligible role at physiological concentrations, confirming that it is the neglect of the ion-channel interaction that is responsible for the failure of PB/PNP theories, and not the neglect of ion-size or correlation effects.

As the continuum theories are designed for use in situations containing a large number of ions, they need to be constantly tested if they are to be applied to ion channels in which only a few ions are present. Here we used a simple approach to try to improve the PNP and PB theories for use in ion channels. Although it led to a major improvement, it does not appear to give reliable results in all situations. This is likely to be a common problem with attempts to fix a statistical theory for use in cases with only a few ions—errors are going to be difficult to overcome in all situations. We are thus left to use simulation methods unless, or until, a more sophisticated continuum description can be developed that is applicable in the ion channel environment. Brownian and molecular dynamics are now well developed for use in ion channels. Given that these simulations can be used to predict macroscopic phenomena such as channel currents that used to be the domain of the continuum theories, as well as being able to explore situations that continuum approaches cannot (such as ionic mixtures in BD or microscopic properties in MD), simulation methods provide an attractive alternative to the continuum theories. In the next chapter I apply BD simulations to study a real biological ion channel: the L-type calcium channel.

Chapter 8

A Model of Calcium Channels

8.1 Abstract

The mechanisms underlying ion transport and selectivity in calcium channels are examined using electrostatic calculations and Brownian dynamics simulations. We model the channel as a rigid structure with fixed charges in the walls, representing glutamate residues thought to be responsible for ion selectivity. Potential energy profiles obtained from multi-ion electrostatic calculations provide insights into ion permeation and many other observed features of L-type calcium channels. These qualitative explanations are confirmed by the results of Brownian dynamics simulations, which closely reproduce several experimental observations. These include the current-voltage curves, concentration-conductance relationship, block of monovalent currents by divalent ions, the anomalous mole fraction effect between sodium and calcium ions, attenuation of calcium current by external sodium ions, and the effects of mutating glutamate residues in the amino acid sequence.

8.2 Introduction

A central problem in studies of ion permeation through biological membrane channels is to understand how channels can be both highly selective and yet still pass millions of ions per second. Calcium channels exemplify this problem; they are ubiquitous in excitable cells and extremely selective, passing calcium over sodium at a ratio of 1000:1 [83]; yet, the picoampere currents they support require more than 10^6 calcium ions to pass every second [203]. Unlike potassium channels, which have a narrow selectivity filter and only allow ions of a particular size to pass [3, 6, 58], calcium channels select between ions of almost identical radius, the Pauling radii of sodium and calcium ions being 0.95 Å and 0.99 Å respectively. Moreover, calcium channels are known to admit much larger ions, the largest observed is tetramethy-

lammonium with a radius of about 2.8 Å [138]. Thus, a different mechanism of selectivity from that in the potassium channel must be at play, one that relies on the different charges on the ions. Monovalent ions can permeate through the channel in the absence of calcium at much higher levels of conductance than can any divalent ions [8, 83, 109, 112], but are blocked when the calcium concentration reaches only 1 μM [8, 109]. That this block is dependent on membrane voltage [68, 116, 129] and the direction of ion movement [111, 112] has been taken as evidence for a multi-ion binding (or selectivity and blocking) site residing in the pore. Four glutamate residues in close proximity are believed to line the pore and to be a component of the selectivity filter of the channel, as point mutations of these change the characteristics of selectivity [18, 63, 105, 153, 216]. The glutamate residues are expected to be highly charged and to strongly bind the calcium ions in the channel leading them to block the passage of sodium ions.

A number of theoretical models have been developed to try to explain permeation and selectivity in the calcium channel. Single-file rate theory models in which ions sequentially hop from one site to another have been used most extensively [203]. Because of the difficulty in obtaining both high selectivity and throughput with a single binding site [22], these models originally contained two sites in which repulsion between ions in neighbouring sites increases transit rates [8, 84]. As the two-site models could not accommodate the mutation data, a new rate model was recently proposed, where a single-site is flanked by lower affinity sites to aid the exit of ions from the central site [51]. Other mechanisms involving single sites have also been developed, such as competition between calcium ions for the binding charges [14, 216]. These rate theory models have provided many useful insights as to how calcium channels may achieve their selectivity with a high throughput. However, as previously noted, they cannot be used to relate the structural parameters of the channel to functional elements [137]. For example, in these theories no physical distances or shapes are used and there is no direct connection between energy minima used in the theory and physical sites in the pore.

A first attempt to relate the observed properties of the calcium channel to its structure was made using PNP theory [151]. The shortcomings of the PNP theory as applied to a model calcium channel were pointed out by McCleskey [137] and Miller [143]. These criticisms have been given a solid foundation in the comparisons of PNP theory with BD simulations (chapter 6), which show that the mean field approximation used in the PNP theory completely breaks down in narrow channels such as the calcium channel. The good agreement between the PNP results and the channel data, often put forward as a proof of its validity, is seen in hindsight as

a fortuitous outcome of mixing incorrect physics with unrealistic parameter values. For example, the calcium diffusion coefficient employed in the PNP fits (10^{-5} times the bulk value) is 10,000 times smaller than the microscopic estimates obtained from molecular dynamics simulations, which suggest at most a ten-fold reduction in calcium diffusion compared to the bulk value [7]. Agreement with experiment also relies on the inclusion of *ad hoc* chemical potentials whose electrostatic origin is not clear.

The failure of the mean field approximation in narrow channels indicates that any theory that aspires to relate channel structure to its function must treat ions explicitly. Because all the atoms in the system are treated explicitly in molecular dynamics, it would provide the ultimate approach to the structure-function problem. Unfortunately, as noted in chapter 2, the computation of most channel properties (e.g. conductance) using molecular dynamics is still beyond the capabilities of current computers. The only remaining alternative is BD simulations. Multi-ion interactions were found from BD to be instrumental in explaining the high throughput of potassium channels [40], and are expected to play a similarly significant role in understanding the high conductance of calcium channels.

The aim of this chapter is to construct a simple model of the structure of calcium channels and examine its various properties using electrostatic calculations and BD simulations. The parameters in the model are determined from either molecular dynamics or a variational principle that optimizes the quantity in question. Thus there are no free parameters that are fitted to data, nor *ad hoc* chemical potentials that are arbitrarily chosen. The model relates structural features to functional roles and, as will be seen, successfully predicts many of the observed properties of the calcium channel using only the principles of electrodynamics.

8.3 Channel model

The crystal structure of calcium channels is not known at present. Nevertheless, through a judicious use of important clues from various experiments one can develop a simplified model of the calcium channel that should be sufficiently accurate for the purposes of electrostatic calculations and BD simulations. The cross section of the channel model employed in this work is shown in Fig. 8.1. A three-dimensional shape of the channel is generated by rotating the curves in Fig. 8.1 about the axis of symmetry (z axis) by 180° (see figure 3.1 for a diagram of the 3D BD system). The channel extends from $z = -25$ Å to 25 Å, long enough to span a typical membrane. In constructing this model, we have followed the basic topology

of the potassium channel; that is, a narrow selectivity filter, connected to a wide chamber that tapers off as it approaches to the intracellular side. One significant difference from the potassium channel is the existence of a relatively short vestibule on the extracellular side with a fairly wide opening. This is suggested by molecular modeling studies [56, 57, 76, 184] of the known amino acid sequences of the calcium channel [60, 142, 197]. A larger external mouth compared to the internal one is required to explain the asymmetry between the inner and outer saturation currents [110].

The radius of the selectivity filter is determined from the size of the largest permeable ion (tetramethylammonium) as 2.8 Å [138]. Interpretation of the mutation data in reaction rate theories suggests that the four glutamate residues (EEEE locus) in the selectivity filter must be in close proximity in order to form a single binding site [18, 63, 216]. This is further supported by the voltage dependence of calcium block, which suggests that calcium binds at the same location whether entering the channel from the inside or outside [112]. Therefore we have chosen the length of the selectivity filter to be 5 Å, which is much shorter than in the potassium channel (12 Å). The position of the selectivity filter in the channel is not known, though it is suspected to be towards the external side of the channel as it is more accessible to ions from the outside of the channel than from the inside [112]. Our trials with various positions of the selectivity filter in the channel also confirm this conjecture: when the filter position is further removed from the external mouth, it is not possible to reproduce most of the known properties of calcium channels. The wide chamber near the middle plays a similar stabilizing role to that in potassium channels, providing a water filled cavity for ions exiting from the selectivity filter [178].

The highly charged glutamate residues forming the selectivity filter play an essential role in determining the channel conductivity and selectivity, and therefore, choosing their positions and charges correctly is of critical importance. The four glutamate residues are modeled by 4 fixed charges located in close proximity, but spread asymmetrically in a spiral pattern 1 Å inside the channel wall. The placement of charges in an asymmetric pattern rather than in a ring helps to account for the mutagenesis studies which show that the removal of each charge has a different effect on channel conductance. The four charges are located at $z = 10.50$, 11.83, 13.17 and 14.5 Å and each rotated by 90° from the last (only two are shown in Fig. 8.1). Finally to overcome the large image forces at the intracellular end of the channel we have placed 4 mouth dipoles, 5 Å in length, with their inner ends 1 Å inside the pore wall at $z = -17.5$ Å. The charges on glutamates and mouth dipoles are

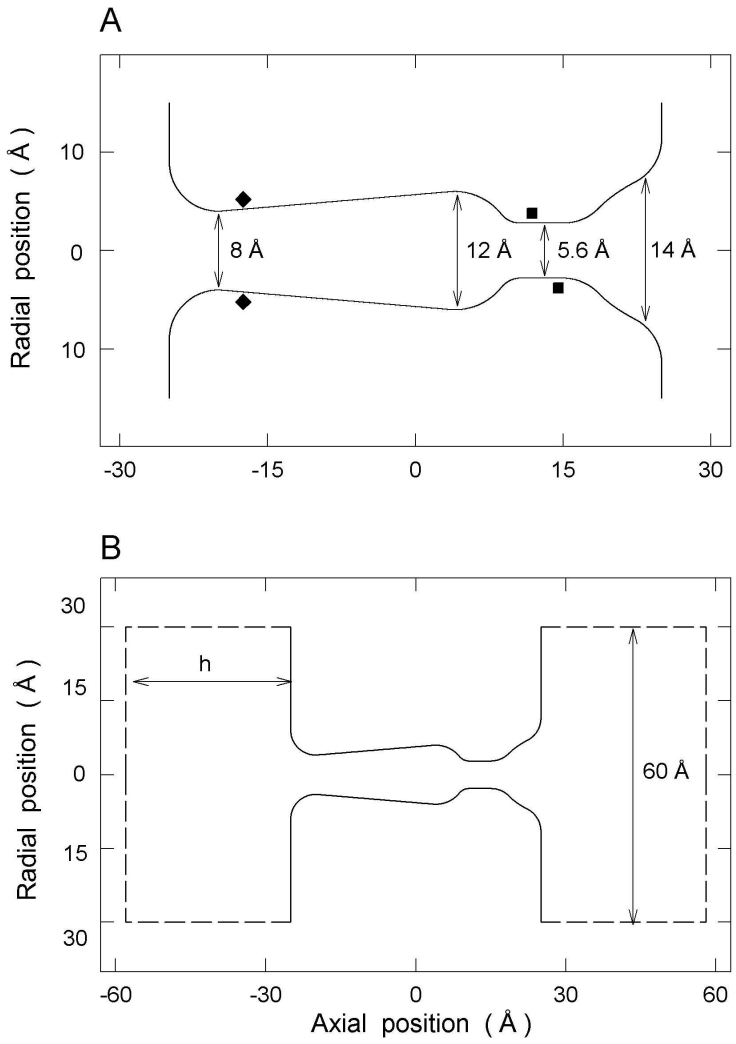

Figure 8.1: Model calcium channel. The three dimensional channel model is generated by rotating the curves about the central axis by 180°. The positions of two of the four glutamate groups are shown by the squares, and the inner end of 2 of the 4 mouth dipoles by the diamonds. The other two groups lie into and out of the page. The intracellular end of the channel is on the left and the extracelluar side on the right.

optimized to obtain the maximum ionic currents as discussed below.

The dielectric constant of the channel protein is taken uniformly as $\epsilon = 2$. The dielectric constant of water inside the channel environment is not well known as it is difficult to determine its value directly from experiments. Recent molecular

dynamics simulations of water inside narrow channels have suggested that it may be considerably lower than its bulk value [183]. On the other hand, BD simulations of ion permeation in potassium channels indicates that current ceases to flow if ϵ in the channel is lower than 40 [40]. In view of these uncertainties, we have adapted the minimal value of $\epsilon = 60$ that allows large conductance through the model channel. Further justification for this choice will be given later.

8.4 Channel parameters

The three channel parameters that are not known experimentally and need to be determined by other methods, are the magnitude of the charges on glutamate residues and mouth dipoles, the dielectric constant of water and the diffusion coefficient of ions in the channel. A straightforward fit of these parameters to the available data is not very satisfactory since one is likely to find many possible sets that eventually have to be distinguished on their physical merits. Therefore, we prefer using guiding principles such as optimization or a more explicit theory (e.g. molecular dynamics) in estimating these quantities.

The determination of the molecular structure of the proteins may help to find the magnitude of the charge of residues in the channel. In the mean time, we expect that the charges in the channel would have evolved to maximize the transit rate of calcium ions. In Fig. 8.2 A we show the dependence of the calcium current on glutamate charges. The BD simulation results in this figure are obtained using symmetric 150 mM $CaCl_2$ or NaCl solutions with an applied field of -2×10^7 V/m (corresponding to a potential of approximately -200 mV producing an inward current). As the charge on the glutamate groups is systematically increased (while the charge on the mouth dipoles is held fixed), the calcium current found from BD simulations sharply increases from zero to a narrow peak at a charge of 1.3×10^{-19} C before dropping steeply again at greater charge strengths. In fact, no calcium current is measured during our simulations if the charges are less than 1.0×10^{-19} C or greater than 1.6×10^{-19} C. The sodium current also peaks at the same value, but conducts over a greater range of glutamate charges as is shown by the open circles. It is noteworthy that the peak calcium current occurs for such a narrow range of glutamate charges. A fully charged glutamate group has a charge of e (1.6×10^{-19} C). However, in an electrolyte solution the charges are likely to become protonated, leading to a lower effective charge on the residues. [35, 36, 145, 167]. As the amount of protonation is not known, we use the optimum value of the glutamate strengths, 1.3×10^{-19} C, for the remainder of this study.

In a similar investigation, the strength of the mouth dipoles is varied whilst the glutamate charges are held fixed at their optimal value. As shown in Fig. 8.2 B, the outward calcium current is critically dependent on the charge strengths as in the case of the glutamate residues. The current is maximum when a charge of 0.5×10^{-19} C is placed on each of the four dipoles. A further increase in the dipole strength reduces the current rapidly (filled circles, Fig. 8.2 B). In contrast, the inward current exhibits a different dependence on the mouth dipole strength (diamonds, Fig. 8.2 B). The current increases steeply with the dipole strength and then remains constant with a further increase. In all subsequent simulations, we use a charge of 0.6×10^{-19} C, which falls between the optimum values of inward and outward currents and gives close to the maximum value for each.

Molecular dynamics studies of water in spherical cavities [217] and narrow pores [183] suggest that the dielectric constant ϵ is substantially reduced from the bulk value. The effect of changing the dielectric constant on the results of BD simulations in narrow pores (the potassium channel) has been examined elsewhere [40]. This study also found that the optimum charge strengths are insensitive to the value of the dielectric constant. The dielectric constant of water in the channel is chosen as $\epsilon = 60$. While this value is rather close to the bulk value, the channel ceases to conduct calcium ions if lower values of ϵ are employed. For example, when the dielectric constant ϵ inside the channel is assumed to be 50 and a potential difference of -200 mV is applied, the current across the channel is only 2.4 ± 0.6 pA, compared to 7.1 ± 0.6 pA with $\epsilon = 60$. With a further reduction of ϵ to 40, the current is reduced 0.4 ± 0.2 pA (during a simulation period of 3 μs). Virtually no conduction takes place with an applied potential of -100 mV and ϵ of 50. In a simulation period of 5.5 μs, only one calcium ion crosses the channel, resulting in a current of 0.06 pA.

The diffusion coefficient of ions inside the channel can be estimated from molecular dynamics simulations. There are a number of such studies which indicate that the diffusion coefficient is significantly reduced from its bulk value inside narrow channels [5–7, 131, 175, 190, 191]. Allen et al. [7] have carried out a systematic study of diffusion coefficients of K^+, Na^+, Ca^{2+} and Cl^- ions in cylindrical channels with radius varying from 3 to 7 Å. Here we use their estimates as a guide and use 0.5 times the bulk diffusion coefficient for calcium ions in the channel chamber ($-25 < z < 7.5$ Å) and 0.1 times the bulk in the selectivity filter ($7.5 < z < 20$ Å). Corresponding values of 0.5 and 0.4 times the bulk value are used for sodium. The bulk values are employed in the reservoirs for all ions.

In Fig. 8.3, we illustrate the sensitivity of the channel conductance on the choice

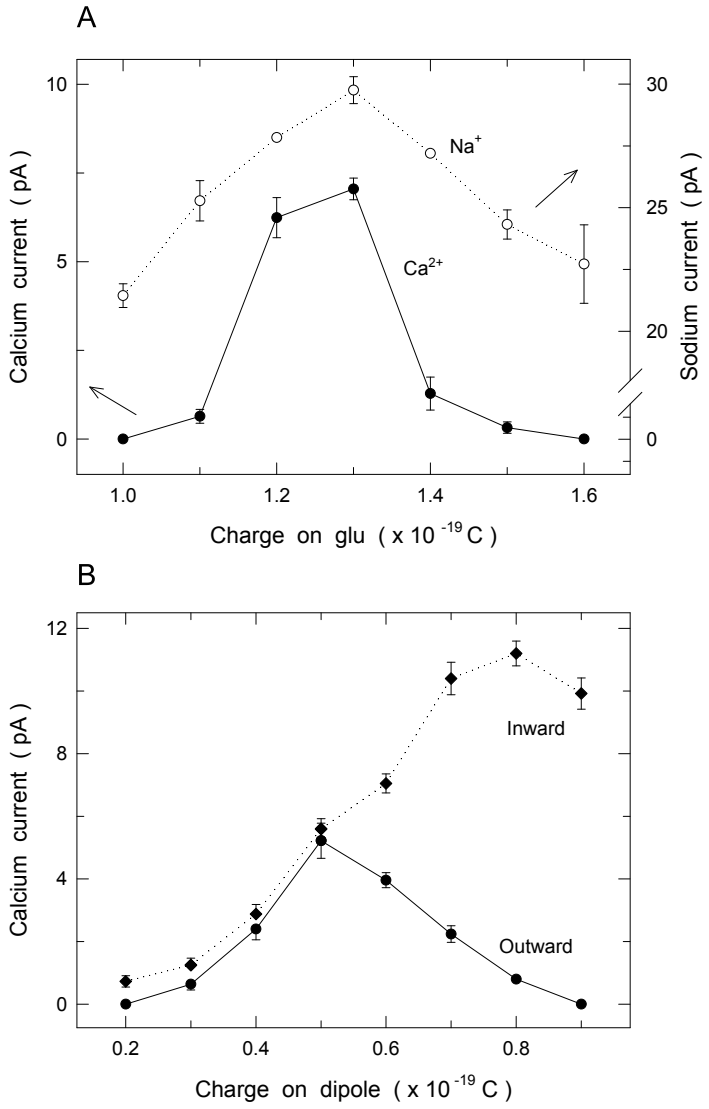

Figure 8.2: Dependence of channel current on fixed charge strengths. (A) The current passing through the channel with 150 mM $CaCl_2$ (filled circles, left side scale) and 150 mM NaCl (open circles, right side scale) under a -200 mV driving potential is plotted against the charge on each of the glutamate groups. The magnitude of the charge on the mouth dipoles is fixed at 0.6 $\times 10^{-19}$ C. Filled circles are obtained from a 1.0 μs and open circles from a 0.5 μs simulation period. (B) The outward (filled circles) and inward (diamonds) current passing through the channel with 150 mM $CaCl_2$ in the reservoirs and a -200 mV driving force is plotted against the magnitude of the charge on each end of the mouth dipoles. The charge on the glutamates is held at 1.3 $\times 10^{-19}$ C. Results are obtained from a 2 μs simulation period. Error bars in this and following figures have a length of one standard error of the mean and are not shown when smaller than the data points.

of diffusion coefficient. Here the diffusion coefficient of calcium ions is systematically varied from 0.05 to 0.5 times its bulk value in the selectivity filter while it is kept at 0.5 times the bulk in the chamber, and the resulting current is plotted. Contrary to intuitive expectations from continuum theories, the current does not increase linearly with the diffusion coefficient but rather saturates as one approaches towards the bulk value. For example, at the chosen value of 0.1 times the bulk, the calcium current is suppressed by only a factor of 2 rather than 10. Thus, we expect the results presented in this paper to be quite robust against variations in the diffusion coefficients.

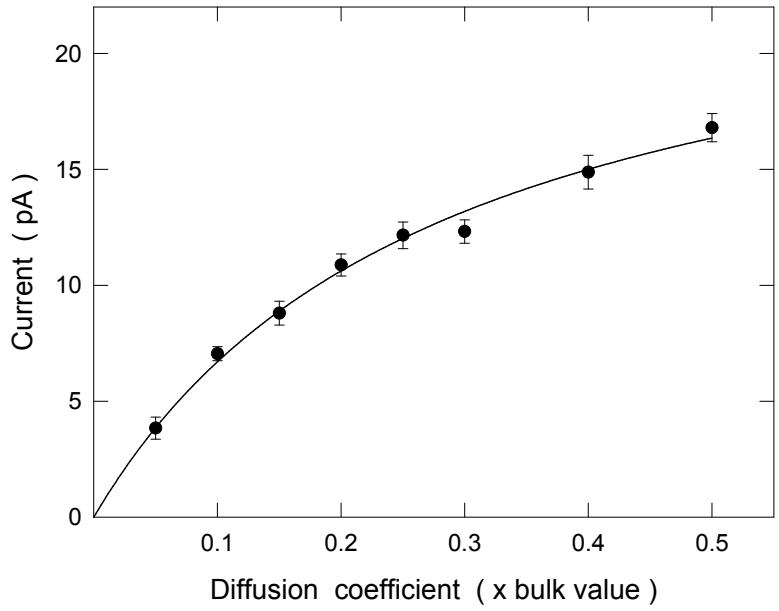

Figure 8.3: Dependence of calcium current on the ion diffusion coefficient in the narrow neck region of the channel (7.5 Å $< z <$ 20 Å) plotted as a fraction of its bulk value (0.79×10^{-9} m^2s^{-1}). A concentration of 150 mM $CaCl_2$ is maintained in the reservoirs and a -200 mV driving force is used. Results are obtained from a 2 μs simulation period.

8.5 Permeation of calcium and sodium ions

The ion-channel and ion-ion interactions hold the clue to understanding ion permeation mechanisms in channels. Therefore we first present a detailed study

of multi-ion potential energy profiles in the model channel to gain some useful insights. A quantitative description of ion permeation that includes the effects of the thermal motion of ions and their interaction with water molecules requires a dynamic approach, which will be discussed in the following sections by performing BD simulations.

8.5.1 Energy profiles

The ion-channel interaction has basically two components; a repulsive force due to the induced charges on the protein boundary and the electrostatic interaction of the ion with charge residues and dipoles in the channel wall. The simple Coulomb interaction between two ions is modified in the channel environment because they also interact via the surface charges induced by each other. All these effects are properly taken into account by solving Poisson's equation with appropriate boundary conditions as mentioned in chapter 3.

For a single ion, a potential energy profile is constructed by calculating the potential energy of the ion held at a fixed z position far from the channel and then repeating these calculations at discrete (1 Å) steps as the ion approaches the channel. While the main pathway of ions in the channel is along the central axis, due to the asymmetric placement of glutamates, an ion's equilibrium position could deviate from the central axis by about 1 Å near the selectivity filter. To take this effect into account, the ion is held fixed only in the z direction but allowed to move in the x and y directions to ensure that it is equilibrated in the $x-y$ plane. To construct multi-ion profiles, one or more ions are placed in the channel at equilibrium positions, and the potential energy of another ion is calculated as it is brought into the channel in 1 Å steps. Before calculating the potential energy of this ion at each fixed position, the ions in the channel are always equilibrated so that the force on them is zero and the system energy is at a minimum. As in the single ion case, only the z position of the external ion is fixed, and it is allowed to equilibrate in the $x-y$ plane. The profile constructed in this way is equivalent to the total electrostatic energy required to bring the charge on the ions from infinity in infinitesimal amounts. The method used in minimizing the energy is detailed elsewhere [40].

The profile for an ion moving through the channel with no fixed charges in the walls is shown in Fig. 8.4. An ion entering the channel meets a steeply rising potential barrier, which is proportional to the square of the ion charge. Thus the barrier height for calcium ions (28 kT, *solid curve labeled a*) is four times larger than for sodium ions (7 kT, *dashed curve labeled b*). When the ring of four mouth dipoles

and four glutamate charges are included in the model, this barrier is turned into a deep well. Again this well is deeper for divalent ions (58 kT, *solid curve labeled d*) than for monovalent ions (36 kT, *dashed curve labeled c*), though the difference is much less pronounced because ion-charge residue interaction is proportional to the ion charge (the energy difference between *a*-*d* is exactly twice that between *b*-*c*). For both types of ions, the well is deep enough so that a single ion would be permanently trapped in the selectivity filter.

Once an ion has entered the energy well, a second ion will see a very different profile, altered by the presence of the first. The profile seen by a second calcium ion when a first ion is in the energy well under a driving potential of -100 mV is shown in Fig. 8.5. The curve on the right (dashed) shows the potential energy of the second ion as it approaches the channel from the right while the one on the left (solid) shows the same when it enters from the left. Clearly both ions can still reside in local energy minima indicated by the arrows in the figure. The ion in the left well faces an energy barrier of about 4.7 kT, which it can surmount as a result of their random motions and the mutual Coulomb repulsion. Once this happens, the ion on the left will move toward the interior mouth of the channel under a steep potential gradient. When the channel is occupied by two calcium ions, a third ion meets a very steep barrier preventing its entry into the channel. The above study of multi-ion potential energy profiles thus indicates that the conduction of divalent ions is most likely to be a two-ion process.

For monovalent ions a different picture emerges. The well is in fact deep enough (20 kT) to hold two ions in a stable configuration at $z = 9$ and 13 Å, as indicated by the lower curves in Fig. 8.6. The two disjointed curves again correspond to the second ion being brought into the channel from the left (solid) and right (dashed), respectively. In the absence of divalent ions, two monovalent ions are most likely to be found together in the narrow part of the channel. When two monovalent ions are in the channel, the profile seen by a third ion is also shown in Fig. 8.6 (upper curves). In this case there is no longer a large potential well in the selectivity filter, and only a very small energy barrier (1 kT) preventing the left-most ion in the filter moving to the small well at the interior region created by the mouth dipoles. So the conduction of monovalent ions is expected to be a three-ion process, and because they face a smaller barrier, their permeation rate should be much higher than that of the divalent ions.

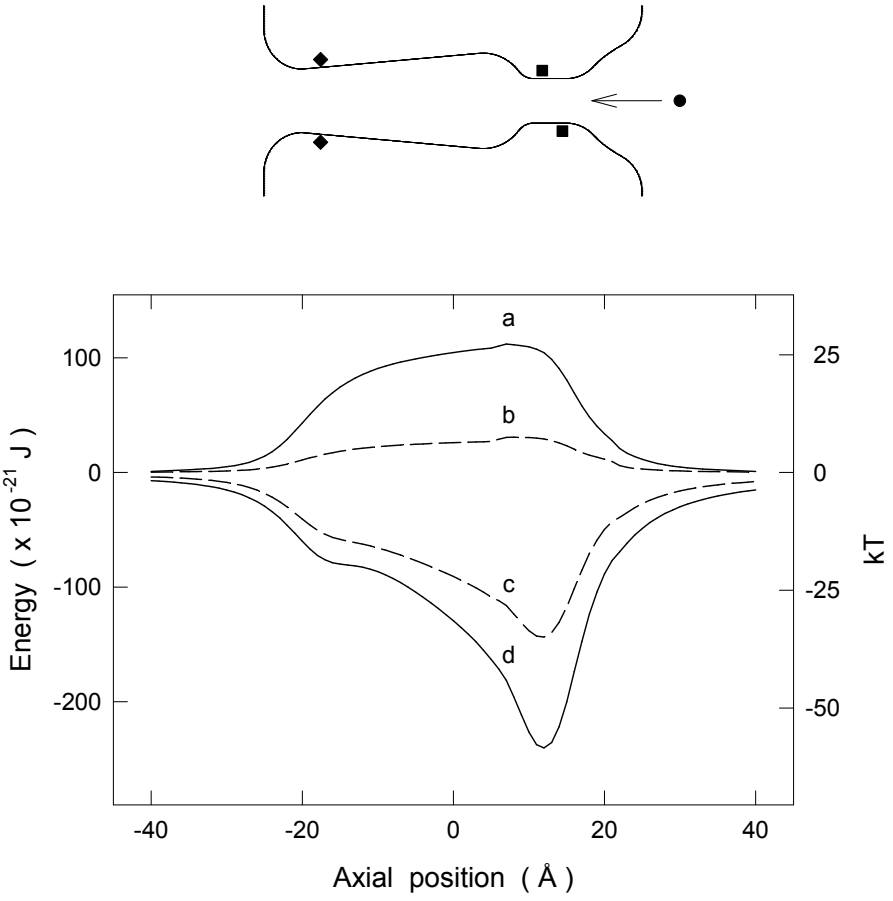

Figure 8.4: Electrostatic energy profile of an ion traversing the channel. The potential energy of an ion held at 1 Å intervals in the z direction but allowed to move to its minimum energy position in the x and y directions is plotted for a calcium ion (solid line labeled a) and a sodium ion (dashed line labeled b) in the absence of any fixed charges. When the glutamate groups and mouth dipoles are included, as shown in the inset, the profiles are replotted for calcium (solid curve labeled d) and sodium ions (dashed line labeled c). No applied potential is used. We note that 1 kT $= 4.11 \times 10^{-21}$ J.

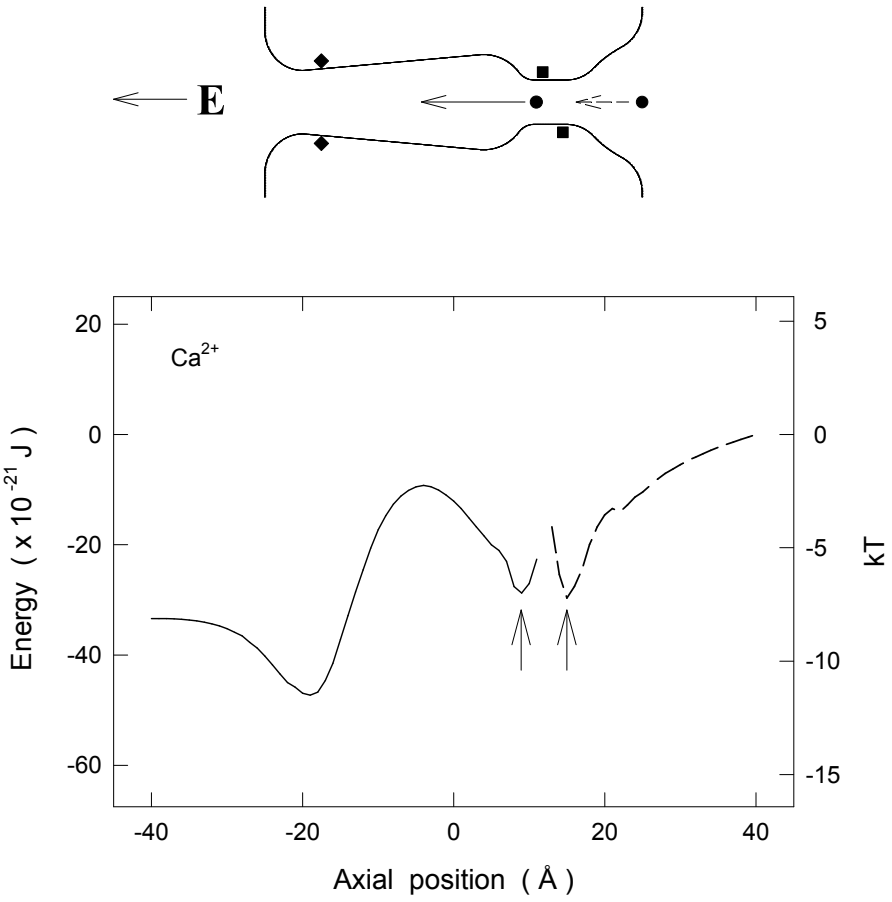

Figure 8.5: Electrostatic energy profiles with 2 calcium ions in the channel under a -100 mV driving force. The potential energy of a calcium ion entering the channel is calculated at 1 Å intervals along the z axis while another calcium ion is resident in the filter (dashed curve). Similarly the potential energy encountered by the left hand calcium ion as it attempts to cross the channel is calculated at 1 Å intervals (solid curve). The second ion is allowed to move to its minimum energy position in the narrow channel neck in both cases. The equilibrium positions of the two calcium ions in the channel are indicated by the arrows. It should be noted that these are 2 distinct curves and the driving potential cannot be calculated from the total energy drop from right to left.

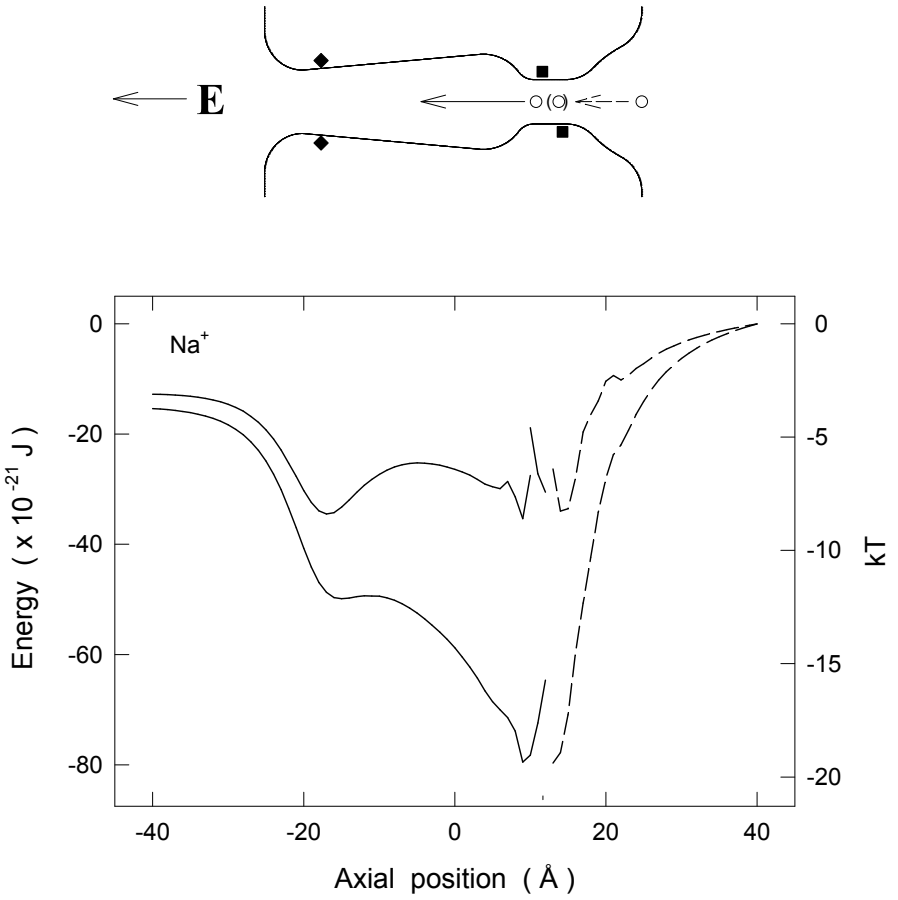

Figure 8.6: The energy profiles as in Fig. 8.5 except for a sodium ion with one (lower curves) or two (upper curves) other sodium ions in the channel neck. An applied potential of -100 mV is used.

8.5.2 Current - voltage relationships

We study the conductance properties of calcium and sodium ions under various conditions by performing Brownian dynamics simulations. The current-voltage relationships shown in Fig. 8.7 A and B are obtained using symmetrical solutions of 150 mM $CaCl_2$ or 150 mM NaCl, respectively and are fitted by the solid lines. Since the calcium current is so small at low applied potentials, it takes exorbitant amounts of simulation time to gain reliable statistics. For this reason values lower than +80 mV and −60 mV are not shown. The current-voltage relationship for the sodium current is fairly linear through the origin although it does show some degree of nonlinearity at large applied voltages. In contrast, the calcium current deviates noticeably from an ohmic relationship as the applied potential is increased beyond ±100 mV. This superlinearity is a result of the large energy barrier in the channel, which presents less of an impediment to ion movement as the driving potential is increased [42]. In both relationships, there is a small asymmetry between the inward and outward currents. The current-voltage relationships obtained experimentally from L-type calcium channels appear to exhibit less asymmetry for both sodium and calcium ions [168, 169]. We find from BD simulations that the symmetry of the calcium current depends crucially on the position and strength of the mouth dipoles. Thus any discrepancy between the experimental findings and the results of our simulations can be improved by adjusting these. With less charge on the dipoles the outward current becomes greater and the inward current smaller (see Fig. 8.3 B). Also, moving the dipoles closer to the interior mouth of the channel produces greater rectification, the inward current becoming much larger than the outward.

At −120 mV and with 150 mM solution, the inward currents for calcium and sodium are, respectively, 1.2 ± 0.2 pA and 14.7 ± 1.6 pA, giving the respective conductance values of 9.7 pS and 122 pS. These values are fairly close to the experimentally determined values of 8 - 9 pS for calcium with 100 - 110 mM solution and 85 - 90 pS for sodium in 150 - 200 mM solution [83, 149, 168]. The superlinearity seen at large applied potentials has been observed in the I-V curves with symmetric solutions [168], which are reproduced for calcium and sodium in the insets of Fig. 8.7 A and B.

8.5.3 Ions in the channel

The average distribution of ions in the channel for calcium and sodium ions under a −200 mV applied voltage is shown in Fig. 8.8 A and B, respectively. To

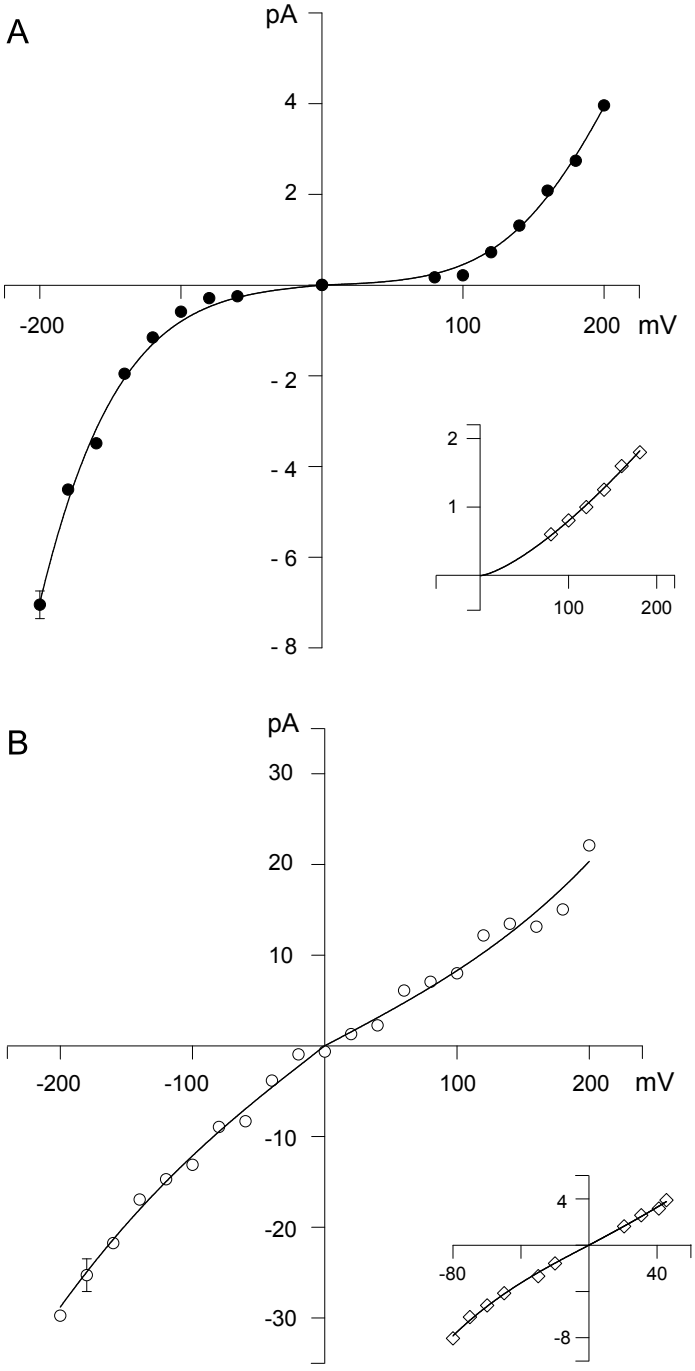

Figure 8.7: Current - voltage relationships. The magnitude of the current passing through the channel with a symmetric solution of (A) 150 mM $CaCl_2$ and (B) 150 mM NaCl in both reservoirs is plotted against the strength of the driving potential. Experimental results [168] in similar conditions are shown in the insets for comparison. A simulation period of 4 to 8 μs is used for calcium and 0.5 μs for sodium.

find the average number of ions in each section of the channel, we divide it into 30 layers of thickness 1.6 Å as indicated in the inset, and compute the average number of ions in each layer throughout the simulation. For calcium ions, there are on average 1.9 ions in the channel, occupying the narrow selectivity filter most of the time. The ion distribution shows two clear peaks, indicating where the ions are most likely to be found at each end of the filter. Again, this supports the conclusion that calcium conduction requires multiple ions. For sodium there are on average 3.1 ions in the channel, and again the ions are most likely to be found in the narrow section. Sodium ions are more likely to occupy the interior end of the channel than the calcium ions, which can be easily understood in terms of the two- and three-ion profiles in Figs. 8.5 and 8.6, respectively.

Our BD simulations support the conjectures derived from the potential energy profiles, that conduction is achieved by the interaction between multiple ions in the channel, and that the channel is always occupied by one or more ions. For 150 mM $CaCl_2$ or 150 mM NaCl at -200 mV, the relative time the narrow section of the channel ($4 < z < 18.5$ Å) is occupied by one or more ions is shown in Table 1. That the filter is so often multiply occupied by calcium suggests that the time taken for one of the ions to move out of the filter, over the energy barrier toward the interior mouth is one of the rate limiting steps. This is shown more conclusively below. For sodium the filter is again occupied most commonly by 2 ions, suggesting that once a third ion enters conduction happens quite quickly. The different times between when an ion enters the channel and an ion traverses it for calcium and sodium reflects the different energy barriers presented in each case: sodium conducts much more quickly as it sees a much lower barrier.

Table 8.1: Relative time selectivity filter is occupied by one, two or three ions in 150 mM $CaCl_2$ or 150 mM NaCl.

	No. ions in filter		
	1	2	3
Ca^{2+}	26 %	74 %	0 %
Na^{+}	5 %	77 %	18 %

Under a +200 mV driving force producing an outward current, the distribution of ions in the channel is very different as is shown for calcium and sodium in Fig. 8.9 A and B. With 150 mM $CaCl_2$ in the reservoirs there is still on average 1.9 calcium

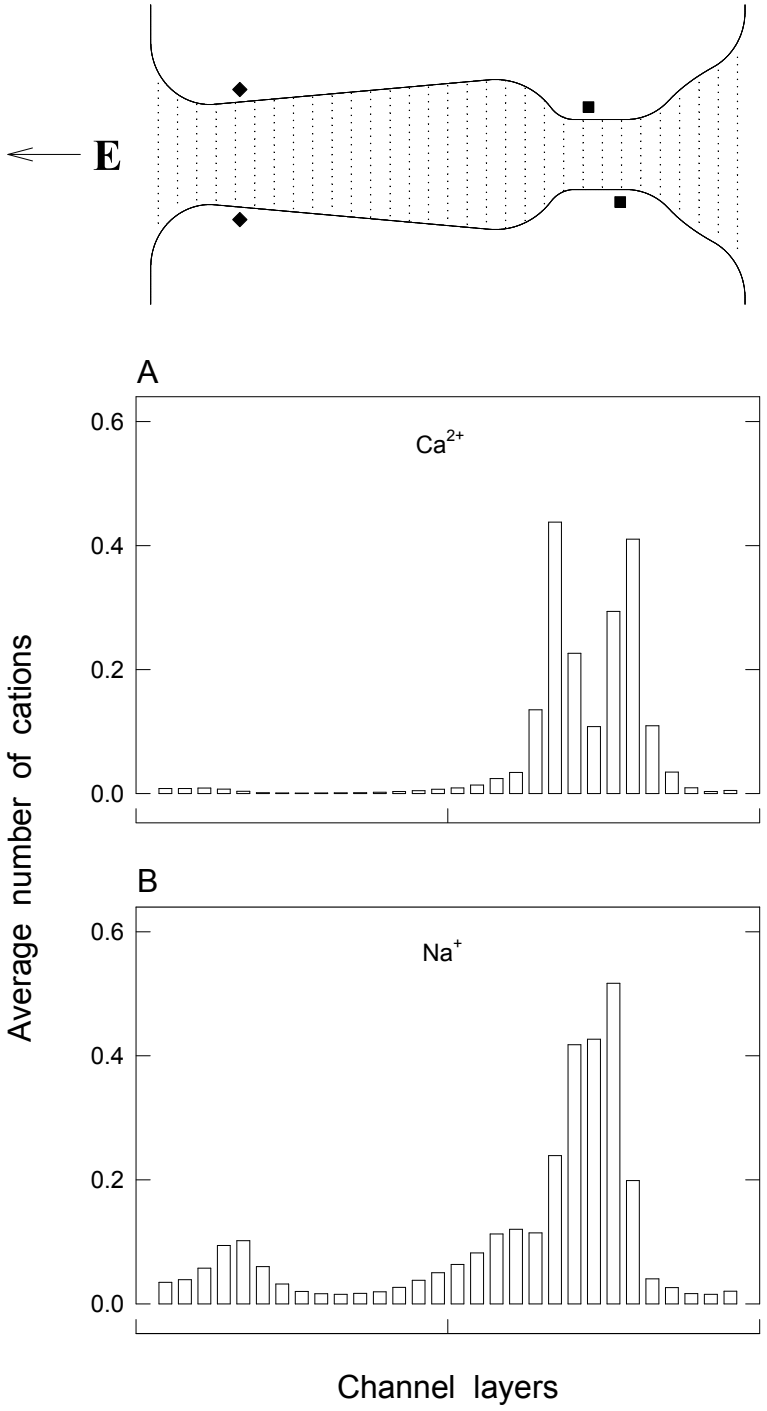

Figure 8.8: Average number of ions in the channel with an applied potential of -200 mV. The channel is divided into 30 sections, as shown in the inset, and the average number of ions in each calculated over a simulation period (0.5 μs) with (A) 150 mM $CaCl_2$ and (B) 150 mM NaCl in the reservoirs.

ions in the channel, but rather than being predominantly located in the narrow neck of the channel as was the case in an inward current, the ions are now almost equally likely to be found near the internal channel mouth as in the narrow filter. Indeed, the region near the internal mouth is occupied 85% of the time. The filter is always occupied, but, in contrast to the situation with an inward current, usually by only one ion (95% of the time). For sodium, the distribution of ions in the channel is very similar under either a -200 or $+200$ mV driving potential. As the energy barriers in the channel are small for sodium, the effect of the driving potential on the barriers does not significantly alter where ions are likely to be found.

Figure 8.10 demonstrates where ions reside in the channel predominantly in a 2-dimensional representation of the system. When there is a -200mV potential driving calcium ions into the cell there are two clear peaks in the narrow region of the channel, indicating that there are usually 2 ions in this region separated by only a few angstroms. There is also a small peak where ions are temporarily delayed at the intracellular end of the channel (Fig. 8.10 A. The ions are repelled from the channel walls by the induced charges, resulting in a region of no concentration around the channel walls. When calcium ions are driven in the other direction, as in Fig. 8.10 B, a clear peak is seen at the intracellular end of the channel, and only one peak in the selectivity filter. When sodium ions are passing through the channel, as in Fig. 8.10 C the ion concentration is more spread, but clear peaks are still seen in the selectivity filter and at the intracellular end of the channel.

To demonstrate more explicitly the rate limiting steps for inward and outward calcium currents, we show in Fig. 8.11 the time taken for different permeation events. Fig. 8.11 A shows the energy profile presented to a calcium ion as in Fig. 8.5 except under a -200 mV driving potential. The height of the central barrier, V_B, is 2.9 kT. Given that the narrow section of the channel is always occupied, the time for a conduction event can be broken into two parts, τ_1, the time for a second calcium ion to enter the filter from the reservoir; and τ_2 the time for one of the ions in the filter to move across the central energy barrier once the second ion has entered, as indicated in the figure. From a conditional probability analysis of the ion trajectories in our BD simulations, we find that τ_2 takes an average of 33 ns or 74% of the average conduction time of 45 ns, making it the main rate limiting step. The time for the second calcium ion to enter, τ_1 takes most of the remaining time (11 ns), indicating that once an ion crosses the central barrier it exits the channel almost instantaneously. This can also be seen in Fig. 8.8 A which indicates that calcium ions rarely occupy the left hand end of the channel. That the time spent waiting for one of the ions to cross the centre of the channel is the rate limiting step

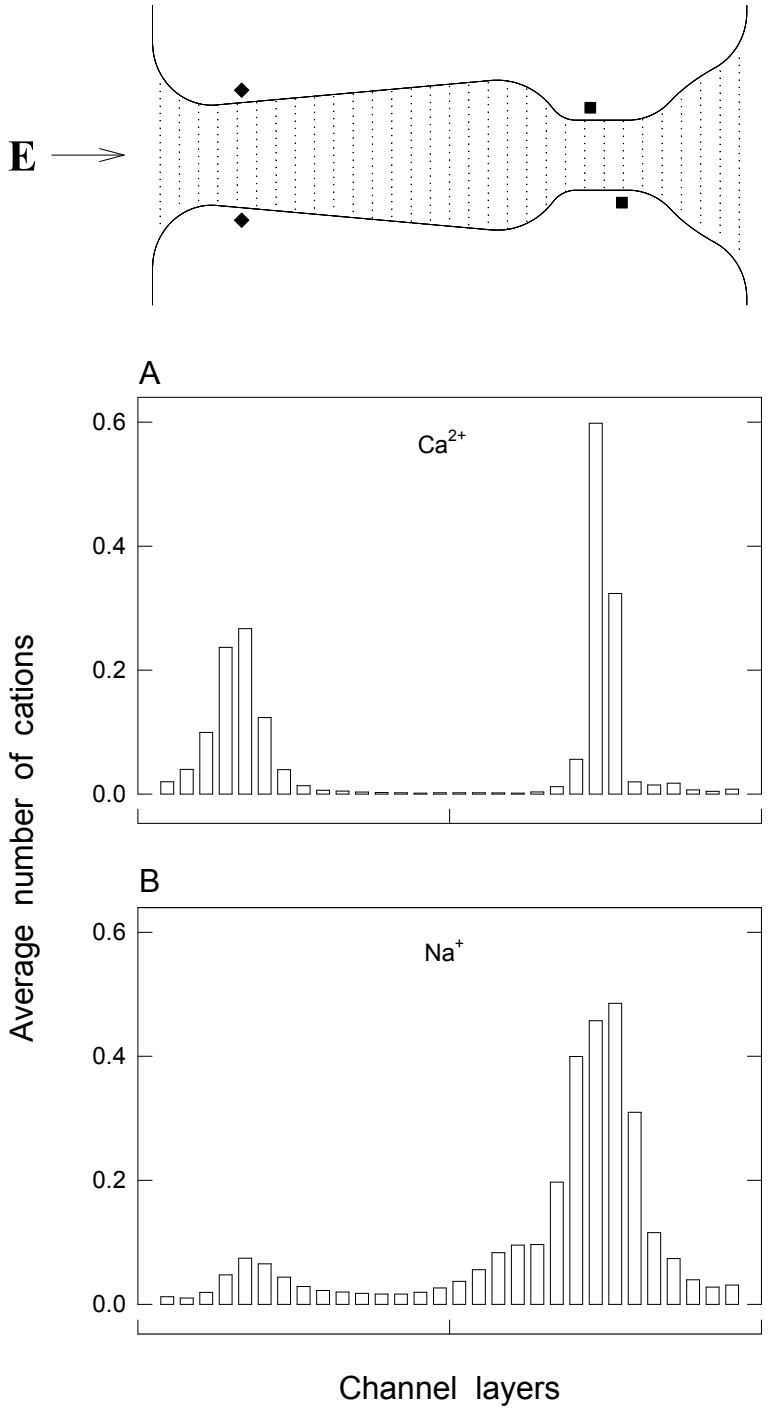

Figure 8.9: Average number of ions in the channel as in Fig. 8.8 except with an applied potential of +200 mV with (A) 150 mM $CaCl_2$ and (B) 150 mM NaCl in the reservoirs.

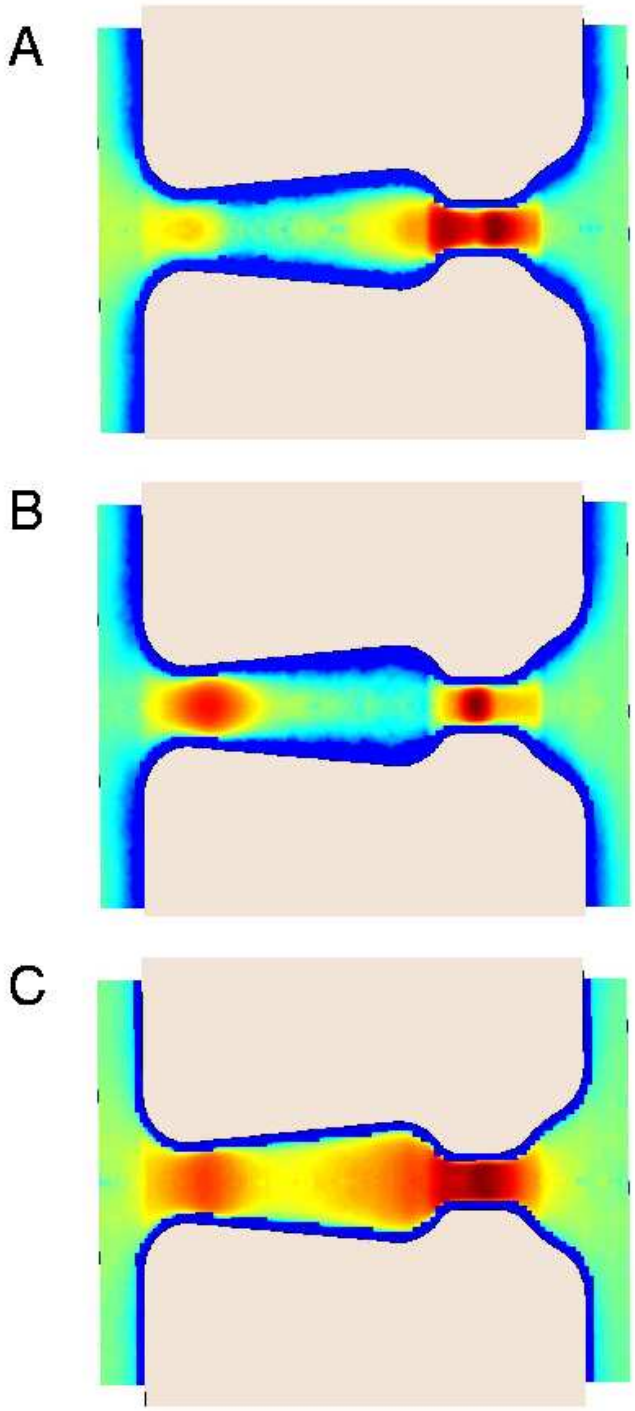

Figure 8.10: Concentration on the calcium channel, showing where ions dwell predominantly with (A) 150 mM $CaCl_2$ in the reservoirs and -200 mV driving potential, (B) 150 mM $CaCl_2$ and +200 mV driving potential, and (C) 150 mM NaCl with a -200mv potential.

for inward currents raises the question of whether an ion moves across the barrier by its own thermal motion and the coulomb repulsion of the second calcium ion, or whether it requires additional repulsion from a third ion entering the channel vestibule. A conditional probability analysis of how many ions are in the right hand half of the channel ($0 < z < 25$ Å) whilst the innermost calcium ion is crossing the central barrier ($-10 < z < 0$ Å) shows that 99 % of the time there is only one ion, and so the entry of a third ion into the channel is not required for calcium transit.

A similar analysis is shown for a +200 mV driving potential creating an outward current in Fig. 8.11 B. The conduction process is divided into the time for an ion to enter the left hand end of the channel, τ_1, and the time for it to move across the central energy barrier ($V_B = 3.7$ kT) into the filter, τ_2 as indicated. Again, the rate limiting step is the time to climb the central barrier, τ_2, which takes an average of 61 ns, accounting for 85% of the total conduction time (81 ns). The time spent waiting for an ion to enter the internal mouth of the channel accounts for most of the remaining time (16 ns), indicating that once two ions enter the filter one quickly exits. This is clearly explained by examining the energy profile which shows that there is virtually no barrier preventing this external exit.

Since climbing over the central barrier is the main rate limiting step in calcium permeation, calcium conductance will depend crucially on the barrier height. The height of the barrier, V_B decreases fairly linearly for both inward and outward currents as the driving potential is increased, which, not surprisingly, results in larger currents. However, this does not mean that the current will also vary linearly as can be seen in the current-voltage curves (Fig. 8.7).

8.5.4 Conductance - concentration relationships

If the transport of ions is dependent on two processes, one of which depends on concentration (access to the channel) and one which does not (permeation in the channel), then we expect the current, I, to eventually saturate with increasing ion concentration c, leading to a current-concentration relationship of the Michaelis-Menten form [40]:

$$I = \frac{I_{\max}}{1 + K_s/c}. \tag{8.1}$$

Here $I_{\max}$ denotes the saturation current and K_s the concentration at half-maximum current.

The current-concentration relationship found from BD simulations indeed has this form and is in close agreement with the experimentally observed shape [69, 83]. In Fig. 8.12 A the current-concentration relationship obtained from BD simulations

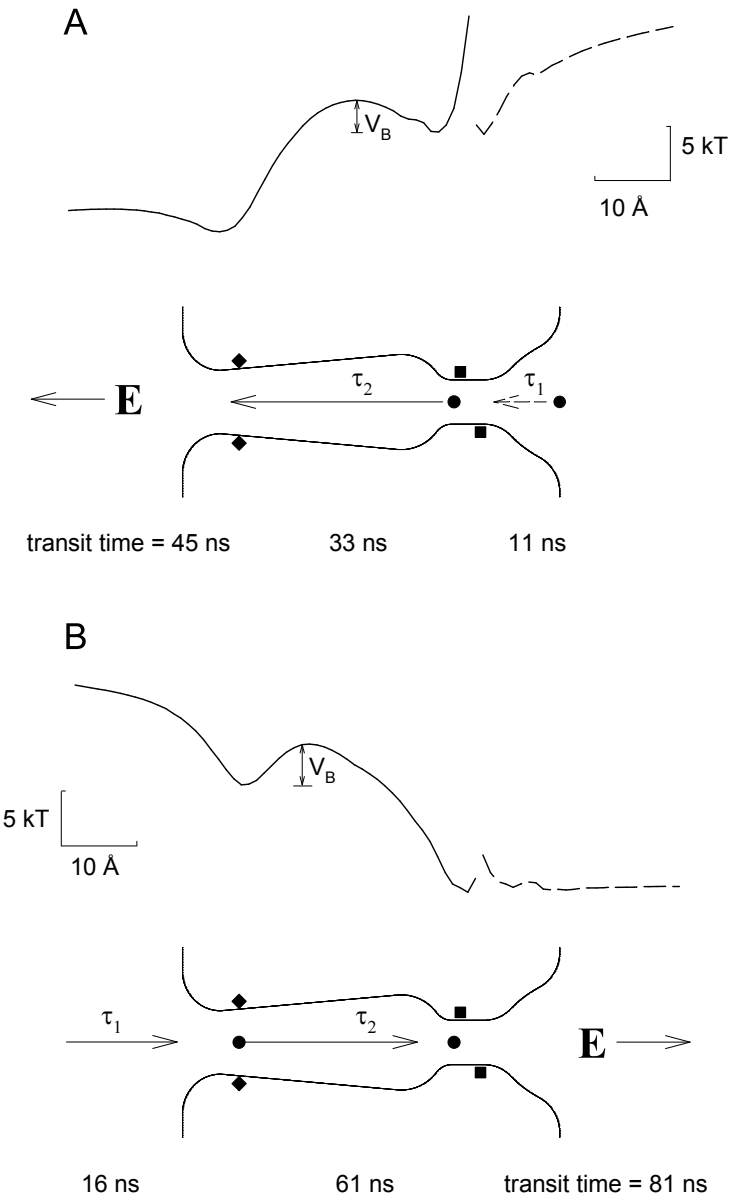

Figure 8.11: Rate limiting steps for ion permeation. The energy profile presented to a calcium ion as in Fig. 8.5 and the main time consuming steps for ion permeation are shown for (A) a -200 mV and (B) a $+200$ mV driving potential. In A the ions permeate from right to left and meet a central energy barrier $V_B = 2.9$ kT. In B the ions permeate in the opposite direction and meet a barrier of 3.7 kT. The time taken for a second ion to enter the channel, τ_1, and the time for an ion to cross the central barrier, τ_2, are indicated.

(filled circles) are compared to the experimental results of Hess et al. [83] (diamonds and dotted line). The BD data has been fitted using Eq. 8.1 (solid line) with a maximum current $I_{\max} = 7.5$ pA and point of half maximum $K_s = 13.9 \pm 2.5$ mM. This compares well with the K_s value of 13.9 mM found experimentally. The different scales in the figure arise as a higher applied potential is used for the BD simulations as required to obtain reliable statistics with a limited amount of computer time.

The current-concentration relationship found with BD simulations for sodium has a similar shape, but saturates much more slowly as can be seen in Fig. 8.12 B. Again this is fitted by a Michaelis-Menten equation with the value $I_{\max} = 71$ pA and $K_s = 240$ mM. No experimental data is available for comparison in this case. In both plots, a driving force of -200 mV is employed.

8.6 Mixtures of calcium and sodium ions

It is important to see whether our model channel can account for experimental results with more than one ion species present. In particular we look at mixtures of calcium and sodium ions as an example of selectivity between monovalent and divalent ions. To answer such questions as the effect of each type of ion on the permeation of the other and the competition between different types of ions to access the selectivity filter, we again first consider potential energy profiles for mixed ions and then carry out BD simulations.

8.6.1 Energy profiles

We look at the energy profiles with a mixture of calcium and sodium ions to gain an intuitive picture of how the presence of calcium ions may affect the permeation of sodium ions. We construct the energy profiles shown in Fig. 8.13 for a sodium and a calcium ion entering a channel occupied by an ion of the other species so that we can compute the energy required to push a resident calcium ion out of the channel. In this and the following figures, a potential of -100 mV is applied. The profile on the right between $z = 14$ to 40 Å (dashed line) shows the potential energy of a sodium ion as it is moved in 1 Å steps from the reservoir, while the resident calcium ion is allowed to adjust its position so as to minimize the total energy of the system. The initial position of the calcium ion is indicated as a filled circle in the inset and the positions of the sodium ion approaching from the reservoir toward the calcium ion is indicated by the open circle. The profile on the left (solid line) represents the energy barrier seen by the calcium ion as it moves out towards the intracellular space in 1 Å steps while the sodium ion is allowed to adjust its position

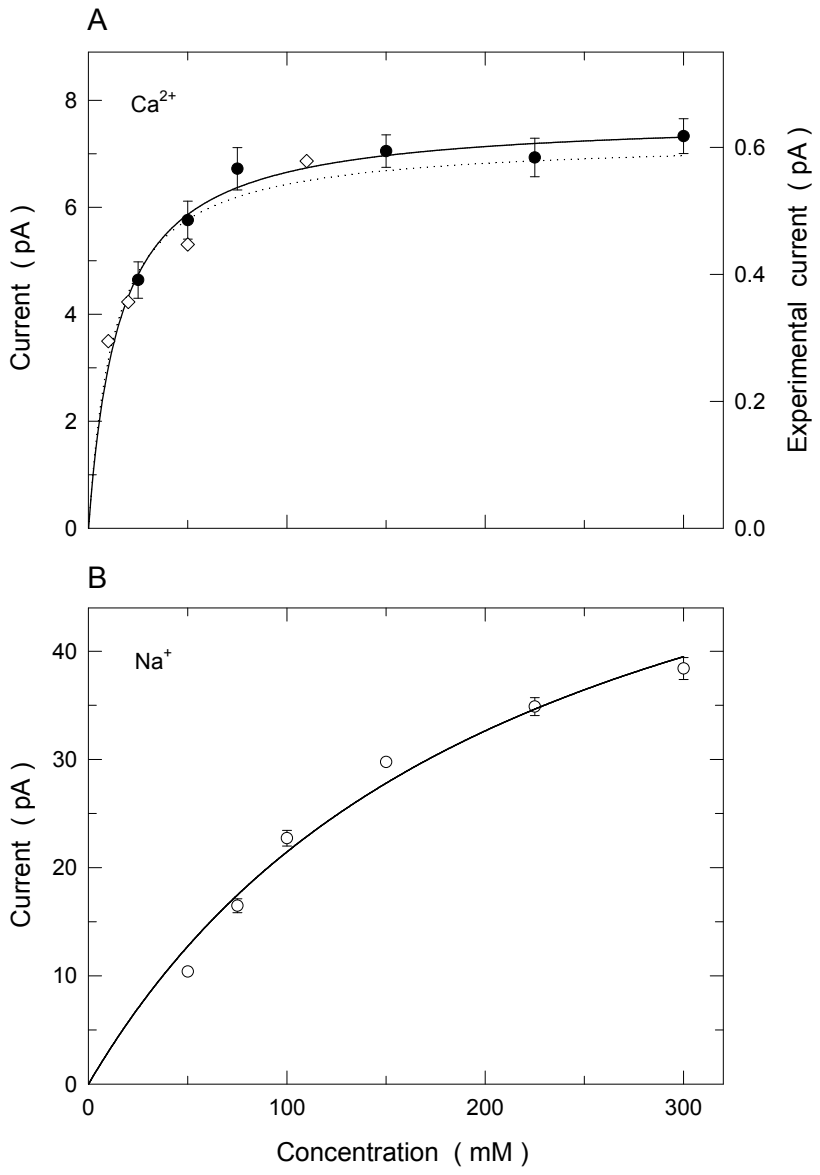

Figure 8.12: Conductance-concentration relationships. The current obtained with symmetrical solutions of varying concentrations of (A) $CaCl_2$ (filled circles) and (B) NaCl (open circles) in the reservoirs. An applied field of -200 mV is used and the data points are fitted by the solid line using Eq. 8.1. In A the experimental data of Hess et al. [83] is shown by the open diamonds and dotted line for comparison. Note that the different scales on the simulation and experimental results are largely due to the different applied potentials in each case. For the BD results a simulation period of 4 to 8 μs and 0.5 μs are used for calcium and sodium respectively.

so as to minimize the total energy of the system. Not surprisingly, the channel can easily hold a calcium and a sodium ion in stable equilibrium. The difference from the two calcium ion case (Fig. 8.5) is that the barrier faced by the calcium ion on the left is increased from 5 kT to 16 kT in the present case, which is insurmountable. Clearly, the Coulomb repulsion provided by a sodium ion is inadequate for ejecting the resident calcium ion from the selectivity filter.

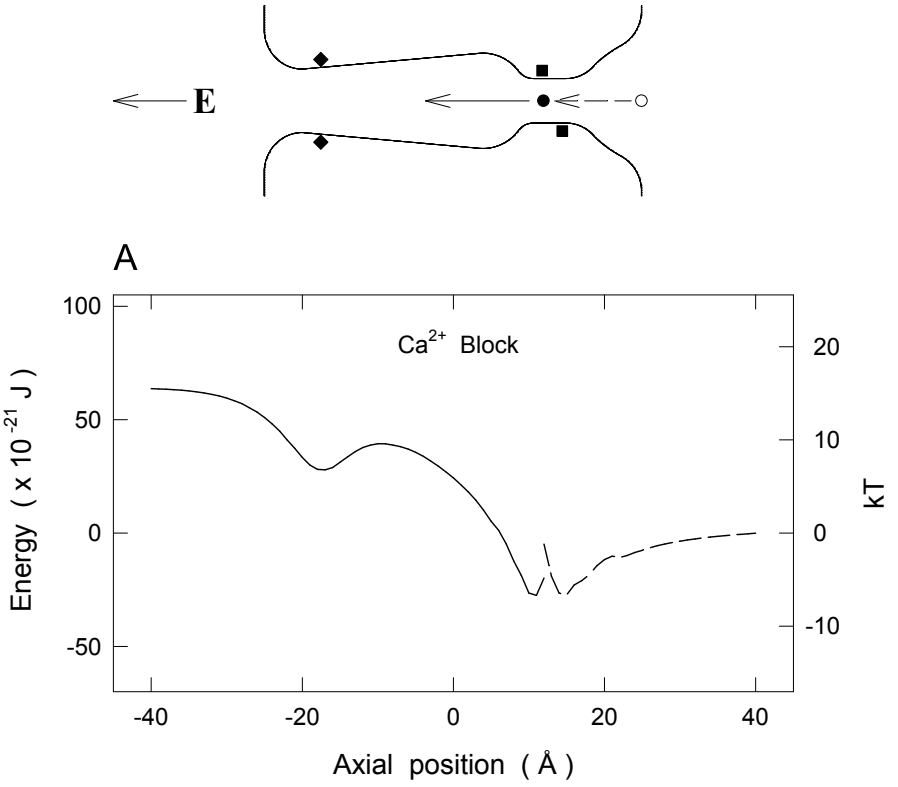

Figure 8.13: Energy profiles indicating calcium block. The right curve (dashed line) shows the potential energy of a sodium ion given that there is a calcium ion in the filter as indicated in the inset. The left curve (solid line) shows the potential energy of a calcium ion given that there is a sodium ion in the filter. The energies are calculated at 1 Å intervals as in Fig. 8.4 under a -100 mV driving potential.

If another sodium ion is brought in from the extracellular reservoir, while a calcium and a sodium ion are resident on the left and right sides of the selectivity filter respectively, it meets a steeply rising Coulomb barrier. In fact, unlike all the previous cases shown in Figs. 8.5, 8.6 and 8.13, there is no stable equilibrium for

one calcium and two sodium ions in the channel. The Coulomb barrier prevents the second sodium ion from moving towards the channel interior so that it is unable to dislodge the calcium ion from its minimum energy position. Even if a second sodium ion enters the exterior mouth through random motions, this will be a temporary event as it will be ejected quickly under the strong Coulomb repulsion from the resident ions. Thus, we expect from the study of the energy profiles that once a divalent ion enters the selectivity filter of the channel, it will permanently block the passage of monovalent ions.

We next examine if the presence of one or more sodium ions in the channel is likely to block the passage of calcium ions. As before, we place one sodium ion in the selectivity filter and examine the profile encountered by a calcium ion as it enters from the right (solid line in Fig. 8.14 A), and the profile encountered by a sodium ion as it attempts to traverse the channel under the influence of the electric field as well as the repulsive Coulomb force exerted by the calcium ion (dashed line in Fig. 8.14 A). The calcium ion sees a large potential drop attracting it in to the channel and there is only a small barrier preventing the sodium ion from exiting the channel. Thus, a single sodium ion in the filter will not prevent a calcium ion entering. The same conclusion is reached with two sodium ions in the channel (Fig. 8.14 B). The calcium ion still sees an attractive potential (solid line) and will easily access the channel. The profile on the left (dashed line) shows the potential energy of the inner sodium ion as it attempts to exit the channel to the intracellular side. As this is a well rather than a barrier, the left-most sodium ion will be easily pushed out once a calcium ion enters the channel. Thus, monovalent ions cannot prevent divalent ions from crossing the channel. Experimentally, however, a high sodium concentration attenuates the calcium current. An explanation of this feature requires BD simulations, and, as shown in a later section, the experimental findings are replicated in our model.

8.6.2 Current - voltage relationships

BD simulations, carried out with a mixture of calcium and sodium ions in the reservoir, confirm the block of sodium current by calcium ions conjectured above from the inspection of the potential energy profiles. Once a calcium ion enters the narrow section of the channel it prevents sodium ions from crossing the channel but not vice versa. The current-voltage relationship obtained in the presence of a combination of calcium and sodium ions is pronouncedly different from that obtained from a solution containing only one cationic species. Fig. 8.15 shows the magnitude of the current as the voltage is varied with 100 mM $CaCl_2$ and 50 mM NaCl in

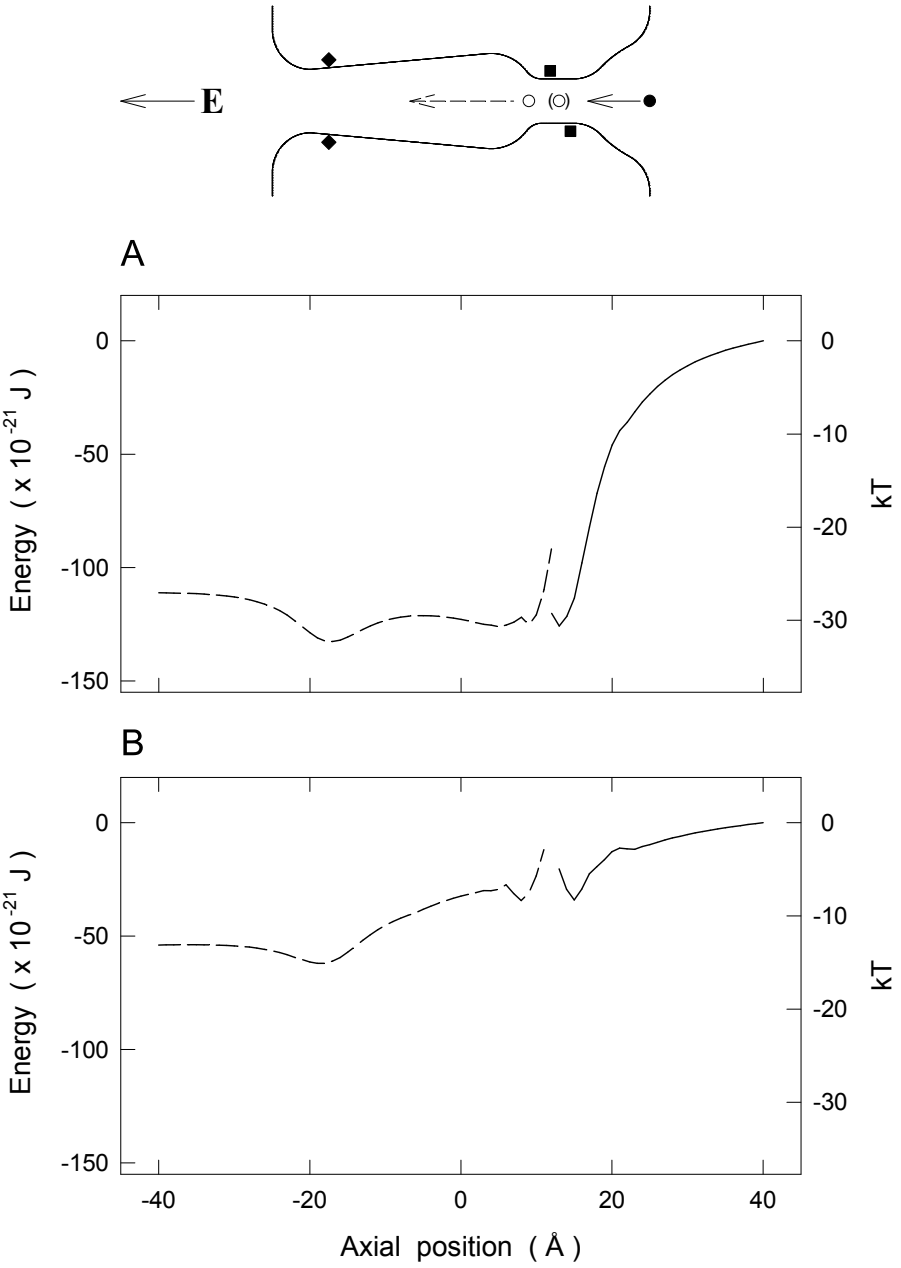

Figure 8.14: Energy profiles as in Fig. 8.13 except with a calcium ion on the right side of either (A) one, or (B) two sodium ions as shown in the inset.

the external reservoir, and only 50 mM NaCl on the internal side. Again we have not carried out simulations between ± 100 mV due to the large simulation times required to gain reliable statistics at low currents. Due to the asymmetric concentrations, the reversal potential is roughly 50 mV. Below this point, the inward current is mostly carried by calcium ions as they block sodium permeation. The conductance value is around 25 % lower than that found for calcium alone. How the presence of sodium lowers the calcium current is discussed below. The external current, however, climbs rapidly above the reversal potential reaching a larger value than the inward current as it is carried by more rapidly permeant monovalent ions. This outward monovalent current, however, displays a different shape to that seen for sodium alone, rising slowly at first and then very rapidly at higher potentials. The reason for this is that calcium ions on the external side of the channel still occasionally move against the driving potential and fall into the channel, blocking the monovalent current. At higher positive applied potentials, this no longer happens and the sodium current is not impeded.

The general shape of this graph agrees closely with that found experimentally in similar conditions by Rosenberg et al. [169] which is represented in the inset. (Note that these experimental results are obtained using Ba^{2+} and Li^{+} ions which have different conductance values to Ca^{2+} and Na^{+}.)

8.6.3 Mole fraction effect

Experimental studies of the calcium channel have shown a remarkable behavior in mixtures of monovalent and divalent ions. As the relative concentration of calcium to sodium is decreased, the conductance of the channel first decreases to a minimum and then increases again to a maximum when there is no calcium present [8]. This so called 'anomalous mole fraction effect' has been a major subject of attention in calcium channel literature (see, for example, [51, 151, 203]).

To investigate this behavior in our channel model, we conduct BD simulations holding the sodium concentration fixed at 150 mM (8 ions in each reservoir) and measure the calcium and sodium currents in the channel at different calcium concentrations as shown in Fig 8.16 A. The calcium current is determined at higher concentrations ($\geq$ 37.5 mM) through BD simulations. As noted in the previous sections, sodium only conducts through the channel until it becomes blocked by a calcium ion. Thus, to calculate the sodium current we need only find how long it takes for a calcium ion to enter the channel and the rate at which sodium conducts before this. The time taken for a calcium ion to enter the channel is determined at 18 mM and above by repeatedly running BD simulations and calculating an average

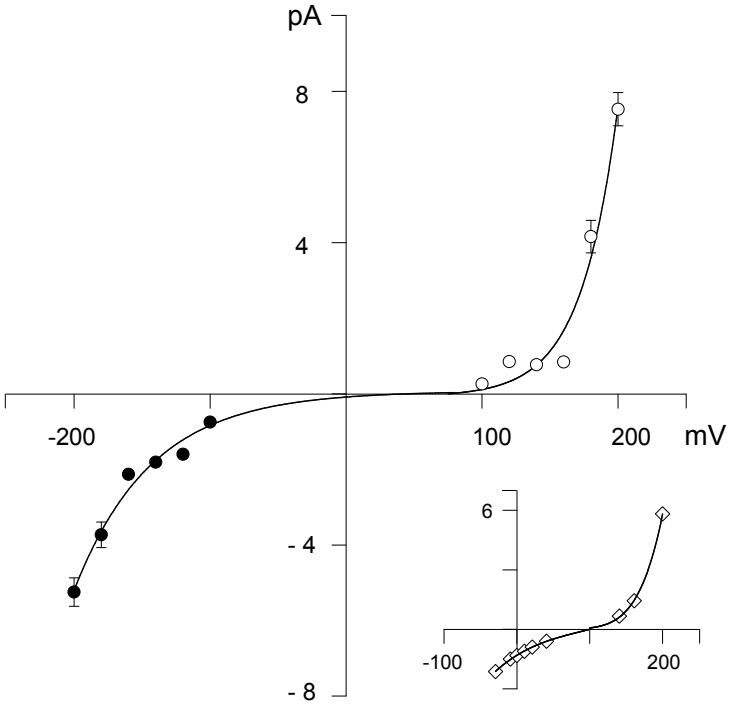

Figure 8.15: Asymmetric I-V curve with a mixture of Ca^{2+} and Na^{+} ions. The calcium (filled circles) and sodium (open circles) current passing through the channel is calculated at various applied voltages with 100 mM $CaCl_2$ and 50 mM NaCl in the external reservoir and 50 mM NaCl in the internal one. Data points represent the results of 2.5 to 7.5 μs simulations. Experimental data with a similar mixture of Ba^{2+} and Li^{+} ions [169] is shown in the inset for comparison.

time for calcium entry. At low calcium concentrations, we can expect that sodium will conduct up until this point as if there were no calcium ions present.

This same technique, however, does not allow us to probe calcium concentrations lower than 18 mM, as we must have a very large reservoir to include a calcium ion. In such cases the BD simulations become cumbersome and impractical as we also have to simulate the motion of a very large number of sodium and chloride ions. To obviate these problems, we extrapolate to lower concentrations using values at higher ones. We note that if our reservoir is larger than about two Debye lengths the effect of the channel and fixed charge environment will be totally screened out at the reservoir edges, allowing us to mimic lower concentrations by letting calcium ions randomly enter the reservoir as if in a larger bulk solution. In other words, the time for an ion to enter the finite reservoirs is inversely proportional to the calcium concentration. (For example, at a concentration of 2 mM we would expect the ion to be in the reservoir only one tenth as long as at 20 mM.) Because sodium only conducts before the channel becomes blocked by calcium or closes through some other gating mechanism, when the time taken for calcium block becomes larger than the mean open time of the channel ($\sim$ 1 ms for an L-type calcium channel [82, 83]) the sodium current saturates at its value in the absence of calcium. Although extrapolating the time to block in this way determines the shape of the sodium current curve, the position of the half maximum current is highly dependent on the time taken for the channel to block at higher concentrations. Thus, comparing this value with experimental data still provides an important test of our model.

The values of the calcium and sodium current at different calcium concentrations normalised by the maximum value of each, are shown by the filled and open circles in Fig. 8.16 A, respectively. (It should be noted that the magnitude of the calcium current is significantly lower than that for sodium.) As the calcium concentration decreases, the calcium current also decreases as was the case in the concentration conductance curve, since it takes longer for a second calcium ion to enter the channel as required for conduction. With further reduction in calcium concentration, it takes longer for a calcium ion to enter and block the channel, meaning more sodium ions are able to pass through the channel before this occurs. Thus the sodium current keeps increasing until it saturates when the time to block reaches the mean open time of the channel.

The resulting picture is the well-known mole fraction effect. As the calcium concentration is decreased, the total current passing through the channel first decreases and then increases again. For comparison, experimental results [8] are shown in Fig. 8.16 B. Our extrapolation from BD simulations predicts the half maximal

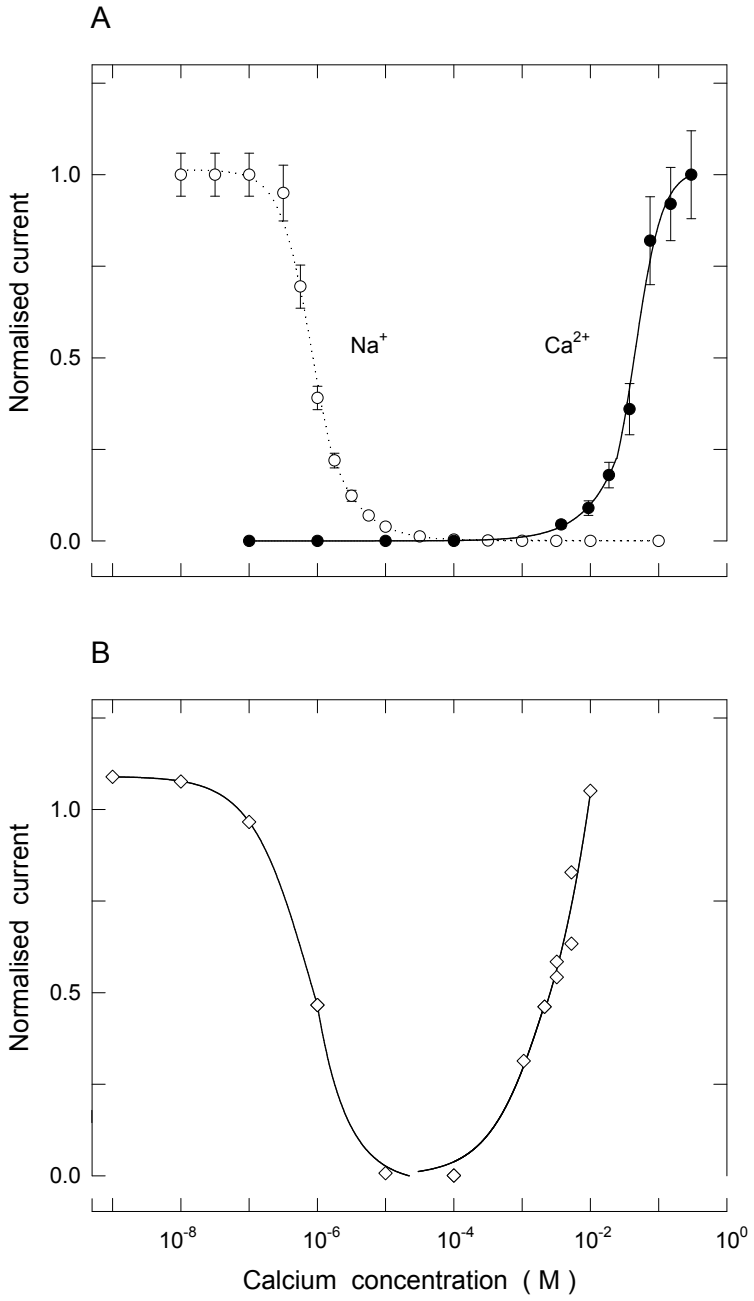

Figure 8.16: Mole fraction effect. (A) The Ca^{2+} (filled circles) and Na^{+} (open circles) currents across the channel determined with different symmetrical calcium concentrations in the reservoirs from BD simulations as described in the text. The sodium concentration is held fixed at 150 mM in both reservoirs and the applied voltage at -200 mV in all cases. (B) A representation of the experimental results from [8] are shown for comparison. Calcium currents come from 2 to 3 μs simulation periods, sodium currents from the simulation of 35 blocking events.

sodium current to occur at a calcium concentration of $\sim 8.6 \times 10^{-7}$ M, close to the experimentally determined value of $\sim 8.8 \times 10^{-7}$ M. Although we have held the sodium concentration at 150 mM throughout, the data points on the right hand side of the experimental figure are obtained with no sodium present. As discussed below, the presence of sodium can attenuate the calcium current, therefore our values of calcium current can be expected to be lower than those in the experimental curve. Also, it is worth noting that the simulation data is normalised by the current at near its saturation value, the experimental data, however, is normalised by a lower value than this. If the saturation current were to be used in the experimental data, the normalised calcium current would be lower than shown.

8.6.4 Attenuation of calcium currents by sodium

We have seen that once a calcium ion enters the channel, it prevents sodium ions from permeating. A number of results suggest that the presence of monovalent ions can also slow the permeation of calcium ions. For example, at physiological concentrations of sodium and calcium, external sodium attenuates calcium current through the channel [158]; in channels carrying outward lithium currents, high extracellular concentrations of lithium ions slow the rate at which calcium ions exit the pore, producing the so called 'lock in effect' [111]; finally increasing the external concentration of lithium is found to slow the entry rate of external calcium ions into the pore [111]. All of these results suggest that the external monovalent ions interfere with the entry and exit of calcium ions on the external side of the pore.

To examine the effect of external sodium ions in our model, we hold the calcium concentration in each reservoir fixed at 150 mM (8 ions in each reservoir) and vary the sodium concentration from 0 to 300 mM. Fig. 8.17 A shows the normalized channel current obtained by dividing the current by that in the absence of sodium. The BD simulation results (filled circles) show that, as the sodium concentration is increased, the calcium current severely decreases. The BD data points are very close to the experimental results of Polo-Parada and Korn [158], which are indicated by the open diamonds and fitted with the equation (dotted line):

$$Y = 1 - ([\mathrm{Na}]^k / IC_{50}^k + [\mathrm{Na}]^k), \tag{8.2}$$

where $IC_{50} = 118.5$ mM and $k = 1.2$. Thus, the blocking of calcium current by external sodium is very well reproduced in this model.

It has been suggested that the block by external sodium is a consequence of calcium and sodium ions competing for the high affinity site in the pore, and Dang and McCleskey [51] take this effect to be evidence for a low-affinity site on the

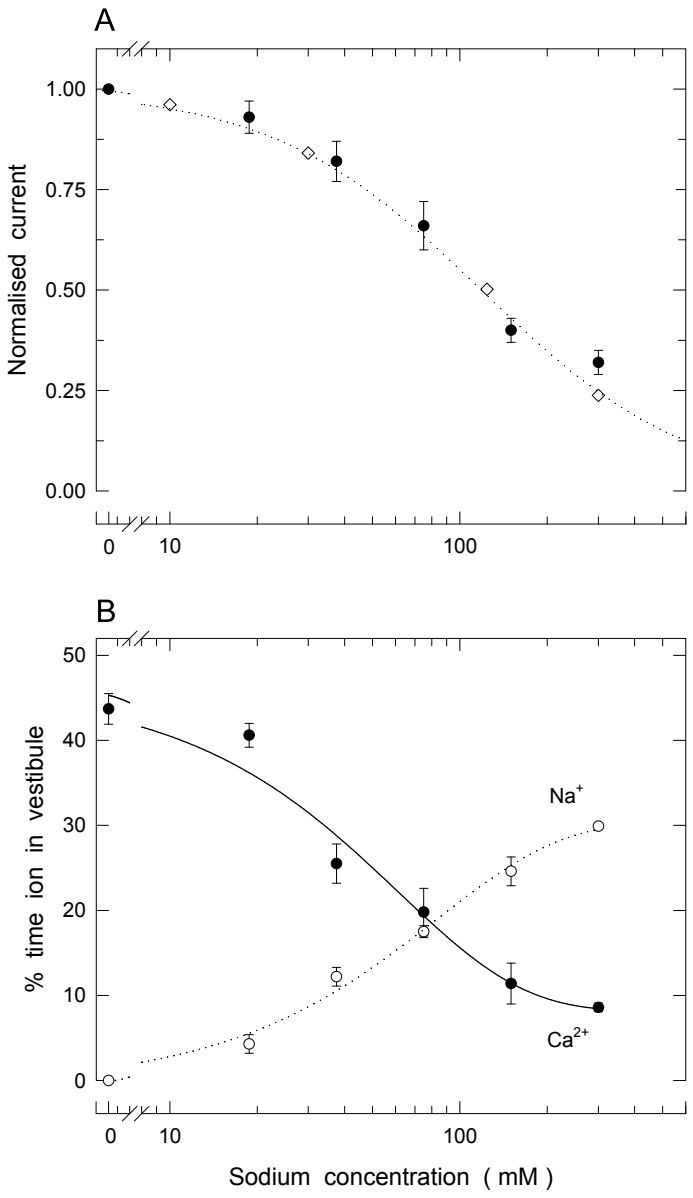

Figure 8.17: Attenuation by external sodium. (A) The normalized channel current, calculated by dividing by the value in the absence of sodium, is shown as the sodium concentration in the reservoirs is varied in BD simulations (filled circles). The calcium concentration is held fixed at 150 mM in both reservoirs throughout and a -200 mV driving potential is used. The experimental data and fit from [158] is shown by the open diamonds and dotted line for comparison. (B) The percentage of time that the external vestibule of the channel is occupied by Ca^{2+} (filled circles) or Na^{+} (open circles) given that there is a calcium ion in the channel neck for the simulations shown in A. A 3 to 4 μs simulation period is used.

outside of the main high-affinity site. To understand the reason behind this blocking, we examine how an increase in the sodium concentration influences the calcium concentration near the external mouth of the channel. In Fig. 8.17 B we show the probability of finding a calcium ion (filled circles) or a sodium ion (open circles) in the external vestibule of the channel given that there is a calcium ion in the filter. In the absence of sodium ions in the electrolyte, the chance of finding a calcium ion in the vestibule while another one is in the filter is 44%. However, when sodium ions are introduced this probability drops rapidly. A sodium ion in the vestibule cannot push the calcium ion out of the filter but it provides sufficient Coulomb repulsion to prevent other calcium ions from entering the vestibule, effectively stopping the conduction process. Due to its random motion, the sodium ion eventually leaves the vestibule and allows the other calcium ions to enter, but as can be seen in Fig. 8.17 B the presence of a sodium ion in the vestibule significantly decreases the chance of a calcium ion finding its way into the entrance of the channel. With a sodium concentration of 300 mM, a calcium ion enters the vestibule while another is in the filter only about 10% of the time. Thus the current is expected to be less than a quarter of its value in the absence of external sodium, consistent with the 75% attenuation observed in experiments. The above analysis suggests that the attenuation of channel current by external sodium is the result of competition between ions accessing the external vestibule of the channel rather than due to the presence of a specific low-affinity binding site.

Chloride ions play an important role in helping to alleviate the attenuation by external sodium. Since the attenuation of current is a result of sodium ions inhabiting the channel vestibule and preventing calcium ions from entering, the calcium current will be strongly dependent on how long it takes for sodium ions to exit from the vestibule once they have entered. As seen in Fig. 8.13, a sodium ion, once inside the channel, faces a sizable barrier (7 kT) to move back to the external reservoir. This would be a very rare event if there were no assistance from counter ions. When chloride ions are prevented from entering the vestibule (through an artificial block introduced into the BD simulations), the sodium ions attenuate the current much more effectively than when chloride ions are free to enter. As an example, with 150 mM calcium and 37.5 mM sodium (8 and 2 ions) in each reservoir, the current when the chloride ions are prevented from entering the vestibule is 3.2 ± 0.8 pA compared to 8.7 ± 0.8 pA when they are free to roam. This example highlights the role played by the counter ions in pulling the sodium ions out of the vestibule with their Coulomb attraction.

8.6.5 Mutation studies

Mutations of the glutamate residues have provided many useful insights into the binding and selectivity of the calcium channel. The replacement of one or more of the glutamate residues with neutral or positively charged residues severely lowers the conductance of the channel for divalent ions, and to a lesser extent for monovalent ions [18, 153]. Also, the block of monovalent currents by divalent ions is severely hampered, only arising at much higher divalent concentrations than for wild type channels [18, 63, 105, 216], giving evidence that the glutamate residues form a single binding zone leading to the high selectivity of the channel.

Here we attempt to replicate these experimental findings using our model calcium channel. In the BD simulations, we mimic the experimental site-directed mutagenesis by removing one of the charges representing the glutamate residues. With only three remaining glutamate residues in the channel, we find that the current is maximized when the charge on each amino acid is a full 1.6×10^{-19} C. That protonation should occur to a lesser degree in the mutated channel is plausible because there is less charge in the channel to attract and bind protons, and protonation is believed to be due to a cooperative effort of two or more glutamates [35, 36, 145].

Examination of the potential energy profiles with three glutamate charges shows that the energy wells become less deep, so they are expected to be less effective in attracting cations. In Fig. 8.18 A we show how the selectivity of the channel for Ca over Na, and the effectiveness of calcium block, diminish when the innermost (squares) or outermost (triangles) glutamate group is removed, compared to when all are present (filled circles). The plot shows the dependence of the sodium current on calcium concentration normalised by the maximum value in the same way as in Fig. 8.16 A. As noted earlier the values in this plot are extrapolated from values at higher concentrations. We find that the removal of one of the glutamate groups results in calcium ions taking longer on average to enter and block the channel, suggesting that sodium ions get more of a chance to permeate through the channel and so it becomes less selective. When one of the central groups is removed we find the shift in selectivity is of similar range to the cases shown. For comparison we have shown some of the experimental data from Yang et al. [216] in Fig. 8.18 B. These curves show the fractional lithium current passing through the channel as a function of calcium concentration and indicate the range of selectivity shift when one of the glutamate groups is replaced with glutamine. Our BD results show a shift in selectivity similar to that found experimentally, but the range of the effect is not as large. Naturally, a more accurate modeling of the channel is required to improve agreement with the experiment.

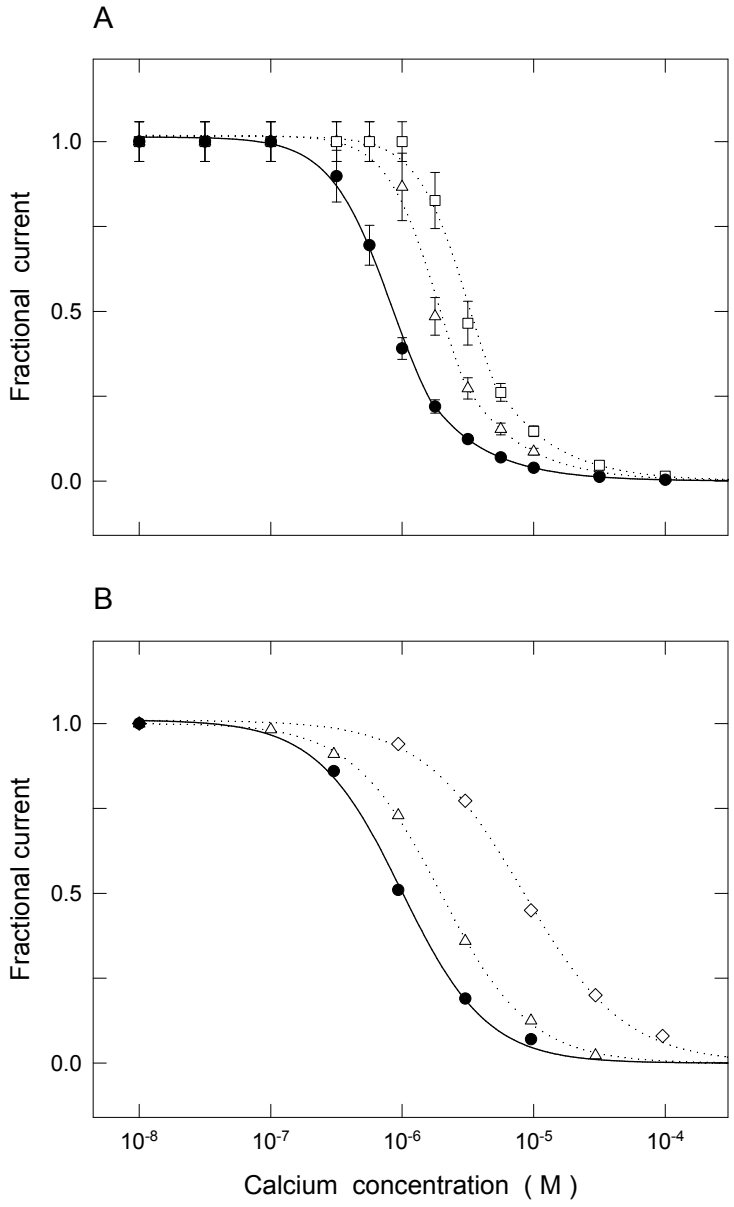

Figure 8.18: (A) The effect of removing glutamate charges on the channel selectivity in our model is shown by plotting the sodium current passing through the channel at different calcium concentrations with all four glutamate charges in place (filled circles), the outermost glutamate charge removed (triangles) and the innermost glutamate charge removed (squares), otherwise all conditions are as in Fig. 8.16 A. Data points come from the simulation of 35 blocking events. (B) A selection of the experimental data with all glutamate residues in place (filled circles) and when two different residues are replaced with glutamine (triangles and diamonds) from [216] is shown for comparison.

8.7 Conclusions

Although the crystal structure of the calcium channel is not yet known, we have constructed a model of the calcium channel using constraints derived from a number of experimental measurements. For the purposes of carrying out electrostatic calculations and BD simulations, this model is a rigid and fixed structure. Most notably the channel contains a narrow region surrounded by the glutamate residues near the extracellular end that forms the selectivity filter of the channel and is responsible for many of the channel's distinctive characteristics. The narrowness of this section of the channel prevents ions from passing each other making this a single file model, a point which is essential for explaining the mechanism of calcium block. The highly charged glutamate groups create a deep potential well which attracts surrounding cations. Once an ion enters this region of the channel, the depth of this well makes it difficult for that ion to exit on its own. Thus, this section of the channel is permanently occupied and roughly corresponds to the binding site discussed in reaction rate models. It is worth noting that binding in this model is simply an electrostatic phenomenon created by the charges on the glutamate residues, and no chemical bonding or flexible amino acid groups are required. The model shape also has a wide but short external vestibule responsible for the attenuation of calcium current by sodium ions. The remainder of the channel is made up of a wider central chamber converging to a narrower intracellular entrance, similar in shape to the recently crystallized KcsA potassium channel.

Despite several gross simplifications in its construction, our rigid model is able to give a very clear explanation for many of the observed properties of calcium channels and reproduces a number of experimental results. We have demonstrated that permeation is a multi-ion process (2 ions for calcium and 3 ions for sodium), and the Coulomb repulsion plays a crucial role in this process. Selectivity arises from the strong electrostatic attraction of a divalent ion in the energy well and the inability of a monovalent ion to push it out. The conductance values of calcium and sodium ions closely match the experimental data. Similarly, the current-voltage and conductance-concentration curves deduced from BD simulations bear close resemblances to those measured experimentally. We also offer plausible physical explanations for the anomalous mole fraction effect between calcium and sodium and the results obtained from studies involving site-directed mutagenesis.

There are several fine details of the channel that stochastic dynamics simulations cannot unravel. Among these are the permeation or selectivity sequence among monovalent and divalent ions (eg. Ba^{2+} conducts more rapidly than Ca^{2+}) and the blockage of the channel by certain divalent ions, such as nickel and zinc. We

expect that the differences between the permeation properties of these ion types is due to differences in how they interact with surrounding water molecules. The physical mechanisms underlying these phenomena may be elucidated by using molecular dynamics simulations, or if that fails, through *ab initio* methods. Because these methods are computationally very intensive, they cannot be used directly in modeling conductance of ion channels. Thus, to capture all these details in one theoretical model we need to develop a computational approach that combines molecular and Brownian dynamics simulations, the former explaining microscopic properties of the channel and providing parameters that can be used in the latter to explain its conductance and other related properties.

Chapter 9

Continuum Electrostatics and the Gramicidin Channel

9.1 Abstract

We investigate the validity of continuum electrostatics in the gramicidin A channel using a recently determined high-resolution structure. The potential and electric field acting on ions in and around the channel are computed by solving Poisson's equation. These are then employed in Brownian dynamics simulations to obtain concentration profiles and the current passing through the channel. We show that regardless of the effective dielectric constant used for water in the channel or the channel protein, it is not possible to reproduce all the experimental data on gramicidin A. Thus continuum electrostatics cannot provide a valid framework for the description of ion dynamics in gramicidin channels. Using experimental data and molecular dynamics simulations as guides, we have constructed potential energy profiles that can satisfactorily describe the available physiological data. These profiles provide useful benchmarks for future potential of mean force calculations of permeating ions from molecular dynamics simulations of gramicidin A. They also offer a convenient starting point for studying structure-function relationships in modified gramicidin channels.

9.2 Introduction

Gramicidin A (GA) is an antibiotic polypeptide that consists of 15 amino acid residues. Its β-helical, head-to-head dimer in membranes forms a single-file ion channel [205] that selectively conducts monovalent cations, binds divalent cations and rejects all anions (for reviews see, [11, 27, 107, 208]). Recent high-resolution structures of the GA channel have been determined from solution NMR [15] and

solid-state NMR studies [103, 104, 186]. In the absence of structural information for biological ion channels, the GA channel has been the main focus of theoretical investigations for a long time [155, 177]. The recent determination of the crystal structure of the KcsA potassium channel [58] has now shifted the attention to biological ion channels. Nevertheless, with its simple and well-defined structure and ample functional data, the GA channel should continue to play a prominent role as a test bed for theories of ion permeation.

Modeling of the GA channel has evolved from simple electrostatic calculations with rigid dielectric boundaries [98, 120, 144] to sophisticated all-atom MD simulations with GA embedded in a lipid bilayer and solvated with water [39, 214, 215]. These developments are reviewed in several articles to which we refer for a complete list of references [155, 161, 177]. Most of the potential or free-energy profiles of ions obtained in these MD studies are in qualitative agreement with the observed binding sites at each end of the channel and a central barrier in between them. However, the calculated energy barriers for the translocation of ions are in the range of 20–30 kT [99, 176], which are too high to predict the experimental conductances. Indeed, these profiles have been tested by McGill and Schumaker [139] by inserting them into a diffusion theory of permeation. They found that the magnitudes of the profiles had to be reduced substantially to reproduce the observed currents. For the microscopic models, the problem with the profiles most likely lies in the force fields used in the MD simulations. Recent high-resolution NMR studies of cation transport in the GA channel [199, 200] have shed further light on this problem by demonstrating that the GA peptide remains rigid upon cation binding and the ion is solvated by just two carbonyl oxygens. In contrast, early microscopic models typically predicted a rather flexible backbone with the carbonyl oxygens swinging by 20–40° so that four carbonyls and two water molecules provide adequate solvation for the cation in the channel. More recent studies suggest that a permeating sodium ion moves off axis to be solvated by the carbonyl oxygens so that the channel may be less flexible. Nevertheless, the carbonyl oxygens are still observed to rotate in substantial amounts in the presence of a sodium ion [215]. In the rigid scenario, the missing solvation energy is presumably provided by the water molecules in the channel having a more ordered structure than in the flexible models. In this regard, inclusion of the polarization effects in the standard MD force fields would be very desirable.

This development is a mixed blessing for the lower-resolution permeation theories such as the PNP equations and BD simulations. On the one hand, the NMR experiments appear to justify the assumption of a rigid channel structure used in

these theories, which is often one of the main criticisms of them. On the other hand, the long range order of the water molecules in the channel imposed by this rigid structure creates even more serious problems for employing continuum electrostatics in PNP and BD approaches. In a bulk solution, the electric field of an ion and hence the polarization of the surrounding water molecules drops as $1/r^2$. Because of the focusing of the electric field by the dielectric boundary, the reduction in the field of an ion in a channel is not as severe as in bulk. Nevertheless, continuum electrostatics predicts a substantial reduction in polarization of channel waters with distance from an ion, in disagreement with the MD predictions that the water dipoles are well aligned along the channel axis. Notwithstanding such criticism from the microscopic quarters [155, 174, 177], the PNP theory has recently been applied to the GA channel, giving an apparently successful description of the current-voltage relations [31, 88, 113]. In view of the problems of the validity of the PNP theory in narrow channels presented in chapter 6, this success is even more remarkable and warrants closer scrutiny. Thus, the main thrust of this work is to perform continuum electrostatic calculations using the high-resolution structure of the GA channel [104] and employ these results in BD simulations to see whether these methods can provide a consistent description of the available experimental data on the GA channel.

There are several outstanding issues in the GA channel that we will attempt to address in this study. The most pressing question is the value of the effective dielectric constant in the channel ε_c, and whether such a uniform value exists at all. While semi-microscopic calculations suggest $\varepsilon_c = 3$–5 [154], the bulk value of 80 is employed in the PNP calculations quoted above. To resolve this question, the whole range of ε_c values will be considered when solving Poisson's equation. A second issue is the origin of cation selectivity of the GA channel. It has been argued that because the GA peptide is charge neutral, there is no obvious mechanism to explain its valence selectivity. Various mechanisms based on intricate ion-peptide-water interactions have been proposed to explain this property [55, 172, 193]. However, in all these semi-microscopic and microscopic calculations, the GA peptide has a flexible structure, and it is not clear how much of these results would carry through if it were rigid. In addition, the PNP calculations of potential and concentration profiles inside the channel suggest that the valence selectivity can be understood simply in terms of the charge distribution in the peptide. It is important to ascertain whether the electrostatic interaction between an ion and GA peptide could indeed discriminate between cations and anions. Such a simple basis would obviate the need to look for more complicated explanations for valence selectivity.

If one cannot trust the free energy profiles obtained from MD simulations, and continuum electrostatics fails to give reasonable potential energy profiles, what other avenues are available for progress? Solving the inverse problem, that is, going from experimental data to potential may provide a more rewarding alternative to direct studies of the GA channel under the present circumstances. Using insights from experiments and simulations, one can construct a potential profile that provides a satisfactory description of physiological data when fed into BD simulations. Such a study was undertaken earlier by relating potential profiles to sodium currents using electro-diffusion equations and one-dimensional BD [38, 95]. This inverse technique is extended here to potassium permeation using 3-dimensional BD. Although one-dimensional BD should do a reasonable job of representing the single file motion in the narrow GA channel, the extension to 3-dimensions has the advantage that the entry and exit of ions to the channel can be explicitly modeled. It also allows ions to move off axis to interact more intimately with the carbonyl oxygens as seen in MD simulation of sodium ions. Compared to the continuum theory, BD accounts for individual ion motions and self energies in a direct manner which the electro-diffusion equations cannot.

Besides providing a better understanding and a united explanation for various channel observables, potential energy profiles found with this 'inverse' technique would also be useful in related studies of the GA channel and its analogs. For example, it could be used in constraining the free-energy calculations in MD simulations when searching for more appropriate force fields in a channel environment. Another area rich in applications is the structure-function relationship in modified GA channels [107]. Changes in the GA structure have ranged from mutations in the amino acid sequence to fluorination of specific residues that modulate dipole strengths [10, 12, 24, 28, 49, 152]. Especially in the latter case, where changes in dipole strength can be easily incorporated in the potential profile for the native structure, one could predict the expected functional changes with a minimal computational effort. Here we construct a potential profile for potassium ions that could be used for such purposes in modified GA channels.

9.3 Gramicidin A structure

A high-resolution structure of the GA channel has recently been determined from solid-state NMR spectroscopy via refinements of the initial structure against both the experimental constraints and the CHARMM global energy [104]. Here we use the atomic coordinates stored in the Protein Data Bank with the accession

code 1MAG. This structure is slightly different from that of Arseniev et al. [15], which has been employed in most of the GA model studies in the past (see below for a comparison of the two structures). For consistency with the high-resolution structure, the partial charges on the atoms are taken from the all-atoms PARAM22 [133] version of the CHARMM force field. The effect of using partial charges from another force field (AMBER, [46]) will be discussed in the Results Section.

To define the surface of the channel (and hence the dielectric boundary), the radii of atoms in the GA peptide are required. We employ the minimum set derived by Li and Nussinov ([126], Table VI). Following their recommendation, the Coulombic radius is used for the polar N and O atoms and the van der Waals radius for the rest of the non-polar atoms. (Had we used the van der Waals radius for all the atoms, the channel radius would be about 10% smaller, leading to a slightly higher self-energy for ions.) Slices of channel profiles generated by this data set are shown in Fig. 9.1 A and B.

The GA dimer is embedded in a neutral membrane of length 33 Å, modeled as a uniform dielectric medium (with dielectric constant equal to that of the GA peptide) without any charges or dipoles. This length and model matches that of relatively neutral glycerylmonoolein (GMO) membrane. It is also close to the thickness of diphytanoylphosphatidylcholine (DPPC) (35 Å), so that results of BD simulations can be compared with experiments involving both types of membranes, although the dipoles in the DPPC membrane may affect the current. Since GMO is wider than the GA dimer, hydrophobic matching is used in smoothly joining the membrane to the GA head groups [79] as indicated in Fig. 9.1. Finally, to complete the simulation system, cylindrical reservoirs of 30 Å radius and length are connected to each end of the channel. When filled with an electrolyte solution, these reservoirs provide an adequate representation of the intra- and extra-cellular baths.

As described in chapter 3, the calculation of potentials is too slow to be carried out at each time-step during BD simulations, and is too cumbersome to be pre-calculated and stored when employing a complete 3-dimensional shape. For this reason, in BD simulations, an axially symmetric form of the channel boundary is employed for convenience (Fig. 9.1 C). This shape is generated by averaging the radial distance around the circumference and modifying it further until the calculated potential profile roughly matches the one obtained from the original shape shown in Fig. 9.1 A and B. Provided these potential profiles are very similar, the use of a symmetric shape should not modify our results.

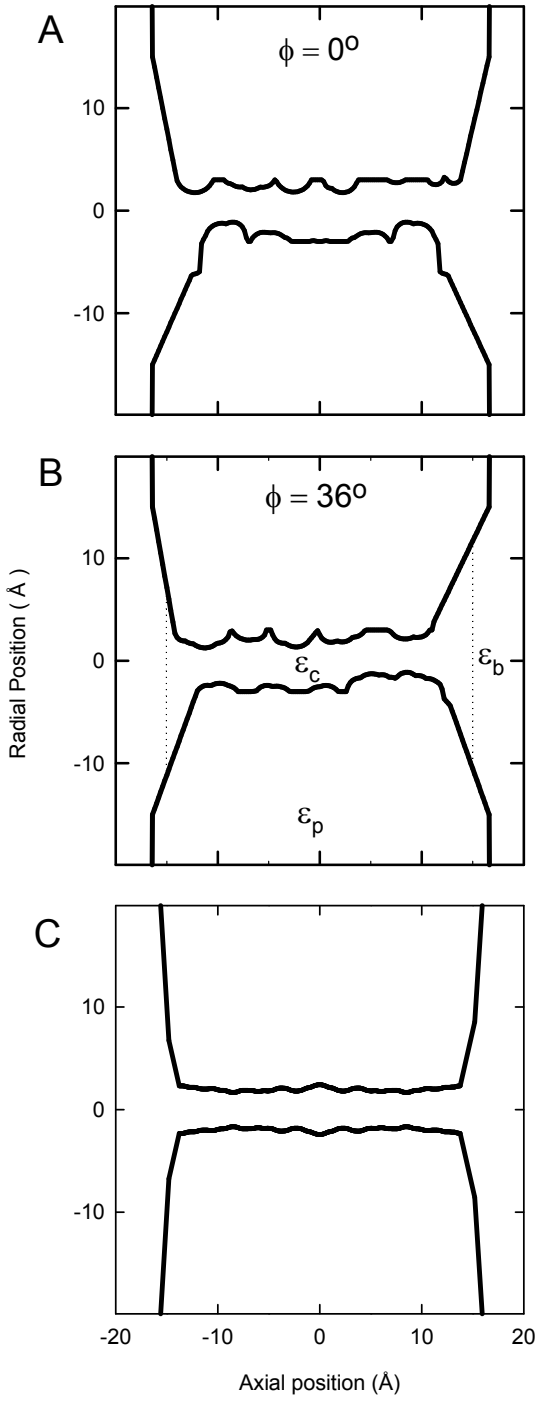

Figure 9.1: (A) and (B) Two slices of the channel boundary down the central axis at different azimuthal angles ϕ. The regions of different dielectric constant are noted in (B). The values shift from the channel value (ϵ_c) to the bulk value (ϵ_b) smoothly over a 5 Å distance centered about the dotted lines. (C) A transverse section of the axially symmetrized channel shape.

9.4 Modifications to BD simulations

Due to the narrowness of the gramicidin channel, ions and water molecules must move in single file. This presents a further constraint on the motion of ions in the channel not encountered in previous BD simulations. If there are two ions in the channel, then they will be separated by an integer number of 'trapped' water molecules and the distance between the ions must remain relatively constant. The intervening water molecules will prevent the ions getting closer, and gaining a larger separation would create a vacuum in the channel. We ensured that this condition is held in our simulations by subjecting both ions to the following additional force whenever a second ion entered the channel:

$$F(r) = a(1/r^9 - 1/r_0^9). \tag{9.1}$$

Here r is the distance between the ions and r_0 is a reference separation equal to the nearest integer number of water molecule diameters when the second ion first appears within the narrow section of the channel. This allows the ions to move freely back and forth whilst constraining the separation between them to remain roughly constant while they are both in the pore. The choice of the water diameter in determining r_0 is not of critical importance, and we simply use the canonical value of 2.8 Å.

9.5 Results

9.5.1 Electrostatic calculations

Potential energy profiles of single ions reveal the binding sites and barriers in the channel and thus provide clues on the permeability characteristics of a proposed model. The absence of a well at an observed binding site or presence of a large barrier (which would prevent conduction) would be sufficient grounds to reject a model without carrying out expensive simulation work. The profiles in this section are obtained from a finite difference solution of Poisson's equation using the non-symmetric channel boundary (Fig. 9.1 A and B). In Fig. 9.2 A we show how the potential energy profile of a monovalent cation in the GA channel changes as the effective dielectric constant of channel waters is reduced from $\varepsilon_c = 80$ to 5. Here the dielectric constant of the GA peptide is set to $\varepsilon_p = 2$, representing its electronic polarizability. The very low values of $\varepsilon_c \sim 5$ suggested by microscopic calculations [154], are seen to lead to huge barriers ($\sim 55\ kT$). This will prevent conduction of ions at any realistic applied potential as also noted by Partenskii et al. [154].

When a larger polarizability is assumed for the GA peptide ($\varepsilon_p = 5$), the barriers are reduced by a factor of 2–3 but still remain too large to permit conductance for low ε_c values (Fig. 9.2 B).

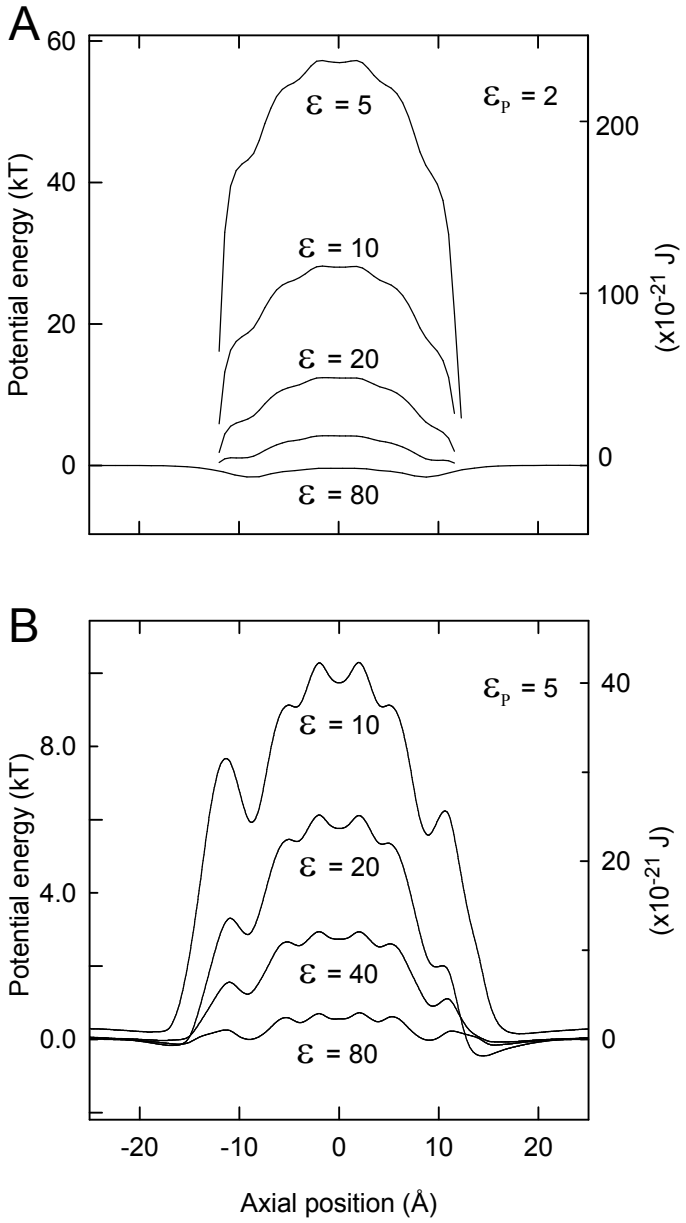

Figure 9.2: Dependence of potential energy profiles on the effective dielectric constant of water in the channel (ε_c). The dielectric constant of the protein is $\varepsilon_p = 2$ in (A), and $\varepsilon_p = 5$ in (B).

At the other extreme of $\varepsilon_c = 80$ employed in the PNP calculations [31, 88, 113], the energy profile is almost flat, as shown in the lower-most profile in Fig. 9.2 A. A more detailed picture of this profile is given in Fig. 9.3. At a first glance, this profile with wells near the entrances and a central barrier appears quite reasonable. However, at only 1.5 kT, the wells are not deep enough to provide binding sites, nor is the barrier enough of an impediment to lead to the saturation of current. These points will become obvious when we present concentration profiles and current-concentration curves obtained from BD simulations below. In contrast, the potential profiles obtained in PNP calculations exhibit a deep potential well across the entire length of the channel. The discrepancy has been shown to arise from the neglect of ion self-energies in PNP (see chapter 6). To make this point more explicit, we decompose the profile obtained with $\varepsilon_c = 80$ and $\varepsilon_p = 2$ into the self-energy part due to the reaction field from the dielectric boundary (calculated by setting the partial charges in the peptide to zero) and the ion-peptide interaction part due to the partial charges, as shown in Fig. 9.4 A. It is seen that the flat profile follows from the near cancellation of these two large components which have opposite signs. One would end up with a deep potential well if the self-energy term were ignored.

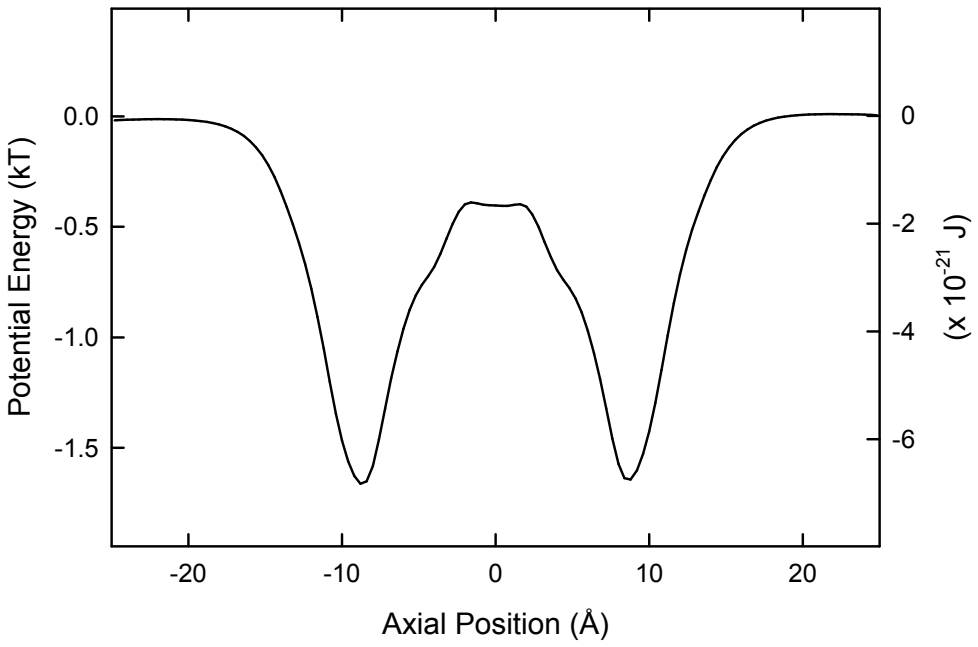

Figure 9.3: A more detailed picture of the bottom profile shown in fig. 9.2 A, i.e. $\epsilon_c = 80$ and $\epsilon_p = 2$.

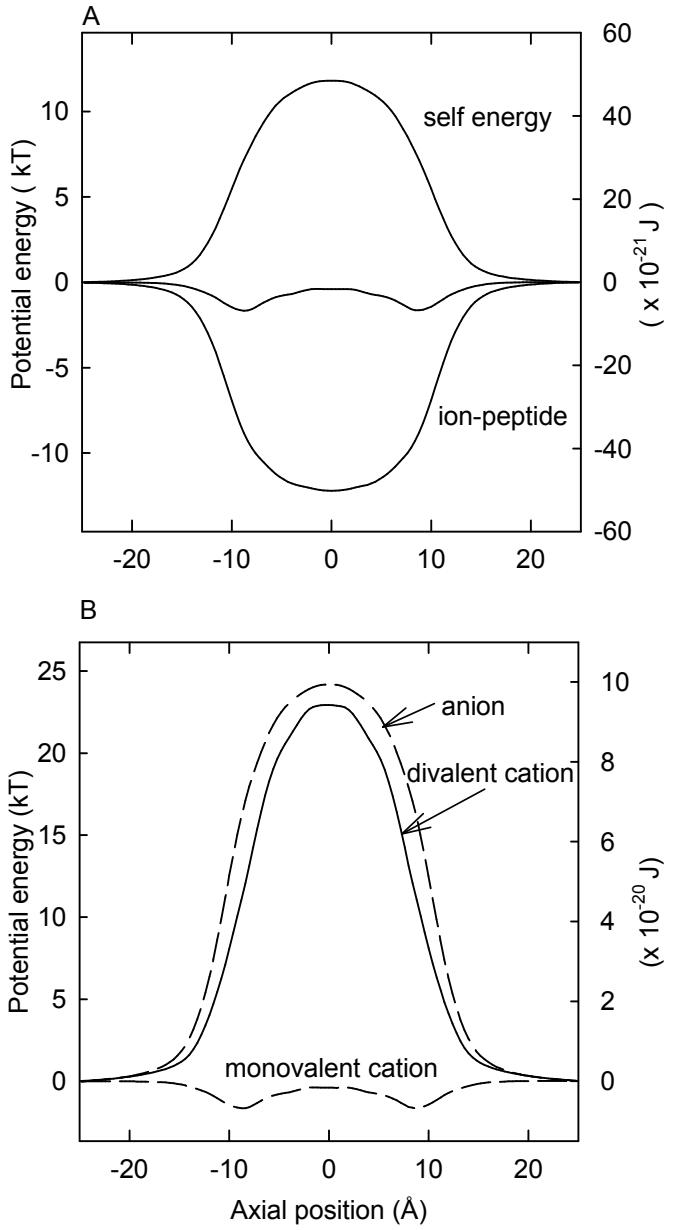

Figure 9.4: (A) Individual contributions to the the energy profile for $\varepsilon_c = 80$ and $\varepsilon_p = 2$ (middle) from the self-energy (top) and ion-peptide interaction terms (bottom). (B) Potential energy profiles for a divalent cation (solid line) and a monovalent anion (dashed line) for the above choice of ε values. The monovalent cation result (dashed line) is included for reference.

Values of ε_c in between the two extremes discussed above do not provide any improvement either. While the barrier height increases with decreasing ε_c (see,

Fig. 9.2), the wells nearly disappear, thus disagreeing with the observed binding sites. This point will again be made clearer with the BD simulations below. In the following continuum electrostatic calculations, we will use the common $\varepsilon_c = 80$ and $\varepsilon_p = 2$ values as we have seen that variations from these only lead to a worse agreement with the experimental data.

We next consider the potential energy profiles for divalent cations and monovalent anions (Fig. 9.4 B). Experimentally, the former bind and block the GA channel and the latter are rejected. From a continuum electrostatics viewpoint, comparing the energy profiles provides a stringent test of the model, because they are not independent quantities but follow directly from the monovalent ion results in Fig. 9.4 A. In fact, if we denote the valence of the ion by z, the self-energy term of a monovalent ion by U_s and the ion-peptide term by U_p, the profile for a divalent cation is given by $U_2 = 4U_s + 2U_p$ and the one for monovalent anion by $U_{-1} = U_s - U_p$. Because $U_p \approx -U_s$, one expects $U_2 \approx U_{-1} \approx 2U_s$. This explains the similarity of the profiles for divalent cations and monovalent anions in Fig. 9.4 B. The absence of any potential wells in the divalent cation profile provides the most direct and clear evidence for the failure of continuum electrostatics in the GA channel. When such a large barrier is used in BD simulations, it results in negligible ion concentrations inside the channel in contradiction with the experimentally observed binding of divalent cations (see below). The large barrier for anions, on the other hand, provides an obvious mechanism for valence selectivity of the GA channel. Just like the divalent cations, anions would not enter the channel in the presence of a 25 kT barrier.

One may question the reliability of such an inference on valence selectivity from a continuum electrostatics calculation; after all, we have just condemned its use in the GA channel. To answer this query, we need to consider the results in Fig. 9.4 in more detail. From microscopic calculations, we know that both the self-energy and ion-peptide interactions are largely underestimated in electrostatic calculations with $\varepsilon_c = 80$. The large barriers observed at lower ε_c values would be canceled by the ion-dipole interactions due to the ordered channel waters, which is ignored in the continuum calculations. Clearly, these interactions are even more important for divalent cations so as to provide the permanent binding sites at the channel entrance. Switching the sign of a monovalent cation, however, changes basically the sign of the ion-peptide interaction leaving the other terms more or less intact. If the electrostatic results in Fig. 9.4 are underestimates as indicated by microscopic calculations, then the barrier for valence selectivity can only go up in more realistic calculations. Thus the proposed valence selectivity mechanism based solely on the distribution of charges in the GA channel appears to be a robust result.

It is important to check the sensitivity of the above results against variations in the GA structure. Two significant parameters in this respect are the coordinates and magnitude of the partial charges of the peptide atoms. In Fig. 9.5 A, we compare the profile obtained using the structure of Arseniev et al. [15] with that of Ketchem et al. [104]. The new profile has no wells and a 4 kT barrier, and could only lead to worse agreement with experimental data than the old one. Not surprisingly, the energy-minimized Ketchem structure leads to a lower profile than the Arseniev one. In Fig. 9.5 B, we show the effect of changing the partial charges from the CHARMM set (solid line) to AMBER (dashed line). The two sets have similar charges on the backbone atoms but the CHARMM charges are a factor of 2 to 3 larger for the side chain atoms. This explains the relative increase in the AMBER profile at the entrances (less negative charges) and decrease at the middle (less positive charges). Although the change in the profile is not significant, the disappearance of the central barrier can be viewed as a backward step. It is also worth noting that the failure to reproduce divalent binding sites is likely to be less dependent on the precise atomic structure than the monovalent profiles. As the divalent profile is dominated by the self energy, large variations in the position of the boundary would be required to obtain binding sites.

9.5.2 Brownian dynamics simulations

The potential energy profiles presented above explain in qualitative terms why continuum electrostatics fails in the GA channel. To make contact with experimental data and thus demonstrate this inadequacy more quantitatively, we next perform Brownian dynamics simulations. The axially symmetric boundary is employed in solving Poisson's equation here for reasons discussed in section 9.3.

There have been many experimental I–V measurements in the GA channel, and the success of the PNP equations in matching these have been used as an argument for its applicability in narrow channels [31, 88, 113]. Here we wish to point out that, as long as the diffusion coefficient of ions in the channel is a free parameter, fitting linear I–V curves poses no problem for any channel model. As an example, the I–V curve obtained from BD simulations of a 500 mM KCl solution with $\varepsilon_c = 80$ (filled circles) is compared to experimental data [9] (open squares) in Fig. 9.6. The bulk values of the diffusion coefficients are employed for both ionic species in the reservoirs but the diffusion coefficient of K^+ ions inside the channel, D_K^{ch}, is reduced by 80% in order to fit the data. Note that such a reduction is not required for the Cl^- ions because they do not enter the channel. It is worthwhile to emphasize that unlike the PNP equations, the current in the channel is not linearly proportional to

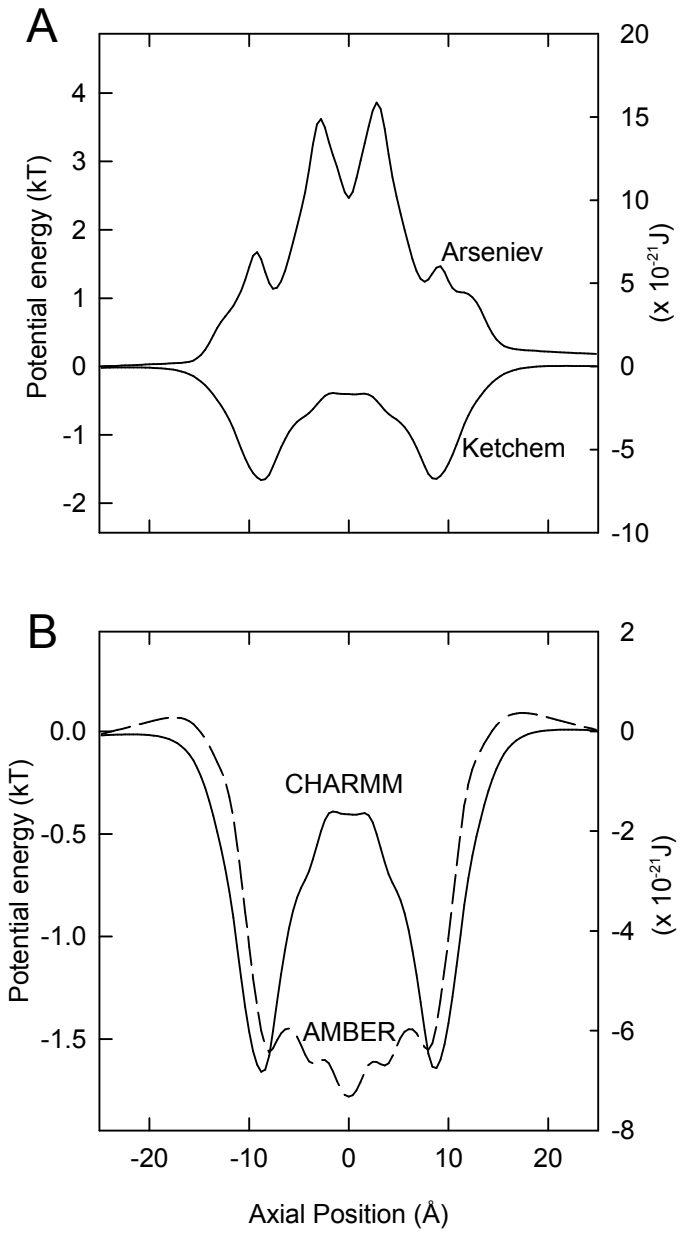

Figure 9.5: (A) Comparison of the potential energy profiles obtained using the structure of Ketchem et al. [104] and Arseniev et al. [15]. CHARMM partial charges are employed in both cases. (B) Effect of using different sets of partial charges on the potential energy profiles; CHARMM (solid line), AMBER (dashed line). Ketchem et al. [104] structure is used in both cases.

the diffusion coefficient in BD simulations. This shape of the current vs. diffusion coefficient depends on the depth of the energy well and height of the energy barrier (see Fig. 9.11 later). For the energy profile used to obtain Fig. 9.6, the current is reduced by less than a factor of 2 when $D_{\mathrm{K}}^{\mathrm{ch}}$ is suppressed down to 10% of its bulk value. A further reduction causes a steep decrease in current. It is worth noting that ions never pass each other in the channel during simulations, the single file nature of GA permeation is reproduced.

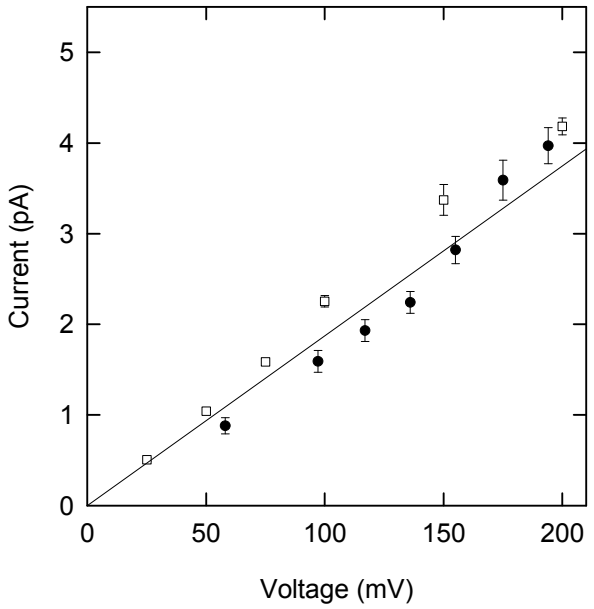

Figure 9.6: Current-voltage relationships obtained from BD simulations of a 500 mM KCl solution (filled circles fitted with a line). Error bars have length one standard error. Experimental data [9] is shown by the open squares.

The results plotted in Fig. 9.6 show that this model has no difficulty in fitting the I–V data of the GA channel. However, we next show that this continuum electrostatic model of the GA channel fails completely when its predictions are compared with the observed binding sites and conductance-concentration curves. In Fig. 9.7, we show the concentration profiles of K^+ ions in the channel without an applied potential (A), and with a 200 mV applied potential (B) obtained from BD simulations using a 500 mM KCl solution as above. The potassium concentration in the channel displays little hint of the expected binding sites at around ± 11 Å [199]. To be consistent with this data, we should see two large concentration peaks

separated by an obvious depression. In our BD data, the central barrier causes a dip in the concentration profile in the absence of a driving force (A), but as soon as a potential difference is applied, this dip disappears (B) as ions can easily climb it. Thus both the wells and the barrier in the potential energy profile are too weak to yield a concentration profile consistent with experiments. It is interesting to note that the channel is only occupied about 10% of the time, and almost never doubly occupied. The PNP calculations also predict featureless profiles similar to BD, except that the cation concentration in the GA channel is enhanced by an order of magnitude compared to the bath solution, which is a direct consequence of the energy well created by neglecting ion self-energies as discussed earlier [31, 113].

In Fig. 9.8, we show the concentration profile for Ca^{2+} ions obtained under similar circumstances (500 mM $CaCl_2$ solution, 200 mV applied potential). As emphasized above, the large barrier (Fig. 9.4 B) prevents the entry of Ca^{2+} ions into the GA channel. Because the barrier gets higher with decreasing ε_c, we will not see binding sites for any value of dielectric constant. The lack of binding sites for Ca^{2+} ions in GA thus provides the most direct evidence for the failure of continuum electrostatics.

A final piece of evidence demonstrating the failure of continuum electrostatics in the GA channel is its inability to describe the observed saturation of conductance with increasing concentration. This saturation is a direct result of rate limiting steps in the channel and will not occur unless the ion has to climb substantial energy barriers with heights greater than 1.5 kT to move out of the energy wells in the channel [42]. In this respect, the barrier in the GA channel is too small to induce the saturation behavior (Fig. 9.2 A). A BD study of the current-concentration curve for symmetric KCl solution confirms this expectation as shown in Fig. 9.9. The potassium current keeps increasing with concentration with no sign of saturation, in disagreement with the experimental data in which currents clearly saturate with a half-maximum value of $K_s \approx 0.23$ M [9].

So, although this model accurately reproduces the observed I–V data, it fails to predict the observed binding sites or the saturation of current with increasing concentration. Given these results one clearly has to look beyond the I–V curves to test the validity of a theoretical approach. On the basis of the complete evidence presented above, we have to conclude that this continuum electrostatics model fails in the GA channel.

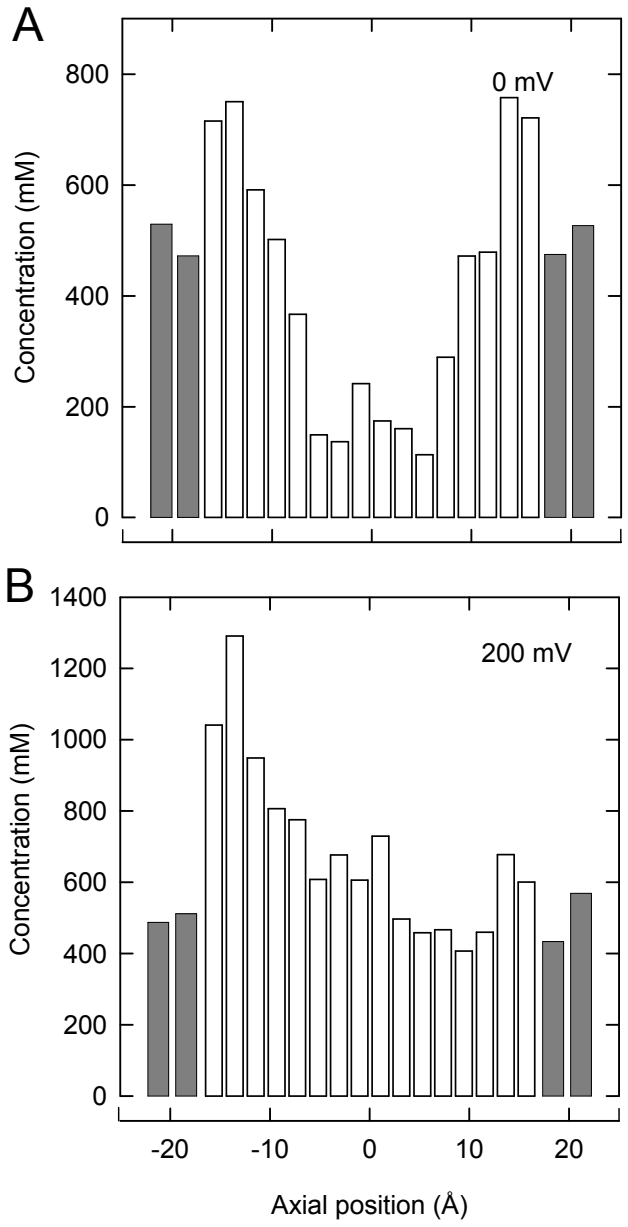

Figure 9.7: Concentration profiles for potassium ions in the GA channel with no applied potential (A) and 200 mV applied potential (B). In both cases, a 500 mM KCl solution is used in the reservoirs. The pore region is divided into 16 equal segments, and each reservoir into two segments. The reservoir concentrations are represented by shaded bars.

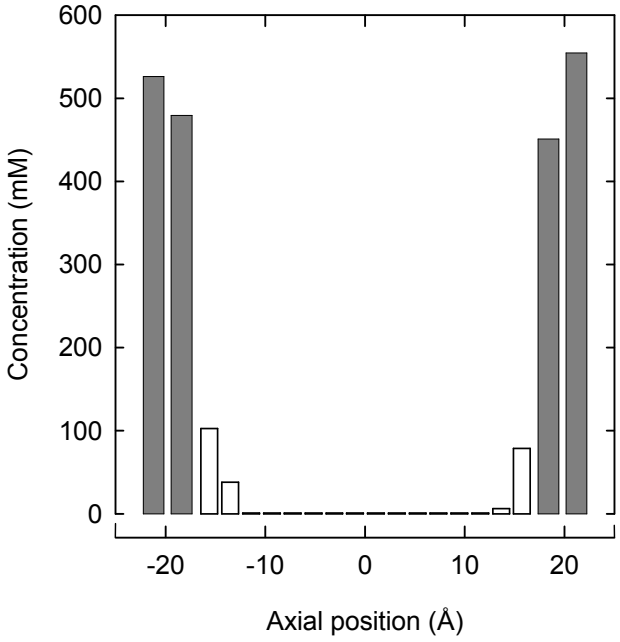

Figure 9.8: Concentration profiles for calcium ions in the GA channel, obtained using a 500 mM $CaCl_2$ solution and 200 mV applied potential.

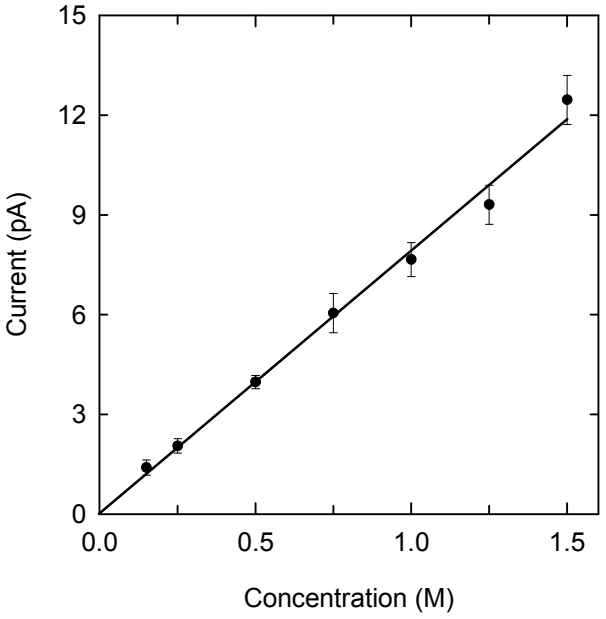

Figure 9.9: Conductance-concentration curve for potassium ions obtained with a 200 mV applied potential fitted by the solid line.

9.5.3 Potential energy profiles

The failure of continuum electrostatics in the GA channel leaves MD as the only reliable method for the calculation of forces on ions in this channel. Unfortunately, as noted in the introduction, none of the MD simulations of GA carried out so far have yielded free-energy profiles that can reproduce experimental currents. The force fields currently used in MD can be improved by including polarization effects, and hopefully, once this is done, MD calculations of potentials of mean force will give more satisfactory results. In the mean time, one can pursue the study of structure-function relationships in GA indirectly by "guessing" the potential profile that will reproduce the available data. Here we give an example of this inverse method by constructing a potential energy profile for potassium ions in the channel.

The fact that GA is a very narrow, single-ion channel (except at high concentrations) makes this task relatively easy. As a first approximation, we can find the profile along the channel axis and supplement it with a harmonic constraint in the radial direction, thus reducing the search to a one-dimensional problem. The shape of the axial profile is, of course, well known from both the experiments and MD simulations. As shown in Fig. 9.10, it has two binding sites at about ± 11 Å, and a central barrier in between them. Here we ignore finer details such as small oscillations in the barrier that are not likely to significantly influence the overall conductance properties of GA. Note also that the exact location of the energy wells (for example placing them at ± 9 Å) does not have much bearing on the channel conductance found in BD. This is much more dependent on the depth of the wells, U_{w}, and the height of the central barrier, U_{b}. These are two parameters that need to be determined from the BD simulations by fitting the calculated conductance under different applied potentials and concentrations to the available physiological data. In the profile illustrated in Fig. 9.10, these two parameters, U_{w} and U_{b} are fixed at 8 kT and 5 kT.

The diffusion coefficient of K^+ ions in the GA channel is expected to be considerably suppressed in the GA channel [175]. However, the spread in the estimated values of $D_{\mathrm{K}}^{\mathrm{ch}}$ is too large to be able to choose a particular value. Therefore, we consider $D_{\mathrm{K}}^{\mathrm{ch}}$ as a third parameter to be determined from the BD simulations. The variation of current with $D_{\mathrm{K}}^{\mathrm{ch}}$ is illustrated in Fig. 9.11 for the profile with $U_{\mathrm{w}} = 8\ kT$ and $U_{\mathrm{b}} = 5\ kT$. The current increases linearly with $D_{\mathrm{K}}^{\mathrm{ch}}$ at first but deviates from it with increasing $D_{\mathrm{K}}^{\mathrm{ch}}$. This nonlinearity arises from the fact that ions do not diffuse in a flat energy landscape but have to surmount energy barriers. The results in Fig. 9.11 demonstrate that the channel conductance can be easily fitted by adjusting the diffusion coefficient of K^+ ions.

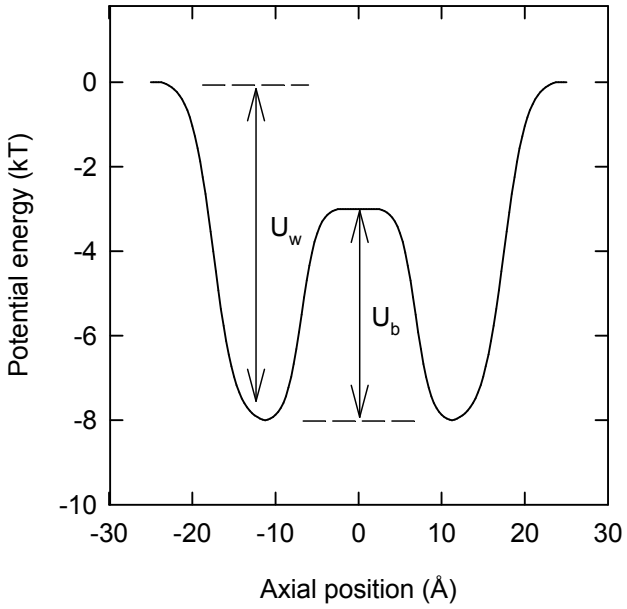

Figure 9.10: Shape of the potential profile used in the inverse method. The two basic parameters are the depth of the wells U_{w} and the height of the barrier U_{b} as indicated by the arrows. Note that the well depth refers to the zero potential in the reservoir but the barrier height is measured with respect to the well minimum. The curved parts are produced using a Fermi function of the form $1/\{1 + \exp[\pm(z - z_0)/d]\}$. The width of the well at half-max is about 10 Å. The profile shown with $U_{\mathrm{w}} = 8\ kT$ and $U_{\mathrm{b}} = 5\ kT$ gives the best description of the physiological data on GA.

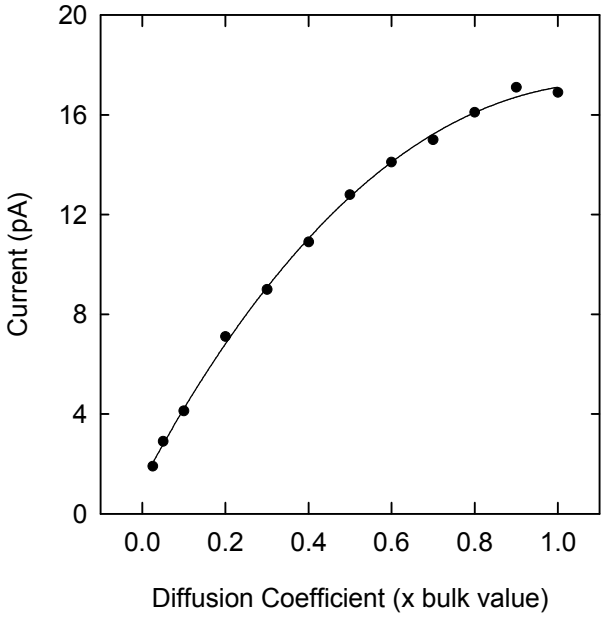

Figure 9.11: Variation of the channel currents with the diffusion coefficient of K^+ in the channel. The depth of the well and height of the barrier used are, respectively, 8 kT and 5 kT. The results are obtained using an applied potential of 200 mV and an ionic concentration of 500 mM.

To see how the U_w and U_b values influence the channel conductance, we have carried out BD simulations using a wide range of values (Fig. 9.12). Here an applied potential of 200 mV is used with a 500 mM KCl solution, and D_K^{ch} is reduced to 0.1 times the bulk value. Each curve in the figure shows how the channel current decreases exponentially with the increasing barrier height U_b for a fixed value of U_w. Note that when U_b is fixed, the current increases with U_w because a deeper well is more successful in attracting the K^+ ions into the channel and thereby facilitating their conduction. The broken horizontal line across the figure indicates the experimentally measured current of 4 pA [9]. Thus, for a given well depth, one can find a matching barrier height that will reproduce the experimental conductance. The requirement that the wells provide binding sites excludes the very low values for U_w (i.e. $U_w > 4\ kT$), but otherwise it does not help in constraining the potential parameters further. This exercise exposes the dangers of relying exclusively on fitting linear I–V curves in model studies. Not only can one fit the channel conductance for a given potential profile by adjusting the diffusion coefficient, but even when D is fixed, there are many sets of potential profiles that can fit the observed conductance. Thus conductance alone cannot provide an adequate test for a phenomenological permeation model.

We next consider the current-concentration curve and study its sensitivity to the potential parameters and diffusion coefficient. The saturation seen in experimental current-concentration curves cannot be reproduced for all values of diffusion coefficient. For a given D_K^{ch} a potential profile cannot necessarily be found which can reproduce the observed saturation. A brief survey of possible diffusion values showed that saturation did not arise when D_K^{ch} was larger than 0.3 times the bulk value. This indicates that the diffusion coefficient is more than just a scaling factor—it plays a dynamical role in ion permeation, influencing the saturation properties of the channel.

A successful description of saturation, however, is possible when the potential parameters are chosen as $U_w = 8\ kT$, $U_b = 5\ kT$, and D_K^{ch} is reduced to 0.1 times the bulk value. In the remaining figures, we study in greater detail the consequences of this chosen parameter set. In Fig. 9.13, the saturation curves obtained under two different applied potentials (100 and 200 mV) are compared to the experimental data of Andersen [9]. The calculated curves follow the experimental result closely at both driving potentials. The simulation results are fitted with a Michaelis-Menten curve as indicated by the solid lines in the figure. The calculated half saturation value of 250 mM is in good agreement with the experimental value of 230 mM at 200 mV. The corresponding values at 100 mV are 90 mM (calculated) and 105 mM (experimental).

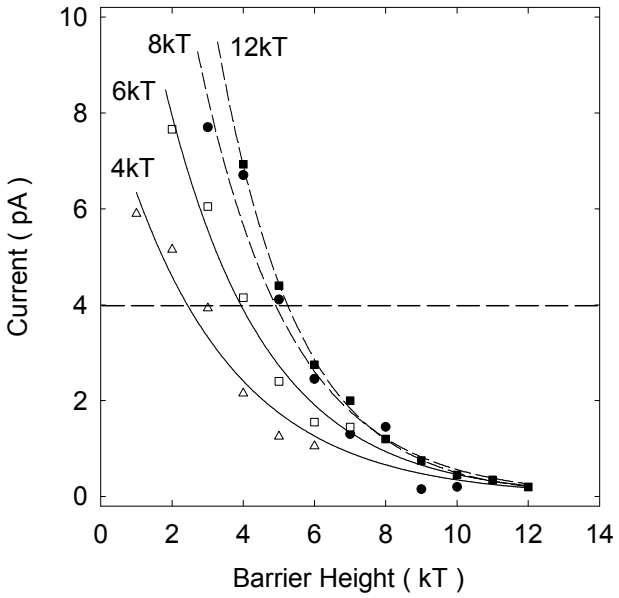

Figure 9.12: Variation of the channel current with the barrier height U_b for fixed values of U_w (indicated at the top of each curve). An applied potential of 200 mV and a 500 mM KCl solution are employed in the BD simulations. The diffusion coefficient of potassium ions in the channel is suppressed to 0.1 times the bulk value. Each set of data is fitted by an exponential decay function (solid and dashed lines). The horizontal dashed line indicates the experimental current value [9].

Fig. 9.14 shows an I–V curve obtained from simulation of a symmetric 500 mM KCl solution. The results of our simulations (filled circles) are compared with the experimental measurements (open circles) [9]. The agreement with the data is again very good.

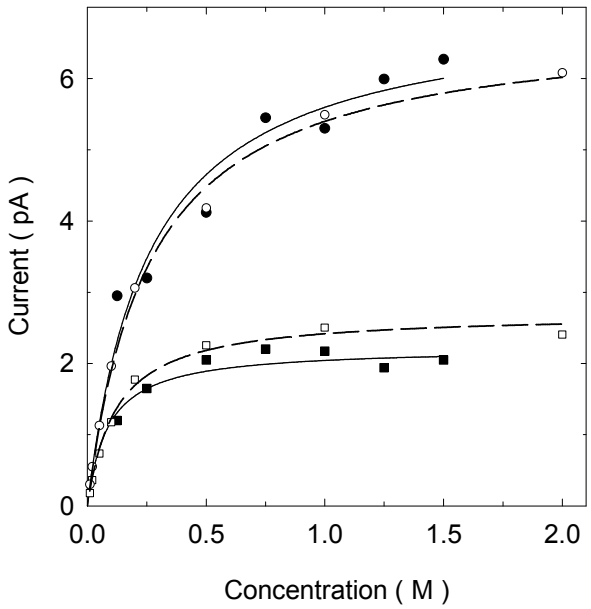

Figure 9.13: Saturation of current with concentration at two applied potentials, 100 mV (bottom curve) and 200 mV (top). The profile in Fig. 9.10 is used in BD simulations with $U_{\rm w} = 8\ kT$, $U_{\rm b} = 5\ kT$ and $D_{\rm K}^{\rm ch}$ reduced to 10% of the bulk value. The experimental data of Andersen [9] are superimposed on the figures (open circles and open squares).

Finally, in Fig. 9.15, we show the concentration profiles for K^+ ions in the GA channel obtained from a symmetric 500 mM KCl solution. As expected, the ion concentration is very large at the binding sites and depressed in the middle, regardless of whether there is an applied potential of 200 mV or not. The magnitude of the concentration may appear too large at first sight. This is simply due to the small volume available at the binding sites. In fact, there are only about 0.75 ions on average at each site in the case shown. This also indicates that the channel is often multiply occupied, unlike when the flatter profile found from continuum electrostatics is used, as the larger wells more easily attract ions into the channel and retain them at the binding sites. The number of ions in the channel increases with concentration, as at higher concentrations ions can find their way into the

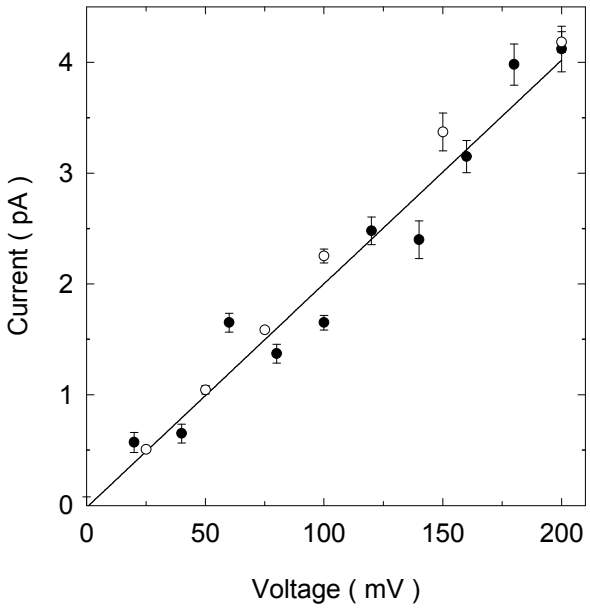

Figure 9.14: Current-voltage relationship obtained with BD simulations using the profile in Fig. 9.10. The results obtained by using 500 mM KCl solution (black circles fitted with a line) are compared with the experimental data [9], shown by open circles.

channel more quickly. For example at 150 mM there are on average 0.8 ions in the channel whilst at 1 M there are 1.75. An analysis of ion trajectories in the multiply occupied channel shows that the inter-ion separation remains roughly constant for any ion pair.

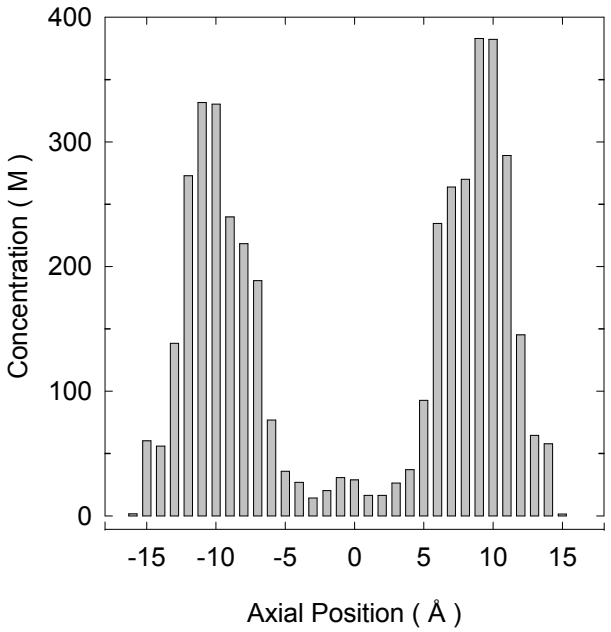

Figure 9.15: Concentration profiles for potassium ions in the GA channel as in Fig. 9.7, but using the profile in Fig. 9.10., with no applied potential.

While it is impossible to prove the uniqueness of the parameter set we have obtained, our results nevertheless suggest that large variations from these values are unlikely to lead to a satisfactory description of the data. For example, Fig 9.12 indicates that the potential parameters $U_{\rm w} = 12\ kT$, $U_{\rm b} = 5\ kT$ may also work, although the larger wells will increase the probability of multiple occupancy. It is also of interest to compare our chosen profile with those of Chiu and Jakobsson [38]. They reproduce sodium conductance properties via electro-diffusion equations using a similar potential profile with the parameters $U_{\rm w} = 5.4\ kT$, $U_{\rm b} = 4.2\ kT$, and a diffusion coefficient for Na^+ ions that is 0.07 times the bulk value. McGill and Schumaker [139] also find that similar well depths and barrier heights are required to match experimental conductances using their diffusion theory. Thus, there is a reasonable congruence between all the sets of parameters.

The saturation property of the GA channel is seen to provide the most sensitive

quantity for the purpose of determining the potential energy profile of ions. In most model studies of ion channels, conductance and I–V curves are studied in great detail while no attention is paid to the saturation curve. In fact, as illustrated here, reproducing the saturation curve provides a more stringent test for a permeation model and should be given more consideration in future studies.

9.6 Conclusions

Our main result is that continuum electrostatics using a rigid protein structure cannot provide a consistent description of all the available data on the GA channel. Surprisingly, the use of a dielectric constant of 80 in the channel seems to give the best results in our continuum electrostatics, despite the fact that from microscopic considerations such a high value seems unreasonable in the narrow GA channel. Although slight changes in the protein structure may alter the energy profiles, the experimental data limits the amount of flexibility allowed, and it seems unlikely that all the problems encountered could be overcome using a different or flexible protein. Given the obvious problems in describing polarization around an ion and the effect of water dipoles, we believe that continuum electrostatics should not be used to model GA. This applies to any model that relies on the solution of Poisson's equation using a dielectric continuum, such as most current BD simulations (in which the forces are calculated from Poisson's equation) and continuum theories such as Poisson-Boltzmann and Poisson-Nernst-Planck equations. This leaves MD as the only method for calculating the forces on ions in the GA channel. But, unfortunately, the force fields currently employed in MD studies are too crude for this purpose and require further refinement to be able to make contact with experimental data. We have used the inverse method to construct a potential energy profile for potassium ions that gives an adequate description of the available physiological data. It will be interesting to compare this profile with future profiles to be determined from MD with improved force fields. In the meantime, the inverse approach can be utilized to relate the structure of the GA channel to its function. Studies of asymmetric and bi-ionic solutions could provide further tests of our proposed potassium potential profile. Also, we expect that profiles for other monovalent ions species can be constructed to match their conductance values by making small changes to the potassium profile. Work in this direction is in progress.

An important question is whether the above results for the GA channel have any bearing on biological ion channels. Because GA was the only channel with a well defined tertiary structure for a long time, it became a model case for all ion channels.

The hope was that insights gathered from the study of the GA channel could be used in understanding the permeation properties of other channels. The determination of the KcsA structure [58] and subsequent studies of the permeation mechanisms in potassium [40, 41] and calcium channels [47] reveal that GA is not likely to fulfill this role. Both in terms of structure (single filing of water vs. presence of water filled cavities and vestibules) and ion dynamics (single-ion vs. multi-ion permeation mechanism), GA is very different to these biological channels. It is the long single-file chain of water molecules that creates problems when using continuum electrostatics to model the GA channel, as the use of uniform dielectric constants cannot mimic their long range polarization. In contrast, the continuum electrostatics-BD approach has been used successfully to reproduce a wide variety of experimental data when modeling biological ion channels, including the KcsA potassium channel [40, 41]. The reason for this is two-fold; first continuum electrostatics works reasonably well in the wider cavity and vestibule regions that form the major part of these channels, and secondly the selectivity filter regions where the single filing occurs are much shorter, involving only a few water molecules sandwiched between ions. That is, there are no long chains of water molecules as in the GA pore which seem to cause the problems seen here. Thus, we believe that GA is a very special channel that needs to be handled with extreme care. The rewards from its study are not to be found in getting direct insights about biological ion channels but rather constructing reliable models of permeation in a difficult test case that can later be applied to other channels.

Conclusion

The work presented in this thesis has been carried out with two broad aims. The first was to present, compare and test various methods used to model ion channels. Ion channels have been modelled using a wide variety of techniques, but this work has focussed only on models that can directly link channel structure to function. The continuum theories of electrolytes provide one way to do this, by treating the channel as a rigid environment and solving equations to find the average ion distributions and flux through the channel. Such theories have been put to good use to show, for example, the relationship between the charge distribution in the protein and the selectivity or permeation rates of ions in the channel. However, by a direct comparison with BD simulations I have been able to show that the mean field treatment of ions in these theories is questionable. As ion channels contain only a small aqueous environment surrounded by protein, in most cases only one or at most a few ions enter the channel at a time. In such cases it is important to treat the ions individually as discrete particles. Treating them via their time averaged concentrations can lead to erroneous results, most notably to an overestimation of the effects of electrolytic screening. For this reason I conclude that the continuum theories should not be used to make quantitative studies of ion channels, and more detailed models are required.

One possible alternative is to use molecular dynamics simulations in which the motions of all the atoms in the system are calculated for a short period of time. I have not focussed on this technique, however, for one main reason: the number of calculations involved makes it currently too time consuming to be used to calculate channel currents, the primary observable quantity. Instead I have presented Brownian dynamics simulations as a middle ground between the continuum and MD approaches. All atom simulations have not been ignored, however, as they can provide estimates for important parameters that can be used in the BD simulations.

Brownian dynamics simulations provide a practical tool for studying the conductance of ion channels. In such simulations the integrity of ions is maintained, but

the protein and water are treated as continuous media, reducing the computational power required to simulate the passage of ions through the channel. In this thesis, the technique is developed and its boundary conditions tested, before it is applied to test the continuum theories and then to study real ion channels. These simulations have been shown to reproduce the bulk properties of electrolyte solutions, and can be used to gain many important insights into the mechanics of ion channels. One must always, however, keep in mind the limitations of a theory. For example, the treatment of water as a continuous medium means that the energy associated with rearranging the water molecules around an ion so as to fit inside the narrow channel is ignored. This makes it difficult to differentiate between like charged ions in BD simulations. It can also be difficult to know how best to calculate the forces acting on ions. In most cases in this thesis, electrostatic forces are calculated by solving Poisson's equation. This seems like a reasonable approach, but may suffer from two main problems. One is that the channel is taken to be rigid when calculating forces, whereas in practice the shape may alter as an ion passes. Using a different channel shape for every position of the ion in the channel could potentially combat this. The other problem, demonstrated here by conducting simulations in the Gramicidin A channel, arises from the description of the water and protein as dielectric media. This picture is meant to describe the average properties of the underlying atoms, but may also be too crude to describe all ion channels accurately. In the narrow GA pore, the dipoles from the water molecules tend to align themselves along the channel, a property that cannot be easily captured in a simple dielectric picture.

The second aim of this thesis has been to apply the appropriate models to try to understand the mechanisms of real biological ion channels. The L-type calcium channel, a channel remarkable for having both a high degree of selectivity and enormous conduction rates, was the main channel studied. As we do not have a crystal structure of this channel, a model was constructed using information from physiological and mutagenesis experiments and molecular models. The most important aspect of the model is a narrow 'selectivity filter' region that creates single filling of ions, surrounded by highly charged glutamate residues whose interaction with ions creates charge selectivity. Using potential energy profiles obtained from the solution of Poisson's equation and Brownian dynamics simulations we were able to explain how this channel can differentiate between sodium and calcium ions whilst retaining high conduction rates. The model can neatly explain and reproduce many physiological experiments yielding confidence in its validity, and demonstrating the explanatory power of these modelling techniques. A similar BD investigation of the KcsA potassium channel (whose crystal structure is known) was carried out by my

colleagues concurrently with those described here, and has also had much success in elucidating the permeation mechanisms of potassium ions in that channel.

There are many interesting directions in which this work could lead. Firstly, given the success of the BD / Poisson's equation modelling technique, an obvious direction for future research is to apply it to different ion channels. The recent determination of the structure of the CLC chloride channel makes it an ideal target. Knowledge of the channel shape and the positions of the partial charges on the protein atoms will take the guesswork out of constructing a channel model. One practical difficulty with this channel, however, is that the shape of the pore does not follow a straight line and is not axially symmetric, unlike those studied previously. The system of storing the solutions of Poisson's equation described in this thesis assumes axial symmetry, and so needs to be extended to deal with this new channel. Work in this direction is currently in progress. Other families of channels can also be modelled. For example, the homology between the voltage gated sodium, potassium and calcium channels means that a model of the former could be determined from the structure and models of the latter two.

Having noted some of the limitations of the models being used, it will be important to refine and improve them accordingly. Extending the solutions of Poisson's equation to deal with three dimensional, non-symmetric structures, as noted above, provides one example. But probably a more important long-term goal is to use more information from all-atom simulations in the BD routine. The current simulations utilise estimates of the ion diffusion coefficients and dielectric constants from MD simulations, but there is no reason to stop there. A more complete approach would be to eradicate the use of Poisson's equation altogether, and instead to calculate forces from the free energy profiles of permeating ions found from MD simulations. This would overcome many of the difficulties and limitations of the current approach. The forces on ions would be determined from MD in which all the atoms and dipoles are modelled, the channel is flexible, no dielectric constants are required and hydration effects can be included. BD would then provide a pathway to determine currents from this data, avoiding the computations required to run MD itself for long enough to do so. Unfortunately, this may not be quite as simple as it sounds. Although free energy profiles have already been determined from MD in the GA channel, as mentioned in chapter 9 they yielded unrealistic energy barriers. It is likely that the classical MD simulations that were designed for use in bulk solutions will have to be improved or reparameterised for use in ion channels before reliable energy profiles can be determined. Alternatively, ab initio techniques in which direct electronic structure calculations are included in the MD

simulations may soon become fast enough to be used to determine MD force fields. As computer power increases, MD is bound to become one of the primary tools in channel modelling. But perhaps a hierarchical approach utilising quantum, MD and BD techniques may provide the most accurate and practical path forward.

Finally, ion channels are fundamental building blocks of living creatures, and although understanding them is of intrinsic interest, the real challenge lies in putting this knowledge to practical use. Hopefully, the insights gained from theoretical models of ion channels can guide experiments that themselves aim to find ways of designing drugs and combatting disease.

References

[1] C. Adcock, G. R. Smith, and M. S. P. Sansom. Electrostatics and the ion selectivity of ligand-gated channels. *Biophys. J.*, 75:1211–1222, 1998.

[2] M. P. Allen and D.J. Tildesley. *Computer Simulation of Liquids.* Oxford University Press, London, 1987.

[3] T. W. Allen, A. Bliznyuk, A. P. Rendelland, S. Kuyucak, and S. H. Chung. The potassium channel: structure, selectivity and diffusion. *J. Chem. Phys.*, 112:8191–8204, 2000.

[4] T. W. Allen and S. H. Chung. Brownian dynamics study of an open-state KcsA potassium channel. *Biochim. Biophys. Acta*, 1515:83–91, 2001.

[5] T. W. Allen, S. Kuyucak, and S. H. Chung. The effect of hydrophobic and hydrophilic channel walls on the structure and diffusion of water and ions. *J. Chem. Phys.*, 111:7985–7999, 1999.

[6] T. W. Allen, S. Kuyucak, and S. H. Chung. Molecular dynamics study of the KcsA potassium channel. *Biophys. J.*, 77:2502–2516, 1999.

[7] T. W. Allen, S. Kuyucak, and S. H. Chung. Molecular dynamics estimates of ion diffusion in model hydrophobic and the KcsA potassium channels. *Biophys. Chem.*, 86:1–14, 2000.

[8] W. Almers, E. W. McCleskey, and P. T. Palade. A non-selective cation conductance in frog muscle membrane blocked by micromolar external calcium ions. *J. Physiol.*, 353:565–583, 1984.

[9] O. S. Andersen. Private communication, 2001.

[10] O. S. Andersen, D. V. Greathouse, L. L. Providence, M. D. Becker, and R. E. Koeppe. Importance of tryptophan dipoles for protein function: 5–fluorination of tryptophans in gramicidin A channels. *J. Am. Chem. Soc.*, 120:5142–5146, 1998.

[11] O. S. Andersen and R. E. Koeppe. Molecular determinants of channel function. *Physiol. Rev.*, 72:89–158, 1992.

[12] D. G. Anderson, R. B. Shirts, T. A. Cross, and D. D. Busath. Noncontact dipole effects on channel permeation. V. Computed potentials for fluorinated gramicidin. *Biophys. J.*, 81:1255–1264, 2001.

[13] J. Aqvist and V. Luzhkov. Ion permeation mechanism of the potassium channel. *Nature*, 404:881–884, 2000.

[14] C. M. Armstrong and J. Neyton. Ion permeation through calcium channels: a one site model. *Ann. NY Acad. Sci.*, 635:18–25, 1991.

[15] A. S. Arseniev, I. L. Barsukov, V. F. Bystrov, A. L. Lomize, and Y. A. Ovchinnikov. ^{1}H-NMR study of gramicidin a transmembrane ion channel: head-to-head right handed single stranded helices. *FEBS Lett.*, 186:168–174, 1985.

[16] F. M. Ashcroft. *Ion channels and disease: Channelopathies.* Academic Press, San Diego, 2000.

[17] N. W. Ashcroft and N. D. Mermin. *Solid State Physics.* Holt, Rinehart and Winston, New York., 1976.

[18] A. Bahinski, A. Yatani, G. Mikala, S. Tang, S. Yamamoto, and A. Schwartz. Charged amino acids near the pore entrance influence ion-conduction of a human L-type cardiac calcium channel. *Mol. Cell. Biochem.*, 166:125–134, 1997.

[19] R.C. Bean, W. C. Shepperd, M. Chna, and J. Eichner. Discrete conductance fluctuations in lipid bilayer protein membranes. *J. Gen. Physiol.*, 53:741–757, 1969.

[20] S. Bek and E. Jakobsson. Brownian dynamics study of a multiply-occupied cation channel: Application to understanding permeation in potassium channel. *Biophys. J.*, 66:1028–1038, 1994.

[21] S. Berneche and B. Roux. Molecular dynamics of the KcsA K^+ channel in a bilayer membrane. *Biophys. J.*, 78:2900–2917, 2000.

[22] F. Bezanilla and C. M. Armstrong. Negative conductance caused by entry of sodium and cesium ions into the potassium channels of squid giant axons. *J. Gen. Physiol.*, 60:588–608, 1972.

[23] J. O'M. Bockris and A. K. N. Reddy. *Modern Electrochemistry*, volume 1. Plenum, N.Y., 1970.

[24] V. Borisenko, D. C. Burns, Z. Zhang, and G. A. Woolley. Optical switching of ion-dipole interactions in a gramicidin channel analogue. *J. Am. Chem. Soc.*, 122:6364–6370, 2000.

[25] B.R. Brooks, R.E. Bruccoleri, B.D. Olafson, D.J. States, S. Swaminathan, and M. Karplus. CHARMM: a program for macromolecular energy, minimization, and dynamics calculation. *J. Comp. Chem.*, 4:187–217, 1983.

[26] F. Buda, G. L. Chiarlotti, R. Car, and M. Parrinello. Proton diffusion in silicon. *Phys. Rev. Lett.*, 63:294–297, 1989.

[27] D. D. Busath. The use of physical methods in determining gramicidin structure and function. *Ann. Rev. Physiol.*, 55:473–501, 1993.

[28] D. D. Busath, C. D. Thulin, R. W. Hendershot, L. R. Phillips, P. Maughan, C. D. Cole, N. C. Bingham, S. Morrison, L. C. Baird, R. J. Hendershot, M. Cotten, and T. A. Cross. Noncontact dipole effects on channel permeation. I. Experiments with (5F-Indole)Trp^{13} gramicidin A channels. *Biophys. J.*, 75:2830–2844, 1998.

[29] M. Cai and P. C. Jordan. How does vestibule surface charge affect ion conduction and toxin binding in a sodium channel. *Biophys. J.*, 57:883–891, 1990.

[30] R. Car and M. Parrinello. Unified approach for molecular dynamics and density-functional theory. *Phys. Rev. Lett.*, 55:2471–2474, 1985.

[31] A. E. Cardenas, R. D. Coalson, and M. G. Kurnikova. Three-dimensional Poisson-Nernst-Planck theory studies: influence of membrane electrostatics on gramicidin A channel conductance. *Biophys. J.*, 79:80–93, 2000.

[32] G. Chang, R. H. Spencer, A. T. Lee, M. T. Barclay, and D. C. Rees. Structure of the MscL homolog from mycobacterium tuberculosis: A gated mechanosensitive ion channel. *Science*, 282:2220–2226, 1998.

[33] D. Chen, J. Lear, and R. S. Eisenberg. Permeation through an open channel: Poisson-Nernst-Planck theory of a synthetic ionic channel. *Biophys. J.*, 72:97–116, 1997.

[34] D. P. Chen, L. Xu, A. Tripathy, G. Meissner, and B. Eisenberg. Selectivity and permeation in calcium release channel of cardiac muscle: alkali metal ions. *Biophys. J.*, 76:1346–1366, 1999.

[35] X. H. Chen, I. Bezprozvanny, and R. W. Tsien. Molecular basis of proton block of L-type Ca^{2+} channels. *J. Gen. Physiol.*, 108:363–374, 1996.

[36] X. H. Chen and R. W. Tsien. Aspartate substitutions establish the concerted action of p-region glutamates in repeats I and III in forming the protonation site of L-type Ca^{2+} channels. *J. Biol. Chem.*, 272:30002–30008, 1997.

[37] W. Cheng, C. X. Wang, W. Z. Chen, Y. W. Xu, and Y. Y. Shi. Investigating the dielectric effects of channel pore water on the electrostatic barriers of the permeation ion by the finite difference Poisson-Boltzmann method. *Eur. Biophys. J.*, 27:105–112, 1998.

[38] S. W. Chiu and E. Jakobsson. Stochastic theory of singly occupied ion channels. II. Effects of access resistance and potential gradients extending into the bath. *Biophys. J.*, 55:147–157, 1989.

[39] S. W. Chiu, S. Subramaniam, and E. Jakobsson. Simulation study of a gramicidin/lipid bilayer system in excess water and lipid. I. Structure of the molecular complex. *Biophys. J.*, 76:1929–1950, 1999.

[40] S. H. Chung, T. W. Allen, M. Hoyles, and S. Kuyucak. Permeation of ions across the potassium channel: Brownian dynamics studies. *Biophys. J.*, 77:2517–2533, 1999.

[41] S. H. Chung, T. W. Allen, and S. Kuyucak. Conducting-state properties of the KcsA potassium channel from molecular and Brownian dynamics simulations. *Biophys. J.*, 82:628–645, 2002.

[42] S. H. Chung, M. Hoyles, T. W. Allen, and S. Kuyucak. Study of ionic currents across a model membrane channel using Brownian dynamics. *Biophys. J.*, 75:793–809, 1998.

[43] R. D. Coalson, M. G. Kurnikova, P. Graf, and A. Nitzan. Brownian dynamics studies of ion permeation through biological channels. *Biophys. J.*, 82:340a, 2002.

[44] K. E. Cooper, P. Y. Gates, and R. S. Eisenberg. Surmounting barriers in ionic channels. *Q. Rev. Biophys.*, 21:331–364, 1988.

[45] K. E. Cooper, E. Jakobsson, and P. Wolynes. The theory of ion transport through membrane channels. *Prog. Mol. Biol.*, 46:51–96, 1985.

[46] W. D. Cornell, P. Cieplak, C. I. Bayly, I. R. Gould, K. M. Merz, D. M. Ferguson, D. C. Spellmeyer, T. Fox, J. W. Caldwell, and P. A. Kollman. A second generation force field for the simulation of proteins and nucleic acids. *J. Am. Chem. Soc.*, 117:5179–5197, 1995.

[47] B. Corry, T. W. Allen, S. Kuyucak, and S. H. Chung. Mechanisms of permeation and selectivity in calcium channels. *Biophys. J.*, 80:195–214, 2001.

[48] B. Corry, S. Kuyucak, and S. H. Chung. Tests of continuum theories as models of ion channels: II. Poisson-Nernst-Planck theory versus brownian dynamics. *Biophys. J.*, 78:2364–2381, 2000.

[49] M. Cotten, C. Tian, D. D. Busath, R. B. Shirts, and T. A. Cross. Modulating dipoles for structure-function correlations in the gramicidin A channel. *Biochemistry*, 38:9185–9197, 1999.

[50] P. S. Crozier, R. L. Rowley, N. B. Holladay, D. Henderson, and D. D. Busath. Molecular dynamics simulation of continuous current flow through a model biological membrane channel. *Phys. Rev. Lett.*, 86:2467–2470, 2001.

[51] T.X. Dang and E. W. McCleskey. Ion channel selectivity through stepwise changes in binding affinity. *J. Gen. Physiol.*, 111:185–193, 1998.

[52] M. E. Davis and J. A. McCammon. Electrostatics in biomolecular structure and dynamics. *Chem. Rev.*, 90:509–521, 1990.

[53] P. Debye and E. Hückel. Zur theorie der elektrolyte. *Physik. Zeitschr.*, 24:185–206, 1923.

[54] G. R. Dieckmann, J. D. Lear, Q. Zhong, M. L. Klein, W. F. DeGrado, and K. A. Sharp. Exploration of the structural features defining the conduction properties of a synthetic ion channel. *Biophys. J.*, 76:618–630, 1999.

[55] V. Dorman, M. B. Partenskii, and P. C. Jordan. A semi-microscopic Monte Carlo study of permeation energetics in a gramicidin-like channel: The origin of cation selectivity. *Biophys. J.*, 70:121–134, 1996.

[56] S. W. Doughty, F. E. Blaney, and W. G. Richards. Models of ion pores in N-type voltage gated calcium channels. *J. Mol. Graph.*, 13:342–348, 1995.

[57] S. W. Doughty, F. E. Blaney nad B. S. Orlek, and W. G. Richards. A molecular mechanism for toxin block in N-type calcium channels. *Prot. Eng.*, 11:95–99, 1998.

[58] D. A. Doyle, J. M. Cabral, R. A. Pfuetzner, A. Kuo, J. M. Gulbis, S. L. Cohen, B. T. Chait, and R. MacKinnon. The structure of the potassium channel: molecular basis of K^+ conduction and selectivity. *Science*, 280:69–77, 1998.

[59] R. Dutzler, E. B. Campbell, M. Cadene, B. T. Chait, and R. Mackinnon. X-ray structure of a CLC chloride channel at 3.0 å reveals the molecular basis of anion selectivity. *Nature*, 415:287–294, 2002.

[60] Williams. M. E., P. F. Brust, D. H. Feldman, S. Patthi, S. Simerson, A. Maroufi, A. F. McCue, G. Velicelebi, S. B. Ellis, and M. M. Harpold. Structure and functional expression of an omega-conotoxin-sensitive human N-type calcium channel. *Science*, 257:389–395, 1992.

[61] R. S. Eisenberg. Computing the field in proteins and channels. *J. Membr. Biol.*, 150:1–25, 1996.

[62] R. S Eisenberg. From structure to function in open ionic channels. *J. Membr. Biol.*, 171:1–24, 1999.

[63] P. T. Ellinor, J. Yang, W. A. Sather, J. F. Zhang, , and R. W. Tsien. Ca^{2+} channel selectivity at a single locus for high-affinity Ca^{2+} interactions. *Neuron*, 15:1121–1132, 1995.

[64] D. F. Evans and H. Wennerström. *The Colloidal Domain.* Wiley-VCH, N.Y., 2^{nd} edition, 1999.

[65] H Eyring. Viscosity, plasticity and diffusion as examples of absolute reaction rates. *J. Chem. Phys.*, 4:283–291, 1936.

[66] H. Eyring and M. Polanyi. Uber einfache gasreaktionen. *Z. Phys. Chem.*, 12:279, 1931.

[67] D. Frenkel and B. Smit. *Understanding Molecular Simulation: From Algorithms to Applications.* Academic Press, San Diego, 1996.

[68] A. Fukushima and S. Hagiwara. Currents carried by monovalent cations through calcium channels in mouse neoplastic B lymphocytes. *J. Physiol.*, 358:255–284, 1985.

[69] V. Y. Ganitkevich and G. Isenberg. Contribution of two types of calcium channels to membrane conductance of single myocytes from guinea-pig coronary artery. *J. Physiol.*, 426:19–42, 1990.

[70] A. Gonzalez, J. A. White, F. L. Roman, S. Velasco, and R. Evans. Density-functional theory for small systems: Hard spheres in a closed spherical cavity. *Phys. Rev. Lett.*, 79:2466–2469, 1997.

[71] E. Guàrdia, R. Rey, and J. A. Padró. Na^+-Na^+ and Cl^--Cl^- ion pairs in water: Mean force potentials by constrained molecular dynamics. *J. Chem. Phys.*, 95:2823–2831, 1991.

[72] E. Guàrdia, R. Rey, and J. A. Padró. Potential of mean force by constrained molecular dynamics: a sodium chloride ion-pair in water. *Chem. Phys.*, 155:187–195, 1991.

[73] L. Guidoni and P. Carloni. Potassium permeation through the KcsA channel: a density functional study. *Biochim. Biophys. Acta*, 1563:1–6, 2002.

[74] L. Guidoni, V. Torre, and P. Carloni. Potassium and sodium binding to the outer mouth of the K^+ channel. *Biochemistry*, 38:8599–8604, 1999.

[75] L. Guidoni, V. Torre, and P. Carloni. Water and potassium dynamics inside the KcsA K^+ channel. *FEBS Lett.*, 477:37–42, 2000.

[76] H. R. Guy and S. R. Durell. Structural models of Na^+, Ca^{2+}, and K^+ channels. *Soc. Gen. Physiol. Ser.*, 50:1–16, 1995.

[77] J. Hall. Access resistance of a small circular pore. *J. Gen. Physiol.*, 66:531–532, 1975.

[78] J. P. Hansen and I. R. McDonald. *Theory of simple liquids.* Academic Press, London, 1976.

[79] T. D. Harroun, W. T. Heller, T. M. Weiss, L. Yang, and H. W. Huang. Theoretical analysis of hydrophobic matching and membrane-mediated interactions in lipid bilayers containing gramicidin. *Biophys. J.*, 76:3176–3185, 1999.

[80] D. Henderson, P. Bryk, S. Sokolowski, and D. T. Wasan. Density-functional theory of an electrolyte confined by thin charged walls. *Phys. Rev. E.*, 61:3896–3903, 2000.

[81] J. Hermans, H.J.C. Berendsen, W.F. van Gunsteren, and J.P.M. Postma. A consistent empirical potential for water-protein interactions. *Biopolymers*, 23:1513–1518, 1984.

[82] P. Hess. Elementary properties of cardiac calcium channels: a brief review. *Can. J. Physiol. Pharmacol.*, 66:1218–1223, 1987.

[83] P. Hess, J. B. Lansman, and R. W. Tsien. Calcium channel selectivity for divalent and monovalent cations : Voltage and concentration dependence of single channel current in ventricular heart cells. *J. Gen. Physiol.*, 88:293–319, 1986.

[84] P. Hess and R. W. Tsien. Mechanism of ion permeation through calcium channels. *Nature*, 309:453–456, 1984.

[85] B. Hille. *Ionic Channels of Excitable Membranes.* Sinauer Associates Inc., MA., 3^{rd} edition, 2001.

[86] S. B. Hladky and D. A. Haydon. Discretness of conductance change in bimolecular lipid membranes in the presence of certain antibiotics. *Nature*, 225:451–453, 1970.

[87] A. Hodgkin and A. Huxley. A quantitative description of membrane current and its application to conduction and excitation in nerve. *J. Physiol.*, 117:500–544, 1952.

[88] U. Hollerbach, D. P. Chen, D. D. Busath, and B. Eisenberg. Predicting function from structure using the Poisson-Nernst-Planck equations: Sodium current in the gramicidin A channel. *Langmuir*, 16:5509–5514, 2000.

[89] U. Hollerbach and R. S. Eisenberg. Concentration-dependent shielding of electrostatic potentials inside the gramicidin a channels. *Langmuir.*, 18:3626–3631, 2002.

[90] B. Honig and A. Nicholls. Classical electrostatics in biology and chemistry. *Science*, 268:1144–1149, 1995.

[91] M. Hoyles, S. Kuyucak, and S. H. Chung. Computer simulation of ion conductance in membrane channels. *Phys. Rev. E*, 58:3654–3661, 1998.

[92] M. Hoyles, S. Kuyucak, and S. H. Chung. Solutions of Poisson's equation in channel-like geometries. *Comp. Phys. Commun.*, 115:45–68, 1998.

[93] W. Im, S. Seefeld, and B. Roux. A grand canonical Monte Carlo-Brownian dynamics algorithm for simulating ion channels. *Biophys. J.*, 79:788–801, 2000.

[94] M. B. Jackson. Perfection of a synaptic receptor: Kinetics and energetics of the acetylcholine receptor. *Proc. Natl. Acad. Sci. USA*, 86:2199–2203, 1989.

[95] E. Jakobsson and S. W. Chiu. Stochastic theory of ion movement in channels with single-ion occupancy. *Biophys. J.*, 52:33–45, 1987.

[96] B. Jayaram, K. Sharp, and B. Honig. The electrostatic potential of B-DNA. *Biopolymers*, 28:975–993, 1989.

[97] Y. Jiang, A. Lee, J. Chen, M. Cadene, B. T. Chait, and R. Mackinnon. Crystal structure and mechanism of a calcium-gated potassium channel. *Nature*, 417:515–522, 2002.

[98] P. C. Jordan. Electrostatic modeling of ion pores. energy barriers and electric field profiles. *Biophys. J.*, 39:157–164, 1982.

[99] P. C. Jordan. Ion-water and ion-polypeptide correlations in a gramicidin-like channel. A molecular dynamics study. *Biophys. J.*, 58:1133–1156, 1990.

[100] P. C. Jordan. Ion permeation and chemical kinetics. *J. Gen. Physiol.*, 114:601–603, 1999.

[101] P. C. Jordan, R. J. Bacquet, J. A. McCammon, and P. Tran. How electrolyte shielding influences the electrical potential in transmembrane ion channels. *Biophys. J.*, 55:1041–1052, 1989.

[102] P.C. Jordan. Microscopic approaches to ion transport through transmembrane channels: the model system gramicidin. *J. Phys. Chem.*, 91:6582–6591, 1987.

[103] R. R. Ketchem, W. Hu, and T. A. Cross. High-resolution conformation of gramicidin A in a lipid bilayer by solid-state NMR. *Science*, 261:1457–1460, 1993.

[104] R. R. Ketchem, B. Roux, and T. A. Cross. High-resolution polypeptide structure in a lamellar phase lipid environment from solid state NMR derived orientational constraints. *Structure*, 5:1655–1669, 1997.

[105] M. S. Kim, T. Morii, L. X. Sun, K. Imoto, and Y. Mori. Structural determinants of ion selectivity in brain calcium channel. *FEBS Lett.*, 318:145–148, 1993.

[106] I. Klapper, R. Hagstrom, R. Fine, K. Sharp., and B. Honig. Focussing of electric fields in the active site of Cu-Zn superoxide dismutase. *Proteins: Structure, function and genetics*, 1:47–59, 1986.

[107] R. E. Koeppe and O. S. Andersen. Engineering the gramicidin channel. *Ann. Rev. Biophys. Biomol. Struc.*, 25:231–258, 1996.

[108] W. Kohn. Nobel lecture: Electronic structure of matter-wave functions and density functionals. *Rev. Mod. Phys.*, 71:1253–1266, 1999.

[109] P. G. Kostyuk, S. L. Mironov, and Y. M. Shuba. Two ion-selecting filters in the calcium channel of the somatic membrane of mollusc neurons. *J. Membr. Biol.*, 76:83–93, 1983.

[110] C. C. Kuo and P. Hess. A functional view of the entrances of L-type Ca^{2+} channels: Estimates of the size and surface potential at the pore mouths. *Neuron*, 9:515–526, 1992.

[111] C. C. Kuo and P. Hess. Characterization of the high-affinity Ca^{2+} binding sites in the L-type Ca^{2+} channel pore in rat phaeochromocytoma cells. *J. Physiol.*, 466:657–682, 1993.

[112] C. C. Kuo and P. Hess. Ion permeation through the L-type Ca^{2+} channel in rat phaeochromocytoma cells: Two sets of ion binding sites in the pore. *J. Physiol.*, 466:629–655, 1993.

[113] M. G. Kurnikova, R. D. Coalson, P. Graf, and A. Nitzan. A lattice relaxation algorithm for three-dimensional Poisson-Nernst-Planck theory with application to ion transport through the gramicidin A channel. *Biophys. J.*, 76:642–656, 1999.

[114] S. Kuyucak, O. S. Andersen, and S. H. Chung. Models of permeation in ion channels. *Rep. Prog. Phys.*, 64:1427–1472, 2001.

[115] S. Kuyucak, M. Hoyles, and S. H. Chung. Analytical solutions of Poisson's equation for realistic geometrical shapes of membrane ion channels. *Biophys. J.*, 74:22–36, 1998.

[116] J. B. Lansman, P. Hess, and R. W. Tsien. Blockade of current through single calcium channels by Cd^{2+}, Mg^{2+}, and Ca^{2+}: Voltage and concentration dependence of calcium entry into the pore. *J. Gen. Physiol.*, 88:321–347, 1986.

[117] P. Laugner and B. Neumcke. Theoretical analysis of ion conductance in lipid bilayer membranes. In G. Eisenman, editor, *Membranes: A sereies of advances*, volume 2. Marcell Dekker, New York, 1973.

[118] A. Lehmani, O. Bernard, and P. Turq. Transport of ions and solvent in confined media. *J. Stat. Phys.*, 89:379–402, 1997.

[119] F. Lehmann-Horn and K. Jurkat-Rott. Voltage-gated ion channels and hereditary disease. *Physiol. Rev.*, 79:1317–1372, 1999.

[120] D. G. Levitt. Electrostatic calculations for an ion channel. I. Energy and potential profiles and interactions between ions. *Biophys. J.*, 22:209–219, 1978.

[121] D. G. Levitt. Strong electrolyte continuum theory solution for equilibrium profiles, diffusion limitation, and conductance in charged ion channels. *Biophys. J.*, 48:19–31, 1985.

[122] D. G. Levitt. Interpretation of biological ion channel flux data – reaction-rate versus continuum theory. *Ann. Rev. Biophys. Biophys. Chem.*, 15:29–57, 1986.

[123] D. G. Levitt. General continuum theory for multiion channel. II. Application to acetylcholine channel. *Biophys. J.*, 59:278–288, 1991.

[124] D. G. Levitt. General continuum theory for multiion channel.I. Theory. *Biophys. J.*, 59:271–277, 1991.

[125] D. G. Levitt. Modeling of ion channels. *J. Gen. Physiol.*, 113:789–794, 1999.

[126] A. J. Li and R. Nussinov. A set of van der Waals and Coulombic radii of protein atoms for molecular and solvent-accessible surface calculation, packing evaluation, and docking. *Proteins*, 32:111–127, 1998.

[127] S. C. Li, M. Hoyles, S. Kuyucak, and S. H. Chung. Brownian dynamics study of ion transport in the vestibule of membrane channels. *Biophys. J.*, 74:37–47, 1998.

[128] M. Lipkind and H. A. Fozzard. KcsA crystal structure as framework for a molecular model of the Na^{+} channel pore. *Biochemistry*, 39:8161–8170, 2000.

[129] H. D. Lux, E. Carbone, and H. Zucker. Na^{+} currents through low-voltage-activated Ca^{2+} channels of chick sensory neurons: block by external Ca^{2+} and Mg^{2+}. *J. Physiol.*, 430:159–188, 1990.

[130] V. B. Luzhkov and J. Åqvist. A computational study of ion binding and protonation states in the KcsA potassium channel. *Biochim. Biophys. Acta*, 1481:360–370, 2000.

[131] R. M. Lynden-Bell and J. C. Rasaiah. Mobility and solvation of ions in channels. *J. Chem. Phys.*, 105:9266–9280, 1996.

[132] A. P. Lyubartsev and A. Laaksonen. Calculation of the effective interaction potentials from radial distribution functions: A reverse Monte Carlo approach. *Phys. Rev. E*, 52:3730–3737, 1995.

[133] A. D. Mackerell et al. Self-consistent parameterization of biomolecules for molecular modeling and condensed phase simulations. *Biophys. J.*, 61:A143, 1992.

[134] A. Mamonov, R. D. Coalson, P. Graf, A. Nitzan, and M. G. Kurnikova. Closer look at the dielectric barrier in the narrow channel, real problem or theoretical artifact? *Biophys. J.*, 82:209a, 2002.

[135] D. Marx, M. Sprik, and M. Parrinello. Ab initio molecular dynamics of ion solvation: The case of Be^{2+} in water. *Chem. Phys. Lett.*, 273:360–366, 1997.

[136] E. Mason and E. McDaniel. *Transport Properties of Ions in Gases.* John Wiley, New York, 1988.

[137] E. W. McCleskey. Calcium channel permeation: a field in flux. *J. Gen. Physiol.*, 113:765–772, 1999.

[138] E. W. McCleskey and W. Almers. The Ca channel in skeletal muscle is a large pore. *Proc. Natl. Acad. Sci. USA*, 82:7149–7153, 1985.

[139] P. McGill and M. F. Schumaker. Boundary conditions for single-ion diffusion. *Biophys. J.*, 71:1723–1742, 1996.

[140] D. A. McQuarrie. *Statistical Mechanics.* Harper Collins, New York., 1976.

[141] M. Mezei and D. L. Beveridge. Free energy simulations. *Ann. (N.Y.) Acad. Sci.*, 482:1b–23b, 1986.

[142] A. Mikami, K. Imoto, T. Tanabe, T. Niidome, Y. Mori, H. Takeshima, S. Narumiya, and S. Numa. Primary structure and functional expression of the cardiac dihydropyridine-sensitive calcium channel. *Nature*, 340:230–233, 1989.

[143] C Miller. Ionic hopping defended. *J. Gen. Physiol.*, 113:783–787, 1999.

[144] H. Monoi. Effective pore radius of the gramicidin channel. Electrostatic energies of ions calculated by a three-dielectric model. *Biophys. J.*, 59:786–794, 1991.

[145] J. A. Morrill and R. MacKinnon. Isolation of a single carboxyl-carboxylate proton binding site in the pore of a cyclic nucleotide-gated channel. *J. Gen. Physiol.*, 114:71–83, 1999.

[146] E. Neher and B Sackmann. Single channel currents recorded from membrane of denervated frog muscle fibres. *Nature*, 260:799–802, 1976.

[147] J. S. Newman. *Electrochemical Systems.* Prentice Hall, Englewood, NJ., 1991.

[148] A. Nicholls and B. Honig. A rapid finite difference algorithm using successive over-relaxation to solve Poisson-Boltzmann equation. *J. Comp. Chem.*, 12:435–445, 1991.

[149] B. Nilius, P. Hess, J. B. Lansman, and R. W. Tsien. A novel type of cardiac calcium channel in ventricular cells. *Nature*, 316:443–446, 1985.

[150] W. Nonner, D. P. Chen, and B. Eisenberg. Progress and prospects in permeation. *J. Gen. Physiol.*, 113:773–782, 1999.

[151] W. Nonner and B. Eisenberg. Ion permeation and glutamate residues linked by Poisson-Nernst-Planck theory in L-type calcium channels. *Biophys. J.*, 75:1287–1305, 1998.

[152] S. Oiki, R. E. Koeppe, and O. S. Andersen. Asymmetric gramicidin channels: Heterodimeric channels with a single F_6Val^1 residue. *Biophys. J.*, 66:1823–1832, 1994.

[153] L. Parent and M. Gopalakrishnan. Glutamate substitution in repeat IV alters divalent and monovalent cation permeation in the heart Ca^{2+} channel. *Biophys. J.*, 69:1801–1813, 1995.

[154] M. B. Partenskii, V. Dorman, and P. C. Jordan. Influence of a channel-forming peptide on energy barriers to ion permeation, viewed from a continuum dielectric perspective. *Biophys. J.*, 67:1429–1438, 1994.

[155] M. B. Partenskii and P. C. Jordan. Theoretical perspectives on ion-channel electrostatics: continuum and microscopic approaches. *Q. Rev. Biophys.*, 25:477–510, 1992.

[156] L. Pauling. *The Nature of Chemical Bond.* Cornel University Press, Ithaca, NY., 1942.

[157] P. S. Phale, A. Philippsen, C. Widmer, V. P. Phale, J. R. Rosenbusch, and T. Schirmer. Role of charged residues at the OmpF porin channel construction probed by mutagenesis and simulation. *Biochemistry*, 40:6319–6325, 2001.

[158] L. Polo-Parada and S. J. Korn. Block of N-type calcium channels in chick sensory neurons by external sodium. *J. Gen. Physiol.*, 109:693–702, 1997.

[159] J. A. Pople. Nobel lecture: Quantum chemical models. *Rev. Mod. Phys.*, 71:1267–1274, 1999.

[160] W. H. Press, B. P. Flannery, S. A. Teukolsky, and W. T. Vetterling. *Numerical Recipes.* Cambridge University Press, Cambridge., 1989.

[161] A. Pullman. Energy profiles in the gramicidin A channel. *Q. Rev. Biophys.*, 20:173–200, 1987.

[162] J. L. Rae, R. A. Levis, and R. S. Eisenberg. Ionic channels in ocular epithelia. In T. Narahashi, editor, *Ion Channels*, volume 1, pages 283–327. Plenum Press, New York., 1988.

[163] K. M. Ranatunga, C. Adcock, I. D. Kerr, G. R. Smith, and M. S. P. Sansom. Ion channels of biological membranes: prediction of single channel conductance. *Theor. Chem. Acc.*, 101:97–102, 1999.

[164] K. M. Ranatunga, I. H. Shrivastava, G. R. Smith, and M. S. P. Sansom. Side -chain ionization states in a potassium channel. *Biophys. J.*, 80:1210–1219, 2001.

[165] D.C. Rapaport. *The Art of Molecular Dynamics Simulation.* Cambridge University Press, Cambridge, 1995.

[166] F. Reif. *Fundamentals of Statistical and Thermal Physics.* McGraw-Hill, Kogakusha, Tokyo, 1965.

[167] M. J. Root and R. MacKinnon. Two identical noninteracting sites for an ion channel revealed by proton transfer. *Science*, 265:1852–1856, 1994.

[168] R. L. Rosenberg and X. H.Chen. Characterization and localization of two ion-binding sites within the pore of cardiac L-type calcium channels. *J. Gen. Physiol.*, 97:1207–1225, 1991.

[169] R. L. Rosenberg, P. Hess, J. P. Reeves, H. Smilowitz, and R. W. Tsien. Calcium channels in planar lipid bilayers: Insights into mechanisms of ion permeation and gating. *Science*, 231:1564–1566, 1986.

[170] P. J. Rossky and H. L. Friedman. Accurate solutions to integral equations describing weakly screened ionic systems. *J. Chem. Phys.*, 72:5694–5700, 1980.

[171] T. K. Rostovtseva, V. M. Aguilella, I. Vodyanoy, S. M. Bezrukov, and V. A. Parsegian. Membrane surface-charge titration probed by gramicidin A channel conductance. *Biophys. J.*, 75:1783–1792, 1998.

[172] B. Roux. Valence selectivity of the gramicidin channel: A molecular dynamics free energy perturbation study. *Biophys. J.*, 71:3177–3185, 1996.

[173] B. Roux. Influence of the membrane potential on the free energy of an intrinsic protein. *Biophys. J.*, 73:2980–2989, 1997.

[174] B. Roux, S. Berneche, and W. Im. Ion channels, permeation, and electrostatics: Insight into the function of KcsA. *Biochemistry*, 39:13295–13306, 2000.

[175] B. Roux and M. Karplus. Ion transport in a gramicidin-like channel: dynamics and mobility. *J. Phys. Chem.*, 95:4856–4868, 1991.

[176] B. Roux and M. Karplus. Ion transport in the gramicidin channel: Free energy of the solvated right-handed dimer in a model membrane. *J. Am. Chem. Soc.*, 115:3250–3262, 1993.

[177] B. Roux and M. Karplus. Molecular dynamics simulations of the gramicidin channel. *Annu. Rev. Biophys. Biomol. Struc.*, 23:731–761, 1994.

[178] B. Roux and R. MacKinnon. The cavity and pore helices in the KcsA K^+ channel: Electrostatic stabilization of monovalent cations. *Science*, 285:100–102, 1999.

[179] B. Roux, B. Prodhom, and M. Karplus. Ion transport in the gramicidin channel: molecular dynamics study of single and double occupancy. *Biophys. J.*, 68:876–892, 1995.

[180] C. Sagui and T. A. Darden. Molecular dynamics simulations of biomolecules: long-range electrostatic effects. *Ann. Rev. Biophys. Biomol. Struct.*, 28:155–179, 1999.

[181] R. Sankararamakrishnan, C. Adcock, and M. S. P. Sansom. The pore domain of the nicotinic acetylcholine receptor: molecular modeling, pore dimensions, and electrostatics. *Biophys. J.*, 71:1659–1671, 1996.

[182] M. S. P. Sansom, C. Adcock, and G. R. Smith. Modelling and simulation of ion channels: applications to the nicotinic acetylcholine receptor. *J. Struct. Biol.*, 121:246–262, 1998.

[183] M. S. P. Sansom, G. R. Smith, C. Adcock, and P. C. Biggin. The dielectric properties of water within model transbilayer pores. *Biophys. J.*, 73:2404–2415, 1997.

[184] J. A. Schetz and P. A. V. Anderson. A reevaluation of the structure of the pore region of voltage activated cation channels. *Biol. Bull.*, 185:462–466, 1993.

[185] T. Schirmer and P. S. Phale. Brownian dynamics simulation of ion flow through porin channels. *J. Mol. Biol.*, 294:1159–1167, 1999.

[186] F. Separovic, S. Barker, M. Delahunty, and R. Smith. NMR structure of C-terminally tagged gramicidin channels. *Biochim. Biophys. Acta*, 67:48–56, 1999.

[187] K. A. Sharp and B. Honig. Electrostatic interactions in macromolecules: theory and applications. *Annu. Rev. Biophys. Biophys. Chem.*, 19:301–332, 1990.

[188] I. H. Shrivastava and M. S. P. Sansom. Simulation of ion permeation through a potassium channel: molecular dynamics of KcsA in a phospholipid bilayer. *Biophys. J.*, 78:557–570, 2000.

[189] P. Smejtek, M. Mense, R. Word, and S. Wang. Electrokinetic properties of the sarcoplasmic reticulum membrane obtained from reconstitution studies. *J. Membrane Biol.*, 167:151–163, 1999.

[190] G. R. Smith and M. S. P. Sansom. Dynamic properties of Na^+ ions in models of ion channels: a molecular dynamics study. *Biophys. J.*, 75:2767–2782, 1997.

[191] G. R. Smith and M. S. P. Sansom. Effective diffusion coefficients of K^+ and Cl^- ions in ion channel models. *Biophys. Chem.*, 79:129–151, 1999.

[192] F. H. Stillinger and A. Rahman. Improved simulation of liquid water by molecular dynamics. *J. Chem. Phys.*, 60:1545–1557, 1974.

[193] S. S. Sung and P. C. Jordan. Why is gramicidin valence selective? *Biophys. J.*, 51:661–672, 1987.

[194] A. Syganow and E. von Kitzing. Integral weak diffusion and diffusion approximations applied to ion transport through biological ion channels. *J. Phys. Chem.*, 99:12030–12040, 1995.

[195] A. Syganow and E. von Kitzing. The drift approximation solves the Poisson, Nernst-Planck, and continuum equations in the limit of large external voltages. *Eur. Biophys. J.*, 28:393–414, 1999.

[196] A. Syganow and E. von Kitzing. (in)validity of the constant field and constant current assumptions in theories of ion transport. *Biophys. J.*, 76:768–781, 1999.

[197] T. Tanabe, H. Takeshima, A. Mikami, V. Flockerzi, K. Takahashi, K. Kangawa, M. Kojima, H. Matsuo, T. Hirose, and S. Numa. Primary structure of the receptor for calcium channel blockers from skeletal muscle. *Nature*, 328:313–318, 1987.

[198] Y. W. Tang, I. Szalai, and K. W. Chan. Diffusivity and conductivity of a solvent primitive model electrolyte in a nanopore by equilibrium and nonequilibrium molecular dynamics simulations. *J. Phys. Chem. A*, 105:9616–9623, 2001.

[199] F. Tian and T. A. Cross. Cation transport: an example of structural based selectivity. *J. Mol. Biol.*, 285:1993–2003, 1999.

[200] F. Tian, K. C. Lee, W. Hu, and T. A. Cross. Monovalent cation transport: lack of structural deformation upon cation binding. *Biochemistry*, 35:11959–11966, 1996.

[201] D.P. Tieleman, S.J. Marrink, and H.J.C. Berendsen. A computer perspective of membranes: molecular dynamics studies of lipid bilayer systems. *Biochim. Biophys. Acta*, 1331:235–270, 1997.

[202] C. Toyoshima and N. Unwin. Ion channel of acetylcholine receptor reconstructed from images of postsynaptic membranes. *Nature*, 336:247–250, 1988.

[203] R. W. Tsien, P. Hess, E. W. McCleskey, and R. L. Rosenberg. Calcium channels: Mechanisms of selectivity, permeation and block. *Ann. Rev. Biophys. Chem.*, 16:265–290, 1987.

[204] P. N. T. Unwin and P. D. Ennis. Two conformations of a channel-forming membrane protein. *Nature*, 307:609–613, 1984.

[205] D. W. Urry. The gramicidin A transmembrane channel: a proposed π_{LD} helix. *Proc. Natl. Acad. Sci. USA*, 68:672–676, 1971.

[206] W. F. van Gunsteren and H. J. C. Berendsen. Algorithms for Brownian dynamics. *Mol. Phys.*, 45:637–647, 1982.

[207] W.F. van Gunsteren and A.E. Mark. Validation of molecular dynamics algorithm. *J. Chem. Phys.*, 108:6109–6116, 1998.

[208] B. A. Wallace. Recent advances in the high resolution structures of bacterial channels: Gramicidin A. *J. Struct. Biol.*, 121:123–141, 1998.

[209] A. Wallqvist and R.D. Mountain. Molecular models of water: Derivation and description. *Rev. Comput. Chem.*, 13:183–247, 1999.

[210] W. Wang, O. Donini, C.M. Reyes, and P.A. Kollman. Biomolecular simulations. *Annu. Rev. Biophys. Biomol. Struct.*, 30:211–243, 2001.

[211] P. Weetman, S. Goldman, and C. G. Gray. Use of Poisson-Boltzmann equation to estimate the electrostatic free energy barrier for dielectric models of biological ion channels. *J. Phys. Chem.*, 101:6073–6078, 1997.

[212] S.J. Weiner, P.A. Kollman, D.A. Case, U.C. Singh, C. Ghio, G. Alagona, S. Profeta, and P. Weiner. A new force field for molecular mechanical simulation of nucleic acids and proteins. *J. Am. Chem. Soc.*, 106:765–784, 1984.

[213] T. F. Weiss. *Cellular Biophysics*, volume 1 and 2. MIT Press, Cambridge, MA., 1996.

[214] T. B. Woolf and B. Roux. Molecular dynamics simulations of the gramicidin channel in a phospholipid bilayer. *Proc. Natl. Acad. Sci. USA*, 91:11631–11635, 1994.

[215] T. B. Woolf and B. Roux. The binding site of sodium in the gramicidin A channel: Comparison of molecular dynamics with solid state NMR data. *Biophys. J.*, 72:1930–1945, 1997.

[216] J. Yang, P. T. Ellinor, W. A. Sather, J. F. Zhang, and R. W. Tsien. Molecular determinants of Ca^{2+} selectivity and ion permeation in L-type Ca^{2+} channels. *Nature*, 366:158–161, 1993.

[217] L. Zhang, H. T. Davis, D. M. Kroll, and H. S. White. Molecular dynamics simulations of water in a spherical cavity. *J. Phys. Chem.*, 99:2878–2884, 1995.

[218] R. Zwanzig. *Nonequilibrium Statistical Mechanics.* Oxford Uni. Press, 2001.